Doctoral Dissertations   Graduate School

8-2015

ION TRANSPORT IN POLYMER ELECTROLYTES

Fei Fan
University of Tennessee - Knoxville, ffan@vols.utk.edu

To the Graduate Council:

I am submitting herewith a dissertation written by Fei Fan entitled "ION TRANSPORT IN POLYMER ELECTROLYTES." I have examined the final electronic copy of this dissertation for form and content and recommend that it be accepted in partial fulfillment of the requirements for the degree of Doctor of Philosophy, with a major in Chemistry.

Alexei P. Sokolov, Major Professor

We have read this dissertation and recommend its acceptance:

Jimmy W. Mays, Charles S. Feigerle, Robert N. Compton

Accepted for the Council:

Carolyn R. Hodges

Vice Provost and Dean of the Graduate School

(Original signatures are on file with official student records.)

ION TRANSPORT IN POLYMER ELECTROLYTES

A Dissertation Presented for the
Doctor of Philosophy
Degree
The University of Tennessee, Knoxville

Fei Fan
August 2015

ACKNOWLEDGEMENTS

The presented research cannot be done without the significant effort from all my colleagues and collaborators at the University of Tennessee and Oak Ridge National Laboratory. I would like to thank Dr. Yangyang Wang for all the guidance, help and advice I have received since day one I joined the group and through my entire graduate school years. He taught me many things and among which, I think the most important is self-discipline and I will keep practicing it no matter what lies ahead in my life. I would also like to gratefully acknowledge Dr. Alexander Agapov, Dr. Masahiro Nakanishi and Dr. Alexander Kisliuk who taught me many things about experimental techniques. I also want to thank my committee members: Dr. Jimmy W. Mays, Dr. Charles S. Feigerle, Dr. Robert N. Compton, for their kindness and effort to serve on my committee and review this dissertation.

I appreciate the collaboration with Dr. Kunlun Hong, Dr. Jimmy Mays and their group members for all the help on synthesis and all the fruitful discussions. I would also want to thank Dr. Che-Nan Sun, Dr. Tomonori Saito, Dr. Shiwang Cheng, Dr. Vera Bocharova, Adam Holt, Dr. Casey Johnson for all their contributions involved in different projects. The presented work could not be done without their efforts.

Lastly, but not the least, I would like to express my sincere gratitude to my advisor Dr. Alexei Sokolov, for providing such an excellent research environment, including those state of the art instruments, opportunity to work with experts from different fields, great collaborators, colleagues, funding, and also for all the guidance and support.

Finally, I want to thank my parents and friends. No words can express how grateful I am to my parents Sizhen Fan and Xiaodong Liu for all their unconditional support. I also would like to thank all my friends, and they are my families in America. And I want to say thank you to myself, for all the hard work, laughs and tears for putting all these together.

ABSTRACT

Batteries with superior performance will advance many technologies, such as the field of energy storage and electrochemical devices. Traditional lithium ion batteries based on liquid electrolytes have intrinsic problems such as leaking, dendrite growth, and those problems are associated with fire or even explosion hazard. Extensive efforts have been devoted to the development of solid polymer electrolytes (SPEs), which would not only reduce the size and weight of the batteries, but also solve safety related issues. However, none of current dry SPEs have reached the desired conductivity of 10^{-3} [0.001] S/cm at ambient temperature. The ion conductivity is controlled by two parameters, the free ion concentration and ion diffusivity. Despite the generally accepted theory that ion diffusion is facilitated by the segmental relaxation of the polymer, the mechanism of ion transport in SPEs is not completely understood.

In this dissertation, the ion transport in different SPEs systems were studied with a combination of experimental techniques: dielectric spectroscopy, differential scanning calorimetry and rheology. The ion transport mechanism was investigated in poly(propylene glycol) (PPG) doped with $LiClO_4$ [lithium perchlorate]. A comprehensive analysis was performed by systematically varying the temperature, pressure, polymer molecular weight and salt concentration. It was found that the ion transport was controlled by the segmental relaxation of the system (or of the "ion-rich" phase if micro-phase separation was observed), which obeyed the traditional theory. On the contrary, decoupling was observed in several

carbonate and styrene based polymer electrolytes. Analysis indicated that the decoupling feature might be related to the packing frustration in those systems.

Polymerized ionic liquids (PolyILs) offer an opportunity of combining the high conductivity of ionic liquids and the superior mechanical strength of polymer. Unlike their small molecule analogue-aprotic ionic liquids, decoupling feature was observed in studied PolyILs. The variation of the pendant group structures altered the fragility index of the samples and thus the degree of decoupling.

Unraveling the mechanisms of the ion transport and structure-property relationship in SPEs is of obvious fundamental and industrial importance. Findings in this work suggested new routes for future design of polymer electrolytes with desired properties.

TABLE OF CONTENTS

LIST OF TABLES

LIST OF FIGURES

xiv

INTRODUCTION

Batteries with superior performance will significantly advance many technologies. For example, batteries play an important role as power supply to cellphones and laptops. To make electric vehicles perform as well as and be cost competitive with traditional gasoline powered vehicles, one needs to have robust batteries. Moreover, the energy we use today is provided mostly from fossil fuels, like coal, oil and natural gas, which are not renewable. While sources like solar, wind and wave provides clean and sustainable energy, in order to achieve an effective usage of them, it is highly desirable to have large-scale batteries to store such energy with low energy loss and production cost. To summarize, the efficient use of energy in nowadays world calls for a breakthrough and innovations in batteries technology.

Traditional lithium ion batteries are based on liquid electrolytes. Those batteries require strong containers which are usually heavy, and those batteries have problems like leaking, dendrite growth which could cause fire or even explosion hazard. To overcome those problems, solid polymer electrolytes (SPEs) have been developed. Use of SPEs instead of traditional liquid electrolytes would significantly reduce the size and weight of the batteries, and solve the safety issues. However, the progress of development of SPEs is relatively slow due to the fact that the mechanism of ion transport in polymers is not completely understood. None of current dry polymer electrolyte system can reach an ambient temperature conductivity of 10^{-3} S cm^{-1}, which is the value required for many practical applications.[1]

In this work a model polymer electrolytes based on poly (propylene glycol) (PPG) doped with LiClO$_4$ was first studied to understand the parameters controlling ionic conductivity. With a basic understanding of the ion transporting mechanism in mind, several polymer electrolytes with targeted structures were synthesized, and the relationship between polymer dynamics and ion transport in those systems was investigated. We found that the picture of ion migration in those systems is different from that in the PPG based polymer electrolytes, which could open new direction for the design of future polymer electrolytes. In the end, a fairly new type of functional materials, the so-called polymerized ionic liquids was studied. Comparison between dielectric and mechanic properties revealed that a decoupling between ion transport and segmental relaxation in all the samples. This dissertation has the following organization.

Introduction gives the organization of this dissertation.

Chapter 1 gives a brief overview of the classic theories in liquid electrolytes and the historical background of solid polymer electrolytes.

Chapter 2 describes experimental techniques and procedures employed in this work. An introduction to the theory and instrumentation of broadband dielectric spectroscopy, differential scanning calorimetry, rheology is presented.

Chapter 3 presents a detailed investigation of the ionic conduction in a model system, poly(propylene glycol) doped with LiClO$_4$. A micro-phase separation into "ion-rich" and "ion-depleted" domains was observed. The modified Walden plot analysis in which the molar conductivity was plotted against the reverse of segmental relaxation time was used. It

revealed that the ionic conductivity is controlled by the "ion-rich" phase and strongly coupled to the segmental relaxation.

Chapter 4 compares the ion transport mechanism in three types of polymer electrolytes based on the modified Walden plot analysis. The concept of "decoupling" is discussed, which states that ionic conduction can be decoupled from segmental relaxation in polymer electrolytes.

Chapter 5 presents a systematic study on several polymerized ionic liquids with different pendant groups. The variation of pendant groups greatly changed the thermal, dielectric, and mechanical properties of the samples. Comparison between dielectric and mechanical results revealed that the ionic conductivity is decoupled from the segmental relaxation in the polymerized ionic liquids studied. Combining data from literature and Chapter 4, it was found that the degree of decoupling increases with the increase of fragility index of polymer due to "packing frustration".

Lastly, there are the conclusions and a brief outlook.

CHAPTER I

CLASSICAL THEORIES IN LIQUID ELECTROLYTES

The motivation for the development of batteries with supreme performance is rooted on the efficient storage and utilization of energy. A battery is composed of a positive electrode, a negative electrode and the electrolyte separating the two electrodes. Outside the battery, electrons flow from the negative electrode to the positive electrode and charge cloud of opposite sign forms near the electrodes. Inside the battery, the ions in the electrolyte neutralize these charges, enabling the electrons to continue flowing.[2] Thus, the electrolyte is as important as the two electrodes, influencing parameters such as the power, electrochemical stability, cycle life, shelf life and safety of a battery.

Lithium-ion batteries have been the most exploited systems mainly for two reasons: first, lithium is the lightest metal element; second, lithium exhibits the highest oxidation potential of any element.[3] Therefore, because of their lightweight and high energy density, lithium-based batteries accounts for 63% of worldwide sales values in portable batteries according to a report published in 2000.[4] Traditional lithium-ion batteries are based on liquid electrolytes, which consist of lithium salts such as $LiPF_6$ dissolved in organic solvents e.g. ethylene carbonate, dimethyl carbonate. To design batteries with better performance, it is crucial to understand the properties of the electrolytes. The next section is devoted to the basic conductivity theories in a liquid electrolyte in general.

1.1 Introduction to an Electrolyte

An electrolyte is made by dissolving a salt in a solvent, and the resulting electrolyte should be capable of conducting ions. A good example would be NaCl water solution. As a solid, NaCl is not conductive since both the cation Na+ and anion Cl- are held tightly in the lattice and cannot diffuse. Once it is dissolved in water, NaCl is pulled apart into free ions Na^+ and Cl^-. The partially negatively charged O end in the water molecules orients towards the cation while the partially positively charged H end rotate towards the anion, forming a solvation shell around the central ion. The stabilization of the ions in the solvent is mediated through heat transfer and increased entropy. The result is that the solution is more thermodynamically stable than the solute and solvent individually. Fig.1.1 illustrates the solvation of NaCl in water.

Since both cations and anions are presented in the solution, ion-ion interaction is inevitable. According to Coulomb's law, the electrostatic interaction between two charged particles immersed in material with dielectric constant ε_r can be described by the equation:

$$F = \frac{1}{4\pi\varepsilon_r}\frac{q_1 q_2}{r^2} \tag{1.1}$$

in which q is the charges on each ion, and r is the distance between them. ε_r is the dielectric constant, or under another name relative permittivity. It is calculated through $\varepsilon_r = \frac{\varepsilon}{\varepsilon_0}$ in which ε is the permittivity of the interested material and ε_0 is the permittivity of vacuum which equals to 8.854187817… $\times 10^{-12}$ F/m (farads per meter).
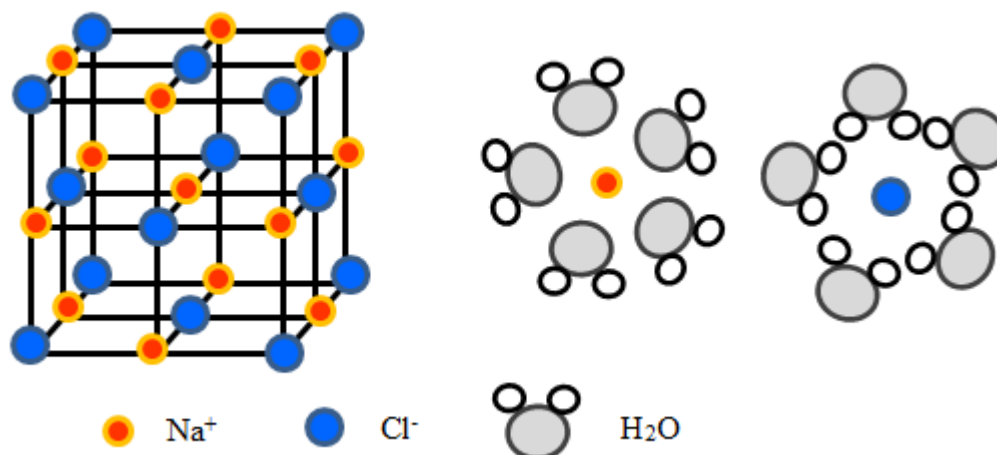
Figure 1.1. NaCl lattice (left), in which Na+ and anion Cl- are hold tightly. Solvation of NaCl in water (right). Water molecules orient different towards cations and anions and form solvation shell around the ions.

The dielectric constant of a solvent represents its ability to screen the electric field raised by the ions dissolved in it. Water, has a dielectric constant of 78.3 at 25°C.[5] Common solvents used as liquid electrolytes in traditional batteries, such as ethylene carbonate has a dielectric constant of 90.5 at 40 °C.[6] The larger the dielectric constant, the smaller the electrostatic interactions between ions at a given distance. In solvents with low dielectric constant, it is easier for cations and anions to form ion pairs or even larger aggregates. It has been suggested by Fuoss's triple ion theory[7] that there are three ion states: unpaired ions which are fully solvated into free ions; separated pairs, where cations and anions are close to each other, but separated by the solvent molecules; and lastly contact pairs, in which the ions are strongly-bounded (Fig. 1.2). The ions are considered as free if the distance between them is larger than

a certain distance D so that the electrostatic effect between ions can be neglected. The

Bjerrum length l_B is usually used for the value D,[8] which is defined as the separation at which

the electrostatic energy between two elementary charges is comparable in magnitude to the

thermal energy scale $k_B T$, through this equation:

$$l_B = \frac{q^2}{4\pi\varepsilon_0\varepsilon_r k_B T} \qquad (1.2)$$

in which k_B is the Boltzmann constant and T is the temperature. For ions within this distance,

they are considered as paired. Normally, if the ions share the first solvation shell, they are

considered as separated pair; if they are in contact and share electrons, they are considered as

contact pairs. Both separated pairs and contact pairs are electrically neutral which means that

they make no contribution to the overall conductivity.
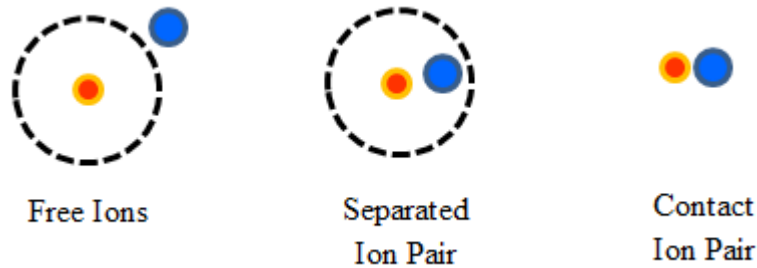
Figure 1.2. Illustration of three different ion states in a solution. The dotted line indicates a distance of D. The Bjerrum length is usually used for this value.

Not only would the property of the solvent, but the type of the salt also influence the salt dissociation efficiency. Ue et al. carried out a systematic study on different lithium salts.[9-11] It turned out that bis(trifluoromethane)sulfonimide lithium (LiTFSI) (Fig. 1.3) has the highest dissociation constant among all compared salts e.g. $LiBF_4$, $LiClO_4$, $LiPF_6$, and $LiAsF_6$. LiTFSI has very low lattice energy, and the charge can be sufficiently delocalized over the imide anion by two trifluoromethanesulfonyl groups. The degree of salt dissociation also depends on the total concentration of the salt. As the salt concentration rises, ions tend to aggregate together. As a result, the free ion concentration first increases with the increase of the total salt amount and after reaching a maximum, it starts to decrease.

$$F_3C-\overset{\overset{\displaystyle O}{\|}}{\underset{\underset{\displaystyle O}{\|}}{S}}-\overset{}{\underset{\underset{\displaystyle Li}{|}}{N}}-\overset{\overset{\displaystyle O}{\|}}{\underset{\underset{\displaystyle O}{\|}}{S}}-CF_3$$
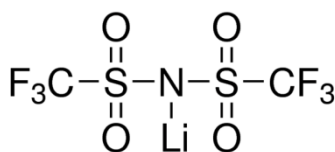
Figure 1.3. Structure of $LiN(CF_3SO_3)_2$ (LiTFSI), Bis(trifluoromethane)sulfonimide lithium salt.

1.1.1 Debye-Hückel Theory

Due to the inevitable electrostatic interactions between ions, the property of an electrolyte deviates from ideality. The Debye–Hückel theory[12] (DH theory) provides the

fundamental treatments to correct for the non-ideality of electrolyte solutions. It was built on the basic assumptions that ions are spherical and are not polarized by the surrounding electric field; each ion is surrounded by a spherically symmetric cloud consisting of ions, namely the ionic atmosphere (Fig. 1.4). The sign of the net charge on the ionic atmosphere and the charge sign on the central ion are opposite. The DH theory also assumes that the solvent has a uniform dielectric constant through the medium and there is no electrostriction.
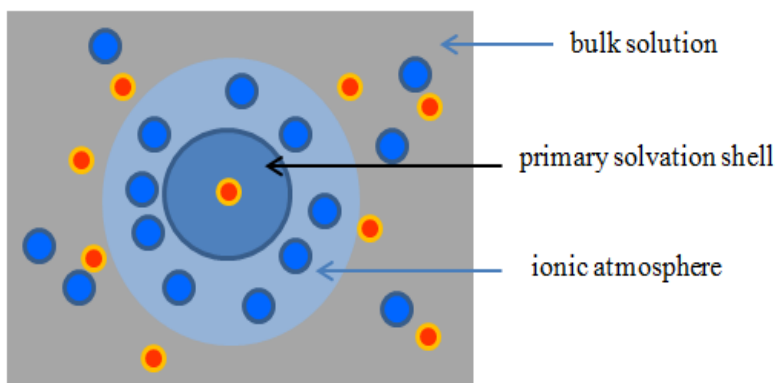
Figure 1.4. Structure of a cation (orange) surrounded by a solvation shell and the "ionic atmosphere" formed by counterions (blue).

First, the ionic strength I of the solution determines the electrostatic interactions.

$$I = \frac{1}{2} \sum c_i\, q_i{}^2 \tag{1.3}$$

in which, c_i is the molar concentration of ion i (either in molality mol/(Kg) or molarity mol/L), q_i is the charge of ion i. The DH theory is only applicable to very dilute solutions in which $I < 0.01$ mol $(Kg)^{-1}$, since it is based on the assumption that the electrolyte is a strong electrolyte and the salt is completely dissociated.

According to the DH theory, the term activity, a, is introduced to accommodate for the deviation from ideal behavior:

$$a = \gamma c \qquad (1.4)$$

in which c is the concentration and γ is the activity coefficient. For an ideal solution, the activity is equal to one. For non-ideal solution, the mean ionic activity coefficient γ can be calculated by the equation:

$$\log \gamma = -\frac{z_i^2 e^3 N_A^{1/2}}{4\pi(\varepsilon_r \varepsilon_0 k_B T)^{3/2}} \sqrt{\frac{I}{2}} \qquad (1.5)$$

in which e is the elementary charge, 1.602×10^{-19}C, N_A is the Avogadro's number 6.022×10^{23}mol^{-1}. Eq. 1.5 does not take into account the effective sizes of the ions.

Although the DH theory is a simplified model based on several assumptions, it predicts accurately the mean activity coefficient for ions in dilute solutions.

1.2 Conductivity of an Electrolyte

Conductivity of an electrolyte is caused by the diffusion of ions, which is a result of concentration fluctuation in different regions of the electrolyte. The conductivity of an electrolyte is given by the equation:

$$\sigma = \sum p_i q_i \mu_i \tag{1.6}$$

in which p is the concentration of free ions, and μ is their electrical mobility. Strictly speaking, one should take the sum over all the ionic species (*i*). In the presented study, $q_+ = q_-$ for the salt $LiClO_4$, LiTFSI etc. In addition, only the average mobility of cations and anions will be considered for simplicity. Therefore, $\sigma = pq\mu$ will be used for the discussion of the general principles governing ionic transport in this work.

The Einstein relation has the form:

$$\mu = \frac{qD}{k_B T} \tag{1.7}$$

where *D* is diffusivity of the ions. Combining eq. 1.6 and 1.7 results in

$$\sigma = \frac{pq^2 D}{k_B T} \tag{1.8}$$

To compare the conductance of different electrolytes, the molar conductivity is often used which is defined as the conductivity σ divided by the total concentration c of the salt.

$$\Lambda = \sigma/c \tag{1.9}$$

Application of an external electric field will cause cations and anions to move in opposite directions. According to Kohlrausch's law, the conductivity measures the sum of the conductivities from migration of both the positive and negative ions. The transference number defines the different fractions of current carried by the cation or the anion. Due to their difference in mobility, cations and anions have different transference number, i.e. they contribute differently to the total conductivity. The sum of the transference numbers of cations and anions equals unity. While the central ion is migrating towards one direction, the surrounding ionic atmosphere is moving towards the opposite direction. As a result, on the conduction path of the central ion, a new ionic atmosphere is formed while the old one has to dissipate or relax. The dissipation of the old ionic atmosphere is relatively slow compared to the migration rate of the central ion. As a result, the charge density of the counter ion behind the central ion is greater than that in the front. This is known as the "asymmetric effect". The movement of the central ion is thus dragged down by the "residue" from the ionic atmosphere on the "tail" of the central ion migration path. This is called the relaxation effect. Besides, in a liquid electrolyte, the solvation shell migrates with the central ions, which adds extra friction to the migration of ions. This is called the electrophoretic effect. Both the relaxation effect and the electrophoretic effect would slow down the migration of ions, resulting in a decrease of molar conductivity of an electrolyte.

The mentioned effects are described by the following equations. The Stokes-Einstein relation connects the diffusion coefficient D to the temperature, viscosity of the solution η and the size of the ions r, including the primary solvation shell.

$$D = \frac{k_B T}{6 \pi \eta r} \tag{1.10}$$

According to the Maxwell equation, for small-molecule solvents $\eta = G\tau_s$, where G is

the glassy modulus and τ_S is the structural relaxation. Combining eq. 1.8 and 1.10,

$\sigma \sim \mu \sim \frac{D}{T} \sim \frac{1}{\eta}$, we arrive at the equation that $\sigma \tau_s T = constant$. It indicates that the

conductivity of an electrolyte is controlled by the structural relaxation of the system. The

structural relaxation and the related glass transition behavior in glass-forming materials will

be discussed in details in the next section.

1.3 Glass Transition and Structural Relaxation

All glass forming materials can be supercooled below their melting temperature

without crystallization, and instead, they go through a process called glass transition. The

glass transition temperature, Tg, is defined as a temperature at which the material transforms

from the liquid state to the solid state without crystallization. It is often defined as when the

structure relaxation time reaches 100s. Properties of the glass forming materials change

drastically in the vicinity of Tg.

The structural relaxation process slows down with the decrease of temperature and its

dependence on temperature deviates from the Arrhenius equation in all glass forming

materials. According to the Arrhenius law,

$$\tau = \tau_0 \exp(E_a / kT) \tag{1.11}$$

13

in which τ is the structural relaxation time of the material, τ_0 is the so-called attempt time of a unit oscillating in the potential well, E_a is the activation energy. Eq. 1.11 can also be used to describe material properties such as viscosity, diffusion rate etc. An Arrhenius behavior indicates that the relaxation dynamics is a pure thermally activated process, during which the relaxing units overcoming a certain potential energy barrier. However, all glass forming materials deviate from the Arrhenius bahavior, and follow another type of temperature dependence under the name Vogel-Fulcher-Tammann (VFT) equation:

$$\tau = \tau_0 \exp\left(\frac{B}{T - T_0}\right) \tag{1.12}$$

T_0 in the VFT equation is related to the so-called thermodynamic Tg, which is usually 30-50K below Tg. It is worth noting that B is different from the activation energy in the Arrhenius equation. The VFT equation describes processes with an increasing apparent activation energy as the material is cooled towards the glass transition temperature, Tg.

The structural relaxation process is generally described by the stretched exponential function, the Kolrausch-Williams-Watts (KWW) function in the time domain:

$$f(t) = \exp[-(t/\tau)^\beta] \tag{1.13}$$

in which τ is the characteristic relaxation time and β is the stretching parameter.

The deviation of the temperature dependence of structural relaxation time from Arrhenius behavior to VFT in the vicinity of Tg is characterized by the fragility index m[13, 14]. It defines the steepness of the temperature dependence of the segmental relaxation time τ_s close to Tg:

$$m = \frac{d \log \tau_s}{d(T_g/T)}\bigg|_{T=T_g} \qquad (1.14)$$

A system is called fragile when it shows non-Arrhenius temperature dependence of segmental dynamics close to Tg. It is called strong when it shows Arrhenius-like behavior (Fig. 1.5). The higher the fragility index, the more deviation it shows from the Arrhenius behavior. Most small molecule liquids show fragility m values between 50 to 100.[15]
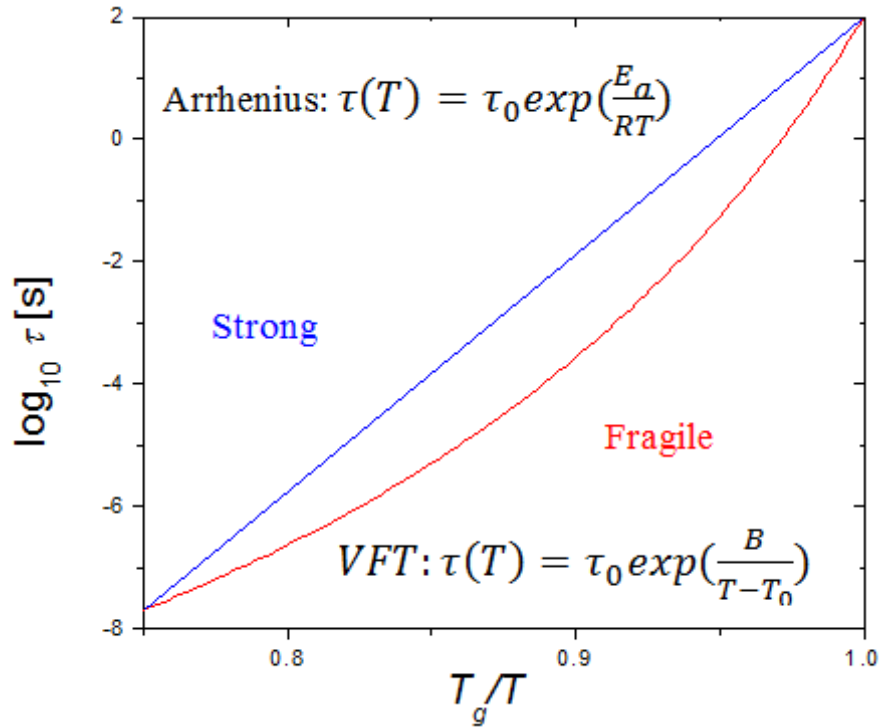
Figure 1.5. Comparison of strong and fragile behaviors. The blue line represents strong behavior and can be fit by the Arrhenius equation. The red curve represents fragile behavior and can be described by VFT function.

1.3.1 Adam-Gibbs Theory

Since the structural relaxation and the ion conductivity are strongly correlated, understanding the structural relaxation helps us to study the ion transport phenomena in electrolytes. Yet, the physical picture underlying the glass transition behavior still remains incompletely understood. One of the most important classic theories has been proposed by Adam and Gibbs (AG theory)[16] since 1965. They defined cooperative rearranging regions which involves z^* molecules (repeating units in the case of polymers). Those regions can surmount simultaneously the individual potential energy barriers, $\Delta\mu$, hindering their cooperative rearrangement, which is a temperature-independent constant. The relaxation time of the supercooled liquid is thus:

$$\tau(T) = \tau_\infty exp\frac{z^*\Delta\mu}{k_B T} \tag{1.15}$$

where τ_∞ is the relaxation time at infinite temperature, and the critical size z^* of the cooperating regions is defined as:

$$z^* = N_A s_c{}^*/S_c \tag{1.16}$$

where $s_c{}^*$ is the critical molar configuration entropy of a region of z^* molecules, S_c is the macroscopic configuration entropy of the system. It states that the size of the region is directly related to the macroscopic configuration entropy. Combining eq.1.15 and 1.16 yields,

$$\tau(T) = \tau_\infty exp(C/TS_c) \tag{1.17}$$

where is C is a temperature-independent constant. As a result of a decrease of temperature, S_c decreases, and the size of the rearranging region increases, the system becomes more densely packed and activation energy increases.

1.3.2 Generalized Entropy Theory

The Generalized Entropy (GE) Theory by Dudowicz, Freed and Douglas[17-19] is one of the many models describing the glass transition behavior in polymer. It was an extension of the lattice cluster theory, combining concepts from the Gibbs-DiMarzio[20] and Adam-Gibbs theories[16]. According to the GE theory, the temperature dependence of structural dynamics is based on the packing efficiency of the system. Their model is based on the assumption that each monomer consists of a set of united atom groups, and each atom occupies a single lattice site. Vacant sites represent the free volume. Therefore, the individual monomer occupies several neighboring lattice sites. The interaction between all united atom groups are simplified as a common monomer averaged van der Waals interaction energy and gauche bending energy penalties ascribed to the backbone (*Eb*) and to the side groups (*Es*).

Thus, polymers can be classified, with simplicity, into three basic categories: flexible-flexible (F-F), flexible-stiff (F-S), and stiff-flexible (S-F) in which the first letter states the stiffness of backbone and the second letter refers to the stiffness of the side groups. The F-F class of polymers are modeled with similar backbone and sidegroup stiffness (*Es = Eb*), which means that backbone and sidegroups are able to adapt to a new conformation at similar

17

rate resulting in efficient packing. As a result, those systems show lower sensitivity to the changes in temperature.

However, in F-S and S-F classes of polymers, due to the big difference in bending energies between backbone and side groups, the polymers will suffer from packing frustration. Thus the change of temperature would greatly affect the structural dynamics, resulting in a higher fragility index.

The GE model gives a qualitative explanation of fragility difference in many glass-forming liquids. In systems suffering from packing frustration, a fragile behavior is expected while in systems with high packing efficiency, it shows a strong Arrhenius behavior. A recent paper by Dudowicz et al. took into account factors such as monomer molecular structure, chain rigidity, and cohesive interaction strength into the GE model.[21]

1.4 Walden Plot

Based on the discussion above, it is clear that the molar conductivity is related to the viscosity of an electrolyte. This is reflected by an empirical relation proposed by Walden in his paper published in 1906.[22] According to the classical Walden's rule, the molar conductivity (Λ) of many small-molecule electrolytes is inversely proportional to its fluidity $=1/\eta$ (η is the viscosity).

$$\Lambda\eta = constant \qquad (1.18)$$

For electrolytes which follow the Walden's rule, eq. 1.18 states that all ions in the electrolytes are free (complete dissociation) and their diffusion is controlled by the macroscopic viscosity. According to the Maxwell equation, for small-molecule solvents $\eta = G\tau_s$, thus η can be substituted with τ_s. The Walden plot analysis serves as a very useful method to classify ionic conductor.[23-26] In a typical Walden plot analysis, the molar conductivity of a given electrolyte is plotted as a function of $1/\eta$ or $1/\tau_s$ on double-logarithmic scale. (Fig. 1.6) Two pieces of important information can be obtained from the Walden plot analysis. First, the Walden plot analysis could reveal the degree of coupling or decoupling between ionic transport and structural relaxation. Using a dilute aqueous solution as a reference (e.g., KCl or LiCl), one can draw an "ideal" Walden line with slope of one on the Walden plot. Completely coupled ionic conductors, such as dilute aqueous salt solutions, would show up as a straight line of slope one very close to the idea Walden line. If ion diffusion is faster than the structural relaxation of the solvent molecules, the Walden analysis would display a line above the ideal Walden line, and those electrolytes are usually classified as superionic. On the other hand, decoupled systems[27-33] would display a slope smaller than one, which indicates that ion transport is less sensitive to the change of temperature than the structural relaxation.

It was Angell[34, 35] who first suggested the decoupling idea. A decoupling ratio was introduced, which is the ratio between structural relaxation time and conductivity relaxation time.

$$R = \tau_s/\tau_\sigma \qquad (1.19)$$
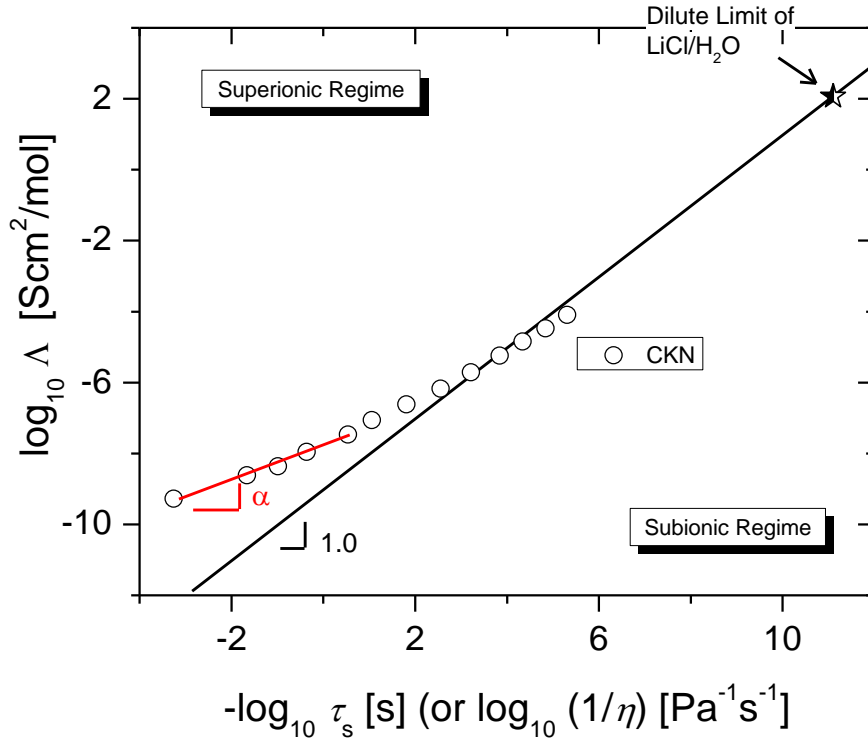
Figure 1.6. Illustration of Walden plot analysis. The ideal line is constructed based on dilute limit of LiCl/H_2O solution. It divides the plot into the superionic regime and subionic regime. The relation between Λ and $1/\tau_s$ or $1/\eta$ typically can be characterized by a power law: $\Lambda\tau_s^{\alpha}$ or $\Lambda\eta^{\alpha} = $ Const., which reduces to the classical Walden's rule when $\alpha = 1$. The slope α provides a measure of the degree of decoupling ε between ionic transport and fluidity. Data from CKN is used as an example of decoupling systems. (Data from ref. [36])

The best vitreous conductors can have R value of order 10^{13} at Tg.[35] It has been shown for Ca-K-NO_3 (CKN), that ionic conductivity is enhanced relative to structural relaxation by nearly three orders of magnitude near Tg.[36] In this case, the ion conduction is less related to the structural relaxation, i.e. it is decoupled from the structural relaxation of the surrounding molecules. (Fig. 1.6)

The relation between Λ and $1/\eta$ or $1/\tau_s$ typically can be characterized by a power law: $\Lambda\tau_s{}^\alpha$ or $\Lambda\eta^\alpha$ = Const, which reduces to the classical Walden's rule when $\alpha = 1$. The slope α provides a measure of the degree of decoupling ε and $\varepsilon = 1- \alpha$, between ionic transport and viscosity or structural relaxation. Second, the Walden plot analysis could reveal the intrinsic conducting ability of an ionic conductor relative to the "ideal" aqueous solution. Solutions with poor ion dissociation would show up in the subionic regime, because only a few ions contribute to conductivity. Those electrolytes are considered as subionic conductors.[24, 25, 37]

1.5 Solid Polymer Electrolytes

Having discussed the ionic transport in liquid electrolytes, this next section will be expanded onto the solid polymer electrolytes, which is considered as a great substitute for liquid electrolytes in batteries.

Polymer electrolytes were first discovered by Peter Wright in the 1970s.[38] The early polymer electrolytes are simply polymers mixed with salts. The area of polymer electrolytes has drawn a great amount of interests, because they are promising candidates to substitute liquid electrolytes. First, SPE is environmentally friendly, free from the problems associated with corrosive, flammable, or toxic liquids. Secondly, SPE can be made into varied geometries due to the flexible solid-state structure of polymers. Moreover, replacement of the liquid electrolytes with SPE results in significant decrease in the weight of the container. Replacement of liquid electrolytes by SPE will speed up the development of other technologies, such as laptops, electric vehicles, which are based on reliable and efficient

energy storage methods.[39, 40] Moreover, progress in the SPE field will help further the

understanding of ion transporting phenomena in fast ion conductors. However, the progress of

development of SPE is relatively slow due to the fact that the mechanism of ion transport in

polymers is not completely understood. None of current polymer electrolyte systems can

reach an ambient temperature conductivity of 10^{-3} S cm^{-1}, which is the value required for

practical applications.[1] A complete and deep understanding of what controls the conductivity

in SPE will greatly boost the development of SPE and guide the design of the SPE for

different applications and to fulfill different requirements.

For a polymer to be suitable for SPE, it must have a donor atom such as O, N such as

poly(ethylene oxide) (PEO) that can coordinate around the cation in order to dissolve the salt,.

Since a polymer is composed of many repeating units connected, the Li$^+$ is usually solvated

by several repeating units of the polymer. For example, in PEO mixed with lithium salt, the

polymer wraps around the cation in a way which is similar to crown ether or cryptand based

coordination compounds. Molecular dynamics simulations showed that the one Li$^+$ is

wrapped by five ether oxygens in PEO chain, isolating Li$^+$ from the counter ion.[41] (Fig.1.7)

The anion is barely solvated by the polymer.

Similar to the situation in liquid electrolytes, the doped salt does not dissociate

completely in the polymer. The Li$^+$ tend to form ion pairs or even larger aggregates with the

counter ion. The polymer has to compete with the counterion for a better solvation of Li$^+$.

However, the interaction between the polymer and the cation cannot be too strong, otherwise

the cation would not be able to diffuse in the polymer. The interaction between ions depends

on the dielectric constant of the hosting polymer. Although PEO has very low dielectric

22

constant (about 5~7), ethylene oxide groups (EO) seem to be excellent solvation groups for

Li$^+$ cation. This is probably due to its special spatial structure.[42-44] The lithium salts that are

commonly used are LiTFSI, LiCF$_3$SO$_3$, LiBF$_4$. LiTFSI. LiTFSI has relatively low lattice

energy, which facilitates ion solvation.
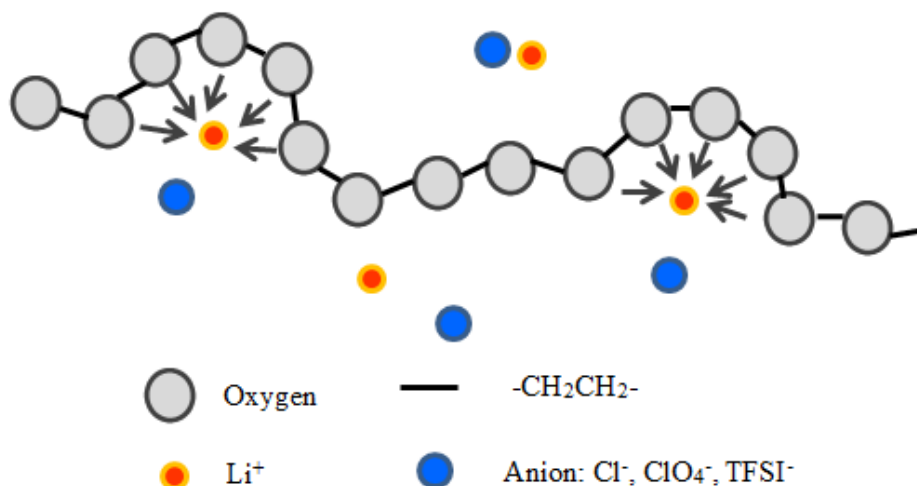
Figure 1.7. Schematic of the solvation of Li+ in the PEO matrix. One Li$^+$ is wrapped by five
ether oxygens in PEO chain, which is suggested by simulation work.[41]

In addition, its spatial structure helps suppress the crystallization of the polymer.[45] The

degree of dissociation decreases with the increase of the amount of salt. Therefore, the free

ion concentration exhibits a maximum with the increase of the total salt amount and then

decreases since the increase of salt amount can no longer compensate for the loss induced by

ion association. The optimal salt concentration is around O:Li=25 in PEO based polymer electrolytes. O:Li is the molar ratio between the number of oxygen (which equals the number of PEO repeating units) and the lithium cations.

Some commonly studied polymer hosts for polymer electrolytes are listed in Table.1. There have been several papers reviewed the development of polymer electrolytes and its application.[46-50]

Table 1.1. Some Selected Polymer Electrolytes Systems

Polymer Host	Repeating Unit	Ref.
Poly(ethylene oxide)	CH_2CH_2O	ref. [1, 8-17]
Poly(propylene oxide)	$CH(CH_3)CH_2O$	
Poly(dimetylsiloxane)	$SiO(CH_3)_2$	ref. [51]
Poly(acrylonitrile)	$CH_2CH(CN)$	ref. [52-54]
Poly(methyl methacrylate)	$CH_2C(CH_3)COOCH_3$	ref. [55, 56]
Poly(vinylidene fluoride-hexafluoropropylene)	$[CH_2CF_2][CF_2CF(CF_3)]$	ref. [57]
Poly(vinylidene fluoride)	CH_2CF_2	ref. [58, 59]
Poly(vinyl chloride)	CH_2CHCl	ref. [60, 61]

1.5.1 Conductivity of Solid Polymer Electrolytes

The ionic conductivity in liquid electrolytes is controlled by two parameters $\sigma = pq\mu$. This also applies for solid polymer electrolytes. The ion transport in liquid electrolytes is controlled by the macro-viscosity of the system. However, polymers are different from small

molecules. A polymer is composed of many connected repeating units. Since Li^+ is solvated by segments of the polymer not the entire chain, the ion transport should be strongly coupled to the local-viscosity instead of the macro-viscosity of the polymer. The local-viscosity of a polymer is determined by its segmental relaxation, which is a cooperative motion of several repeating units. Both theoretical work and experiments have shown that it is indeed the case in several model polymer electrolyte systems, i.e. ion transport occurred in amorphous polymers above Tg and the ion transport is facilitated by the local-viscosity, i.e. segmental relaxation of the polymer.[62-67] One of the models describing the ion transport process in polymer electrolytes is the dynamic bond percolation model.[64, 65] The bond is a vivid metaphor as the temporary bridge between suitable coordination sites for ions to hop to. Above Tg, the segmental motion of the polymer creates coordination sites, facilitating the ion transport through the polymer. As temperature decreases towards Tg, the segmental relaxation becomes slower as well as the ion transport.

The macro-viscosity of the polymer is known to be associated with the chain relaxation of the polymer. The chain relaxation represents the dynamics of the entire chain and it happens at a length scale and time scale larger than the segmental relaxation. It has been reported that chain dynamics and segmental relaxation are decoupled in most polymer systems, i.e. they exhibit different temperature dependence.[68]

Since faster segmental relaxation could facilitate ion transport, a lot of work has been focused on using polymer with flexible backbone, such as poly-siloxane based polymer. Addition of plasticizers have reported to be able to improve the ionic conductivity.[69] Plasticizers are usually low molecular weight liquids of carbonic acid esters and chain-like

esters (e.g. propylene carbonate, dimethyl carbonate, diethyl carbonate, etc.). However, the gain in ionic conductivity is accompanied by a loss of mechanical strength and an increase of safety hazard. So this raised an important question about whether or not we can boost the conductivity through other methods. The answer is yes.[70-73] One of the methods is using nano-composites. Examples of such additives are nano particles, e.g. TiO_2, Al_2O_3 and SiO_2.[74] This is a promising approach, which raises the conductivity and also mechanical strength at the same time. Another method is under the name "polymer-in-salt," or "rubbery" electrolytes, in which lithium salts are mixed with small amount of PEO or PPG.[75, 76] Moreover, traditional views think the ionic conductivity happens in the amorphous phase of the polymer electrolyte. However, it has been discovered that ionic conductivity also exists in crystalline phase.[77]

Another promising method is also quite different from the traditional approach., Since the ion motion is facilitated by the segmental relaxation of polymer according to the traditional theory, as temperature approaches Tg, the ion transport slows down with the reduced segmental relaxation rate. As a result, conductivity decreases drastically. If the ion transport depends less or even becomes independent on the rearrangement of polymer segments, ionic conductivity would not decreases as much as the segmental relaxation rate upon cooling.

This decoupling scenario was first reported in polymers by Sasabe and Saito.[78] In their work, the ionic conductivity is less sensitive to the change of temperature than the segmental dynamics of the polymers in several rigid polymers, e.g. poly(vinyl chloride) (PVC). (Fig. 1.8)
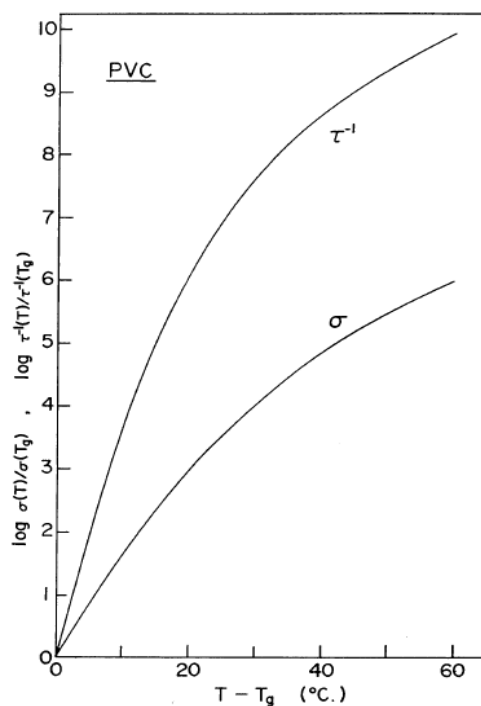
Figure 1.8. Temperature dependence of dc conductivity and reciprocal segmental relaxation time of PVC (ref.[78]).

Agapov et al. [79] discovered that the degree of decoupling ε is higher in more fragile polymers. As introduced in the previous section, fragility m defines the steepness of segmental relaxation time temperature dependence close to Tg. Polymers show fragility m between 20 to 200.[80] Fragility of polymer was found to be dependent on many parameters including monomer structure, molecular weight, tacticity, symmetry, and the relative rigidity between the backbone and sidechain.[80]

To explain this observation, Agapov et al.[79] turned to the general entropy theory proposed by Dudowicz et al.[17-19] and recent theoretical and experimental work.[80, 81] According

27

to these studies, the "relative rigidity" between the polymer backbone and side chain governs the chain packing efficiency and thus affect the polymer fragility: the higher the chain packing efficiency, the lower the fragility. For ion diffusion, a well packed polymer matrix presents more obstacles than that in a loosely packed polymer matrix. Thus the ionic transport requires larger rearrangement of polymer segments. On the contrary, ions may diffuse through the loosely packed polymer matrix even when the segmental dynamics is slow or "frozen". Flexible polymers can pack more efficiently, resulting in a tightly packed structure. As a result, the ion transport is strongly coupled to the segmental relaxation of the polymer.

There has also been evidence of the possibility of decoupling in polymer electrolytes. By incorporating ionogenic groups, Zhang et al.[82] prepared a decoupled system-Li$^+$ion conducting polyimides. By introducing small molecules resembling common organic solvents into the polymer, Yamamoto and co-workers[83] prepared Poly (vinyl alcohol) (PVA) systems with a Tg of 350°C with alkali metal salts that exhibit reasonable conductivities ($10^{-5.5} \sim 10^{-3.5}$ Scm^{-1}) at 20°C. They observed Arrhenius temperature dependence of conductivity (eq.1.11), while in coupled systems it is usually described by the VFT equation (eq.1.12). Results from NMR measurements also support the decoupling phenomenon in the PVA system.[84] Wei et al.[85] prepared poly (vinyl carbonate) based systems having rigid structure with conductivity of 10^{-4} S cm^{-1}. Imrie et al.[86] introduced a "glassy mechanism" strategy in the synthesis of polymer electrolytes and achieved the highest decoupling ratio R at Tg among polymer electrolytes so far (R=1.6×10^6 at Tg). By the inclusion of isophthalic ester linkages and non-solvating side groups (Fig.1.9), they stiffened the backbone, thus stabilizing the ethylene oxide. The resulting excess volume and empty sites facilitated the ion transport.
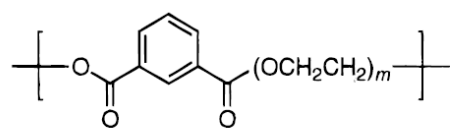
m = 4, 6, 13, 20, 34

(a)
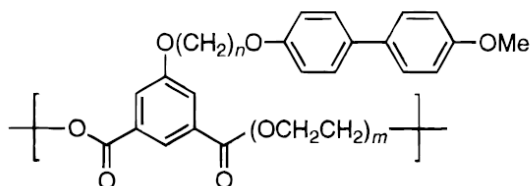
n = 3, 4, 5, 6, 12: m = 4, 6, 13, 20, 34

(b)

Figure 1.9. Molecular structures of the new polymers (a) the one with side-group liquid crystalline polymer (b) the one without the side-group liquid crystalline polymer (ref.[86]).

All the above findings suggest that it might be possible to get high ionic conductivity in polymer electrolytes based on the decoupling concept. With careful structure design, one can control the rigidity of the polymer and thus maximize the decoupling phenomena. Therefore, besides looking for flexible polymers with low Tg, the concept of decoupling suggests a promising alternative direction for the designing of polymer electrolytes with high conductivity.

1.6 Research Objectives

It is clear that the ionic transport mechanism in polymer electrolytes has not been completely understood. In traditional polymer electrolytes, the ion motion is coupled with the segmental dynamics of polymers. The segmental relaxation is related to the glass transition behavior of polymeric materials. As segmental relaxation slows down, the ionic conductivity decreases. Experimental and theoretical work have shown that ionic motion can be decoupled from the segmental relaxation of polymer, which suggests a whole new direction for the design of high conductivity polymer electrolytes.

With that goal in mind, this work is addressing the following problems: First, what controls the ionic conductivity in traditional polymer electrolytes? Secondly, can we improve ionic conductivity with the decoupling concept? Thirdly, can the degree of decoupling be modified through polymer structure design?

CHAPTER II

EXPERIMENTAL TECHNIQUES

Reproduced in part from "Examination of Methods to Determine Free-Ion Diffusivity and Number Density from Analysis of Electrode Polarization" *Physical Review E.* 87 (4), 042308, 2013 American Physical Society.

2.1 Broadband Dielectric Spectroscopy (BDS)

2.1.1 Principles of Dielectric Spectroscopy

Broadband dielectric spectroscopy is capable of probing molecular dynamics on a wide range of time scales. Generally, in a dielectric measurement, a very small perturbation created by a sinusoidal external electric field is applied to the sample. The dipoles within the sample will try to align with the external field and then relax to a new equilibrium state. During this process, the neighboring dipoles, bonds or groups have to rearrange, in this way the dielectric spectroscopy probes different polarization processes, reflecting important properties of the materials.

$$D = \varepsilon^* \varepsilon_0 E \tag{2.1}$$

$$P = D - D_0 = \chi^* \varepsilon_0 E \tag{2.2}$$

$$\varepsilon^* = \varepsilon_\infty - \int_0^\infty \frac{d\varepsilon(t)}{dt} \exp(-i\omega t)\, dt = \varepsilon'(\omega) - i\varepsilon''(\omega) \tag{2.3}$$

in which ε^* is the complex permittivity function of the material. ε' is the real part and it represents the dielectric energy stored in the system. ε'' is the imaginary part and it is proportional to the energy dissipated. ε_0 is the dielectric constant of the vacuum ($\varepsilon_0 = 8.854 \times 10^{-12} F/m$); χ^* is the dielectric susceptibility which describes how hard is it for a dipole to orient with the applied electric field. It is related to the permittivity through equation:

$$\chi^* = \varepsilon^* - 1 \tag{2.4}$$

ε^* is a generalized compliance, and the corresponding modulus is the complex electric modulus:

$$M^*(\omega) = 1/\varepsilon^*(\omega) \tag{2.5}$$

Ion diffusion results in conductive contribution σ^* to the dielectric spectrum.

$$\sigma^* = i\omega\varepsilon^*\varepsilon_0 = i\omega\varepsilon_0/M^*(\omega) \tag{2.6}$$

Different types of polarizations occur at their characteristic frequency range due to the intrinsic mechanism of each process. Electron polarization is the deformation of the electron cloud which occurs at high frequencies near 10^{15} Hz. Atomic polarization is the reorientation of an atom or a group of atoms. This process occurs at approximately $10^{12} - 10^{14}$ Hz. Dipole relaxation describes the rotation and orientation of a molecule with permanent or induced dipoles. Dipole relaxation is impeded by thermal motion and viscosity. The frequency range is typically in the radio frequencies (MHz) and below. Ionic polarization is the translation of ions in the presence of an applied electric field. Ionic polarization is predominately at very low frequencies and it only presents dielectric losses to the system. A special case of ionic polarization is interfacial polarization or so called "Maxwell-Wagner" effect, in which the

ions are accumulated at the boundary between two layers with different dielectric constant. Electrode polarization is a result from charge carriers being blocked at the electrodes.

Due to the stochastic thermal fluctuation of the molecules, the functions defined above fluctuate around their mean values and the auto correlation function of the polarization fluctuation ΔP is defined as:

$$\Phi(\tau) = \frac{\langle \Delta P(\tau) \Delta P(0) \rangle}{\langle \Delta P^2 \rangle} \tag{2.7}$$

The simplest case is a Debye relaxation which assumed that the change of the polarization is proportional to its actual value:

$$\frac{dP(t)}{dt} = -\frac{1}{\tau_D} P(t) \tag{2.8}$$

Where τ_D is a characteristic relaxation time. Combined with Eq. 2.7, the correlation function becomes:

$$\Phi(\tau) = \exp(-\frac{t}{\tau_D}) \tag{2.9}$$

And the complex dielectric function becomes:

$$\varepsilon^* = \varepsilon_\infty + \frac{\Delta\varepsilon}{1 + i\omega\tau_D} \tag{2.10}$$

Fig.2.1a shows a representative spectrum for a Debye relaxation process. The loss peak maximum position is related to the Debye relaxation time τ_D by $\omega_p = 2\pi f_p = \frac{1}{\tau_D}$.
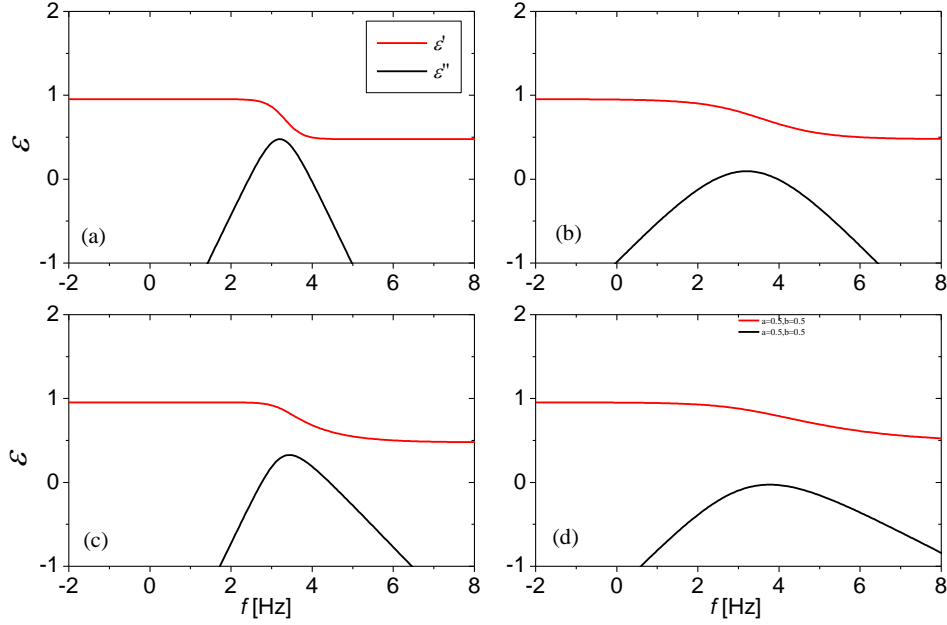
Figure 2.1. Real $\log\varepsilon'$ and imaginary part $\log\varepsilon''$ of the complex dielectric function vs normalized frequency for (a) a Debye relaxation process, τ=0.0001s $\Delta\varepsilon$=6 α=1 β=1 ε_∞=3; (b) α=0.5 (c) β=0.5 (d) α=0.5 β=0.5. The rest of the parameters for (b), (c), (d) are same as those in (a).

However, in reality, the majority cases are not Debye relaxation. Those relaxations are much broader than the Debye spectrum and are usually asymmetric. Therefore, several empirical model functions have been developed to describe the spectra.

Cole/Cole-function (CC):

$$\varepsilon^*(\omega) = \varepsilon_\infty + \frac{\Delta\varepsilon}{1 + (i\omega\tau_{CC})^\alpha} \tag{2.11}$$

in which α describes the symmetric broadening of the peak.

Cole/Davidson-function (CD):

$$\varepsilon^*(\omega) = \varepsilon_\infty + \frac{\Delta\varepsilon}{(1 + i\omega\tau_{CD})^\beta} \qquad (2.12)$$

in which β describes the broadening on the high frequency side.

A combination of CC and CD was introduced by Havriliak and Negami, and the model has the function:

$$\varepsilon^*(\omega) = \varepsilon_\infty + \frac{\Delta\varepsilon}{(1 + (i\omega\tau_{CD})^\alpha)^\beta} \qquad (2.13)$$

Fig.2.1b, 1c, 1d gives a representative spectrum for 3 different processes simulated using eq.2.11-2.13, respectively.

The position of peak maximum depends on both the shape parameters:

$$\tau_{max} = \tau_{HN} \left(\sin\frac{\alpha\beta\pi}{2 + 2\beta} \right)^{1/\alpha} \left(\sin\frac{\alpha\pi}{2 + 2\beta} \right)^{-1/\alpha} \qquad (2.14)$$

Kohlrausch/ Williams/ Watts (KWW) function is always used to describe the non-Debye relaxation behavior in the time domain.

$$\varepsilon(t) - \varepsilon_\infty = \Delta\varepsilon \left[1 - exp\left(-\left(\frac{t}{\tau_{KWW}}\right)^{\beta_{KWW}} \right) \right] \qquad (2.15)$$

in which β_{KWW} is the stretched parameter and τ_{KWW} is the corresponding relaxation time.

2.1.2 Dipoles in Polymers

Polymers can be classified into three different categories based on the dipole moment direction with respect to the polymer backbone (Fig.2.2). Polymers with dipole moments parallel to the backbone are named as type A polymers. Examples are poly(cis-1,4-isoprene),
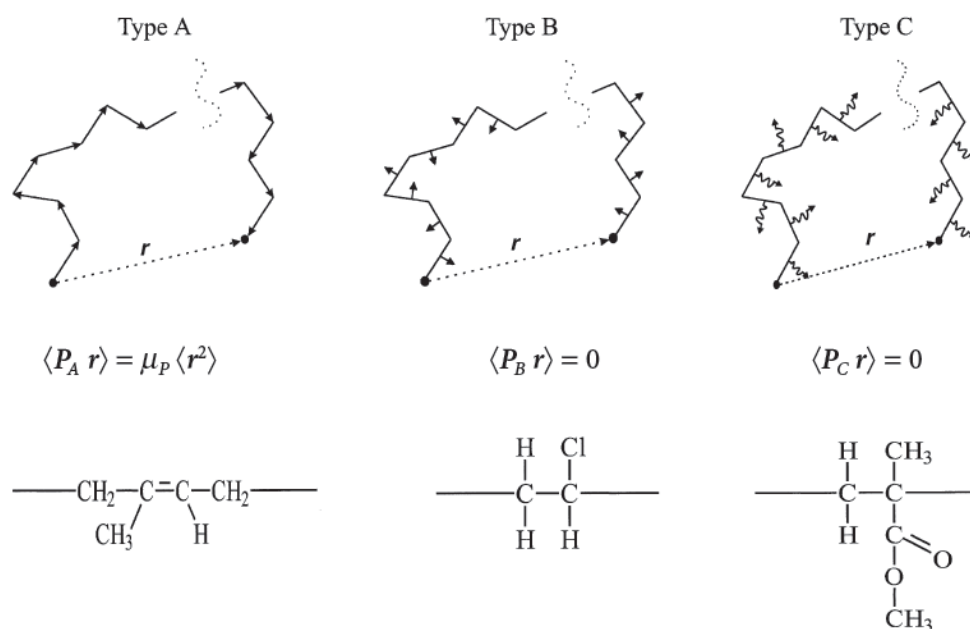
Figure 2.2. The different geometric possibilities for the location of molecular dipoles with respect to the polymer chain. Examples: Type A poly(cis-1,4-isoprene), type B poly(vinyl chloride), type C poly(methyl methacrylate). (ref.[87])

poly(ethylene oxide), poly(propylene glycol). For type B polymer, the dipole moment is

perpendicular to the backbone of the polymer. Examples are poly(vinyl-chloride). The last

category named as type C polymers includes polymers such as poly(methyl methacrylate) in

which the dipole moment is located within the side chain. As for type C polymers, the side

chain has to be flexible enough to orient under the external electric field. Usually, a polymer

is not solely type A polymer. A good example is poly(propylene glycol) which has dipole

moments both parallel and perpendicular to the backbone. The overall polarization is the sum

of dipole density in a unit volume V.

$$P = \frac{1}{V} \sum_{\text{chain}} \sum_{\text{repeating unit}} \mu_i \qquad (2.16)$$

In which μ_i is the dipole moment of the repeating unit *i*.

2.1.3 Analysis of the Dielectric Spectrum

A representative dielectric spectra of PPG with a molecular weight of 425 g/mol mixed with LiClO$_4$ (O:Li=30) at T= -40°C are shown in Fig.2.3.

There are three major components from high to low frequencies: (1) a dielectric relaxation process labeled as α relaxation (2) dc conductivity in the intermediate-frequency region of ε'' and (3) ε' and ε'' in the low-frequency region affected by the electrode polarization effect.

Molecular relaxation is originated from rotation and vibration of molecular dipoles. If the frequency of the molecular dipole orientation corresponds to the frequency of the applied electric field, a peak in the imaginary part and a step-like decrease of the real part would show up with the increase of frequency. This pattern is usually fitted by HN function (Eq. 2.13), and by analyzing the pattern, parameters about the relaxation process can be obtained.

Conductivity shows as an increase of the imaginary part with decreasing frequency. Therefore, in dielectric spectra of materials with high dc conductivity, relaxation peaks in $\varepsilon''(\omega)$ might be completely hidden by the conductivity. On the contrary, the conductivity does not contribute to the real part of permittivity. Thus, the derivative spectra: $\varepsilon''_{\text{der}} = (-\pi/2)\partial\varepsilon'/\partial\ln\omega$, based on the Kramers-Kronig relations is often used to assist the

data analysis.[88, 89] The relaxation process is revealed in the derivative spectrum (Fig.2.3 green). The corresponding relaxation time τ is estimated from the maximum in the derivative of the real part of permittivity ε': $\varepsilon''_{der} = (-\frac{\pi}{2})\frac{\partial \varepsilon'}{\partial \ln f}$, and $\tau = 1/2\pi f_{max}$, as f_{max} being the frequency corresponding to the peak maximum in the derivative spectra. Another way to reveal the molecular relaxation process is to subtract conductivity contribution from the spectrum based on the equivalence $\sigma' = \frac{\varepsilon''}{\varepsilon_0 \omega}$.
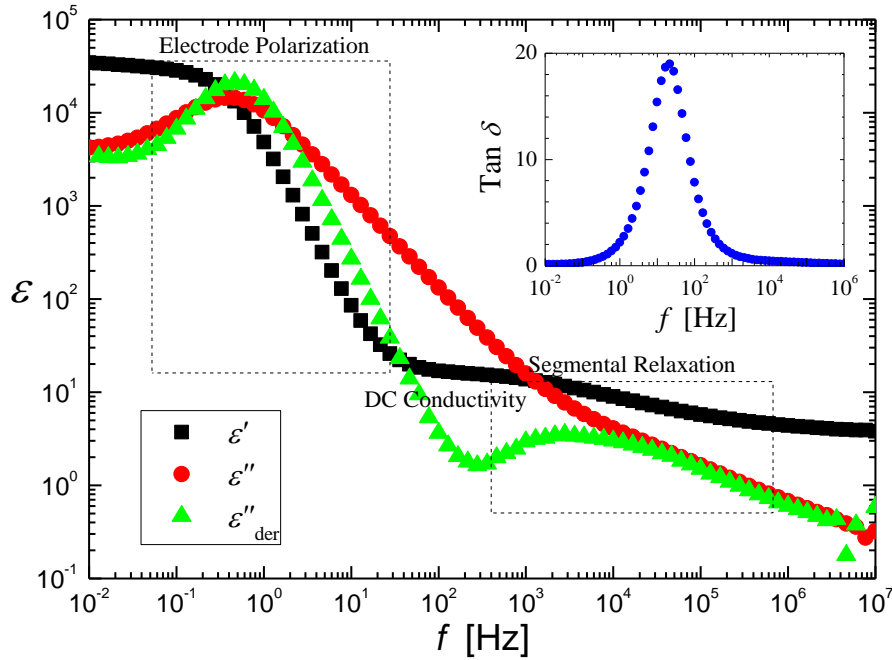
Figure 2.3. Dielectric spectra of PPG with a molecular weight of 425 g/mol with LiClO$_4$ (O:Li=30) at T = -40°C. There are three major components: (1) a dielectric relaxation peak due to segmental relaxation, revealed in ε''_{der}; (2) DC conductivity in the intermediate-frequency region of ε'', and (3) the electrode polarization effect that appears as the sharp increase of ε' and ε''_{der} in the low-frequency region.

The electrode polarization effect is prominent at low frequencies. It will be discussed in details later in this chapter.

To account for all processes mentioned, the complex permittivity spectra can be modeled by the superposition of several Havriliak-Negami (HN) functions, a dc conductivity term and an EP term:

$$\varepsilon^*(\omega) = \varepsilon_\infty + \sum \frac{\Delta\varepsilon}{[1 + (i\omega\tau_{HN})^\alpha]^\beta} + i\frac{\sigma}{\varepsilon_0\omega} + A\omega^{-n} \tag{2.17}$$

Here, $\omega = 2\pi f$ is the angular frequency, ε_∞ represents the value of $\varepsilon'(\omega)$ at infinite frequency, $\Delta\varepsilon$ is the dielectric relaxation strength, τ_{HN} is the Havriliak-Negami relaxation time, α, β are the shape parameters, σ is the dc conductivity, and n is related to the slope of EP's high frequency tail, A is related to the amplitude of EP. Although such a simple treatment of EP by addition of $A\omega^{-n}$ can only describe the EP process at its high frequency side, the inclusion of $A\omega^{-n}$ is helpful for the accurate fitting of the main relaxation process.

The relaxation time τ_{max} is related to the Havriliak-Negami relaxation time τ_{HN}, the shape parameters α and β by Eq. 2.14.

2.1.4 Electrode Polarization

Cations and anions flow to opposite directions in the presence of applied electric field. Once they reach the electrodes, they will accumulate on the electrodes since they are too big to get in the electrodes as electrons do, and form the so-called "electrical double layer" (Electrical DL) (Fig.2.4). This is called the electrode polarization effect (EP effect).
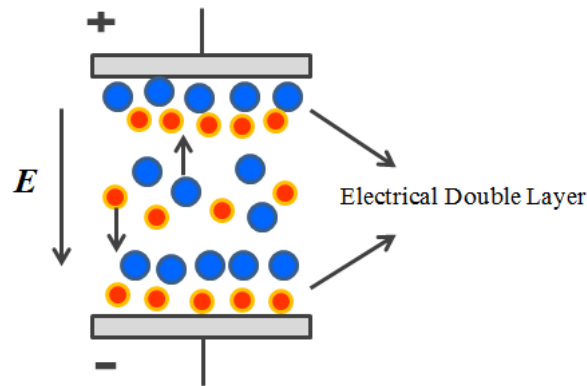
Figure 2.4. Electrode Polarization as ions accumulated at the electrodes, forming electrical double layer.

The EP effect is prominent at low frequencies since it takes some time for ions to reach the electrodes and form the Electrical DL. It appears as a sharp increase of the permittivity response in the dielectric spectrum and fully develops into a Debye like process as frequency decreases (Fig.2.3).

Apparently, the EP effect adds difficulties to the analysis of the spectrum since its dielectric response is so large that it affects the shape, position of other relaxation processes and even covers other relaxation processes. Therefore, it is desirable to reduce the EP effect. First, it would take longer time for the Electrical DL to form if the sample is thicker. At the same time, the impedance resulted from Electrical DL does not depend on the sample thickness. Thus, the employment of thicker sample can move the EP effect to lower frequencies plus the ratio of the electrical DL impedance to the sample impedance would be improved. Secondly, impurities can add extra ions to the sample, thus a thorough cleaning of

the electrodes can help remove the EP effect resulted from unwanted ions. The third method requires two measurements, in which the sample thickness is doubled in the second measurement. With a doubled sample thickness, the impedance of the sample will be doubled while that of the electrical DL will not change. As a result, impedance resulted from the electrical DL can be canceled out after simple math treatment from two sets of data. It should be emphasized, that the third method only works approximately.

The analysis of the EP effect observed by dielectric spectroscopy provides an indirect way to deduce the concentration of free ions and ion diffusivity in ion conductors. It is worth noting that dielectric spectroscopy is capable of discriminating separated ion pair from free ions, because the amplitude of the dielectric response is proportional to the square of the dipole moment of the molecule and the magnitude of the dipole moment is related to the distance between the two ions. On the other hand, a problem with vibrational spectroscopy is that it cannot separate the signals from separated ion pair from that of free ions, since the formation of separated pair provides insufficient change to be measurable by the vibrational spectroscopy.

The analysis of the electrode polarization is based on MacDonald model [90-92] and Trukhan's model [93-95]. For simplicity, let's consider a polymer electrolyte made from salt AB, where A^+ and B^- are monovalent ions with the same mobility μ. The electrode polarization in polymer electrolytes typically can be modeled by a Debye relaxation as:

$$\varepsilon_{EP}^* = \varepsilon' - i\varepsilon'' = \varepsilon_R + \frac{\Delta\varepsilon_{EP}}{1+i\omega\tau_{EP}}, \qquad (2.18)$$

where $\varepsilon_{EP}{}^*$ is the complex permittivity, $\varepsilon_R = \varepsilon_r\varepsilon_0$ is the dielectric constant of the bulk electrolyte without the EP effect, $\Delta\varepsilon_{EP} = (\frac{L}{2L_D} - 1)\varepsilon_R$ in which L_D is the Debye length.

τ_{EP} is the characteristic relaxation time, and it is defined by the bulk resistance R and the interfacial layer capacitance C_{EP} through $\tau_{EP} = RC_{EP}$ and $C_{EP} = \varepsilon_0\varepsilon_R\frac{A}{2L_D}$ with A being the surface area of the electrode.

The free ion concentration (n) or number density, which is the sum of the number densities of free cations (n_+) and anions (n_-), can be related to the Debye length by the following equation:

$$L_D = \sqrt{\frac{\varepsilon_0\varepsilon_R k_B T}{(n_+ + n_-)q^2}} = \sqrt{\frac{\varepsilon_0\varepsilon_R k_B T}{nq^2}} \qquad (2.19)$$

According to the Trukhan model[93-95], the ion diffusivity D can be evaluated from the ω_{max}, and the $(\tan\delta)_{max}$ associated with the electrode polarization, and the sample thickness L(Fig.2. 5c):

$$D = \frac{2\pi f_{max} L^2}{32(\tan\delta)_{max}{}^3} \qquad (2.20)$$

The free ion number density can be obtained from the dc conductivity and ion diffusivity according to the definition of dc conductivity through the Einstein relation,

$$n = \frac{\sigma k_B T}{Dq^2} \qquad (2.21)$$

A representative dielectric spectrum of NaCl–(glycerol-H_2O) is shown in Fig.2.5, where the ε' ε'' and $\tan\delta$ are plotted as a function of frequency. On the high-frequency side,

the real part of permittivity is independent of frequency while the imaginary part increases

with decreasing frequency as $\varepsilon'' \sim f^{-1}$, exhibiting the normal behavior of dc conduction. On the

low-frequency side, the complex permittivity shows a Debye-like shape, due to the electrode

polarization effect. The corresponding f_{max} and $(\tan\delta)_{max}$ can be used to analyze the free-ion

number density and diffusivity using the method outlined above. One can define the onset of

EP as the minimum in σ'' and the "full development" of EP as the maximum in σ''.

The solid lines in Fig.2.5 represent the fits using eq.2.18. The shape of the spectrum

can be clearly approximated by the Debye function up to the "full development" of electrode

polarization. In reality, no electrodes can be perfectly blocking, even in the case of gold. As a

result, substantial deviation from eq.2.18 occurs at low frequencies. In order to describe the

spectra in the whole frequency region, more sophisticated models[96, 97] have to be considered.

However, here the low-frequency response (below the frequency of σ'' maximum) does not

affect the analysis.

In the earlier studies by Colby and coworkers[92, 98], MacDonald's model[90, 91] were used

to calculate the diffusivity from the same EP effect. These two models are actually equivalent

for a Debye-like EP process. According to the MacDonald model[90-92], the dielectric constant

ε_R and the relaxation time τ_{EP} are related to the ion concentration p, the ion mobility μ, and the

sample thickness L by the following equations:

$$\varepsilon_{\infty,EP} = M\varepsilon_R \qquad (2.22)$$
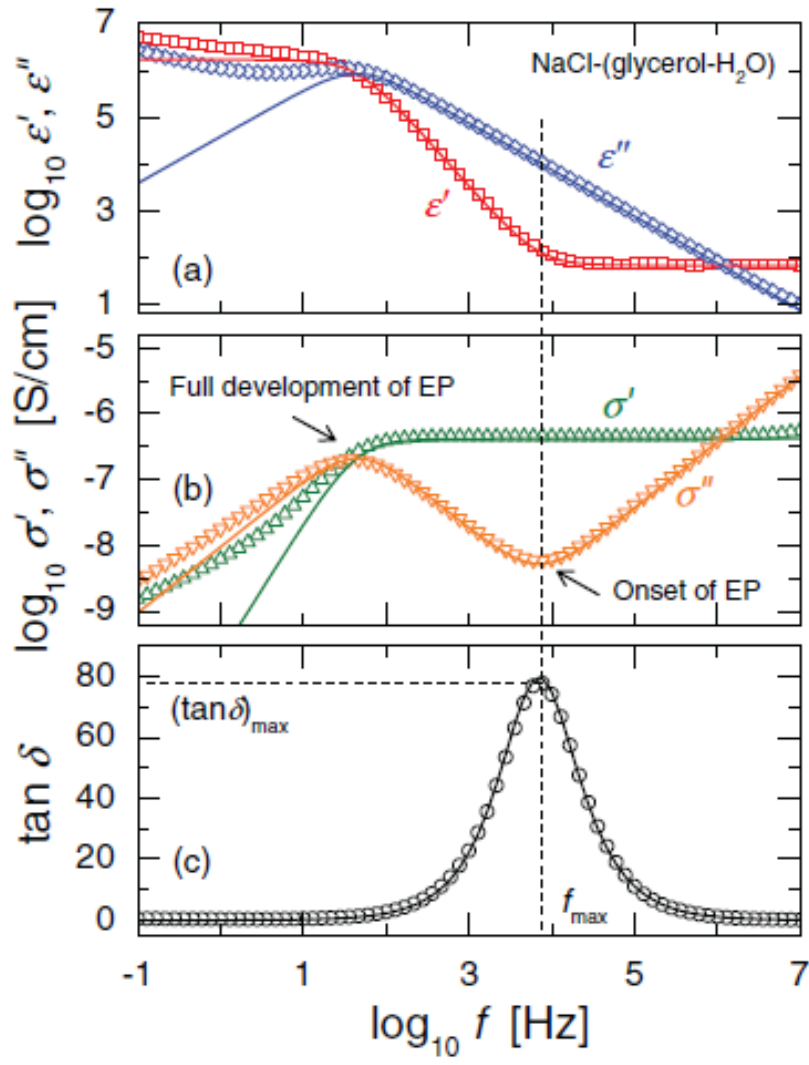
Figure 2.5. Dielectric spectrum of NaCl–(glycerol-H₂O) at -5 °C. (a) Complex permittivity. (b) Complex conductivity. (c) Tanδ. Here, the main "relaxation" is due to electrode polarization. The onset and full development of electrode polarization are indicated by the arrows. (ref.[99])

$$\tau_{EP} = M\tau \tag{2.23}$$

where τ is the relaxation time defined by the ionic conductivity:

$$\tau = \frac{\varepsilon_0 \varepsilon_r}{\sigma_0} = \frac{\varepsilon_R}{pq\mu} \tag{2.24}$$

and M is defined as the ratio of $L/2$ and the Debye length:

$$M = \frac{L}{2L_D} = \frac{L}{2}\sqrt{\frac{pq^2}{\varepsilon_R k_B T}} \tag{2.25}$$

The ion diffusion coefficient D can be calculated by combining eqs. 2.22– 2.25:

$$D = \frac{\mu k_B T}{q} = \frac{\varepsilon_R k_B T}{pq^2 \tau} = \frac{L^2}{4M\tau_{EP}} = \frac{L^2 \varepsilon_R}{4(\varepsilon_R + \Delta\varepsilon_{EP})\tau_{EP}} \tag{2.26}$$

Notice that under our assumption of a Debye relaxation, the ω_{max}, and the $(\tan\delta)_{max}$ can be expressed as functions of ε_R, $\Delta\varepsilon_{EP}$, and τ_{EP}:

$$\omega_{max} = \sqrt{\frac{\varepsilon_R + \Delta\varepsilon_{EP}}{\varepsilon_R}} \cdot \frac{1}{\tau_{EP}} \tag{2.27}$$

$$(\tan\delta)_{max} = \frac{\Delta\varepsilon_{EP}}{2(\varepsilon_R + \Delta\varepsilon_{EP})}\sqrt{\frac{\varepsilon_R + \Delta\varepsilon_{EP}}{\varepsilon_R}} \tag{2.28}$$

After substituting Eqs. (27) and (28) into Eq. (26), one obtains:

$$D = \frac{L^2 \varepsilon_R (\varepsilon_R + \Delta\varepsilon_{EP})^2}{4\Delta\varepsilon_{EP}^3 \tau_{EP}} \approx \frac{L^2 \varepsilon_R}{4(\varepsilon_R + \Delta\varepsilon_{EP})\tau_{EP}} \tag{2.29}$$

which is approximately equal to Eq. (2.20) when $\Delta\varepsilon_{EP} \gg \varepsilon_R$. For the electrode polarization effect, this condition will be always satisfied in practice. Consequently, analyses based on the

MacDonald model and the Trukhan model will yield the same result for ion concentration and diffusivity.

Fig.2.6a presents the free-ion number density, determined from the EP analysis, as a function of $1000/T$ for all the samples in this study. As a first observation, the free-ion number density n decreases with decrease of temperature in all samples except LiCl-H_2O, where n is almost a constant. The temperature dependence of ion number density can be described by the Arrhenius equation $n = n_0\exp(-E_{dis}/k_BT)$. Fig.2. 6(b) shows the temperature dependence of free-ion fraction n/n_{tot}, where the Arrhenius fits are extrapolated to infinitely high temperature, i.e., $1000/T = 0$. The total ion number density n_{tot} is calculated from the total amount of salt in the solution, under the assumption of complete dissociation. If the electrode polarization analysis could indeed quantitatively capture the free-ion concentration, one would expect $\log10(n/n_{tot})$ should be zero at $1000/T = 0$. However, such agreement is not found in all the other samples.

In work done by Wang et al.[99], it was proposed that the true free-ion concentration density can be corrected using a correction factor based on the assumption that all salts will fully dissociate at infinite high temperature. The free-ion concentration n calculated from Macdonald-Trukhan model was rescaled by a factor of $\frac{n_{tot}}{n_0}$.

$$\tilde{n} = \frac{n_{tot}}{n_0}n = \frac{n_{tot}}{n_0}\left[n_0 \exp\left(-\frac{E_{dis}}{k_BT}\right)\right] = n_{tot}\exp(-\frac{E_{dis}}{k_BT}) \tag{2.30}$$

n_{tot} is the total ion number density at complete dissociation, n_0 is the parameter obtained from Arrhenius fitting of the original ion number density n. The corrected diffusivity was rescaled by $\frac{n_0}{n_{tot}}$.
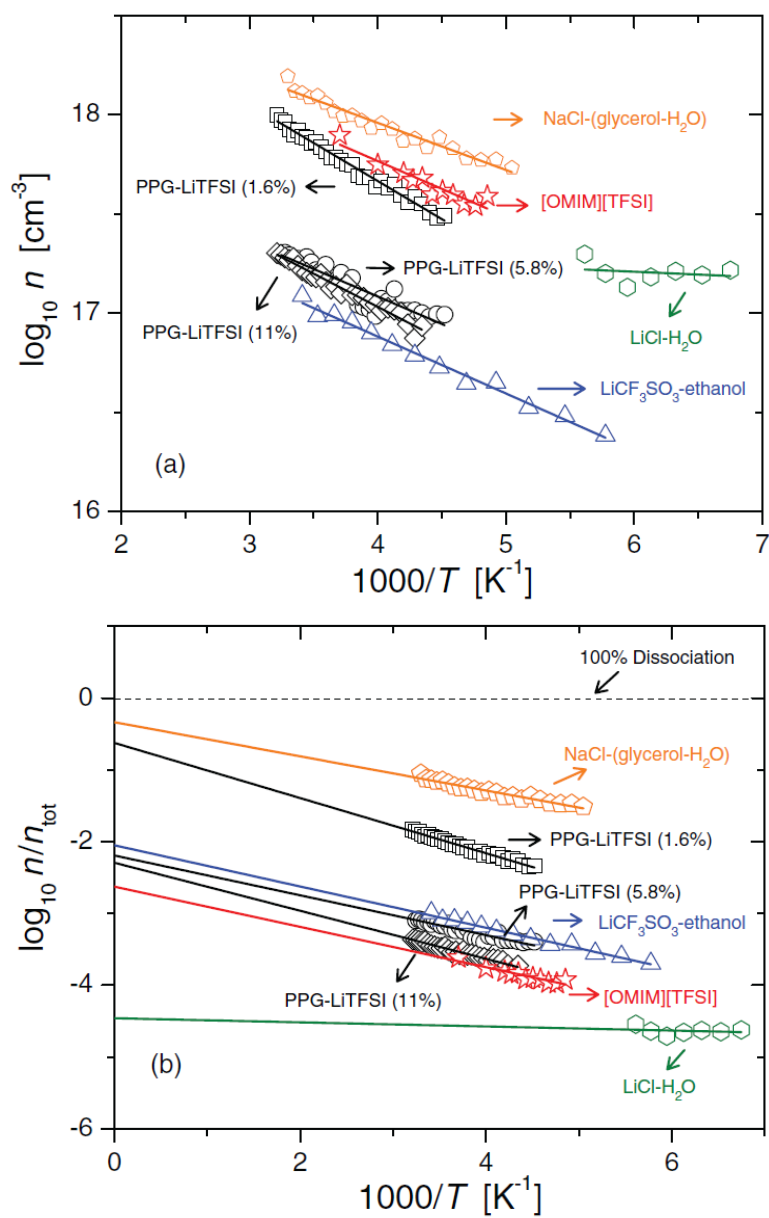
Figure 2.6. Temperature dependence of (a) free-ion number density n evaluated from the electrode polarization effect using the Macdonald-Trukhan model. Solid lines denote Arrhenius fits. The horizontal dashed line indicates the limit of 100 % dissociation.

$$\tilde{D} = D\frac{n_0}{n_{tot}} \tag{2.31}$$

with $\tilde{D}$ being the corrected diffusivity and D the original diffusivity.

The modified ion diffusivity is in reasonable agreement with the values measured by pulse-field-gradient NMR.[99]

2.1.5 Dielectric Measurement Set-up

Broadband dielectric measurements were performed using Novocontrol Concept 80 system, which includes Alpha-A impedance analyzer, ZGS active sample cell interface, and Quatro Cryosystem temperature control unit. The samples were placed between two gold-plated electrodes separated by a Teflon spacer. (Fig.2.7) The use of Teflon spacer is to ensure that the geometry of sample stays the same through the experiment under changed temperatures. Measurements were made in the frequency range of $10^{-2} - 10^7$ Hz. Fig.2.8 illustrates the application of a sinusoidal electric field. There is a phase lag between the applied electric field and the resulting current. Thus the impedance is a complex number. Impedance Z^* is measured as $Z^* = U^*/I^*$, capacitance $C^* = 1/(i\omega Z^*)$ and $\varepsilon^* = \frac{C^*}{C_0}$.
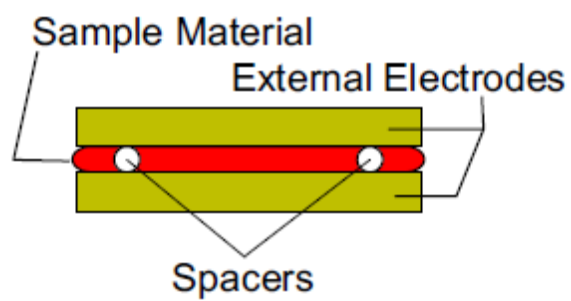
Figure 2.7. Sample cell set up.
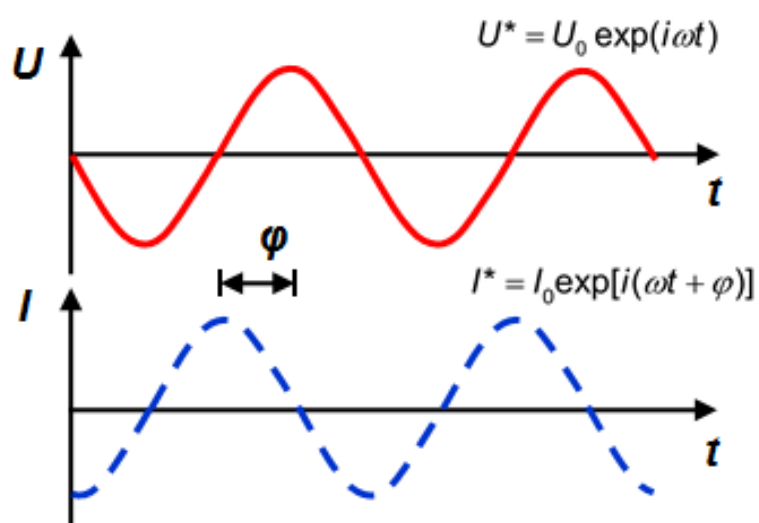
Figure 2.8. A schematic representation of applied voltage and the current in a dielectric spectrometer circuit. φ is the phase difference.

2.2 Differential Scanning Calorimetry (DSC)

2.2.1 Principles of Standard DSC

Differential Scanning Calorimetry is used to study the thermal transitions, e.g. melting, crystallization, and glass transition of a material. In a typical DSC measurement, one pan has sample in it and the other pan is always empty as the reference. During the measurement, both pans are heated at the same specific rate which is determined by the operator. Since one pan has sample the other pan doesn't, in order to keep the same heating rate, the sample pan needs more heat than the reference pan. The instrument measures how much more heat it has to supply for the sample pan than the reference pan. The quantity that describes how much heat Q a sample has to take for it to increase temperature by one degree is called heat capacity $C_p = Q/\Delta T$, in which ΔT is the change of temperature.

Fig.2.9 illustrates the typical curve for the DSC measurement result with an example of Polyethylene Terephthalate (PET). The heat capacity of PET is higher when the temperature is above the glass transition temperature T_g than it is below T_g, since above T_g the molecules have more accessible conformational states, thus higher entropy. Therefore, the glass transition shows as a step on the DSC curve, indicating an increase of the heat flow as PET is heated crossing the glass transition. Crystallization shows up as a peak representing a drop of heat flow as the sample crystalizes since crystallization is an exothermic process. On the other hand, melting process requires heat (endothermic), thus it shows up as a peak indicating an increase of heat flow. Usually, the measurement is repeated several times, and the average values are used. T_g is determined as the mid-point of the incline. Crystallization temperature

and melting temperature are determined as temperatures corresponding to the peak maximum. Not all materials have those features and the same material might have different curves depending on the measurement conditions, such as sample size, heating rate and pre-treatment condition.
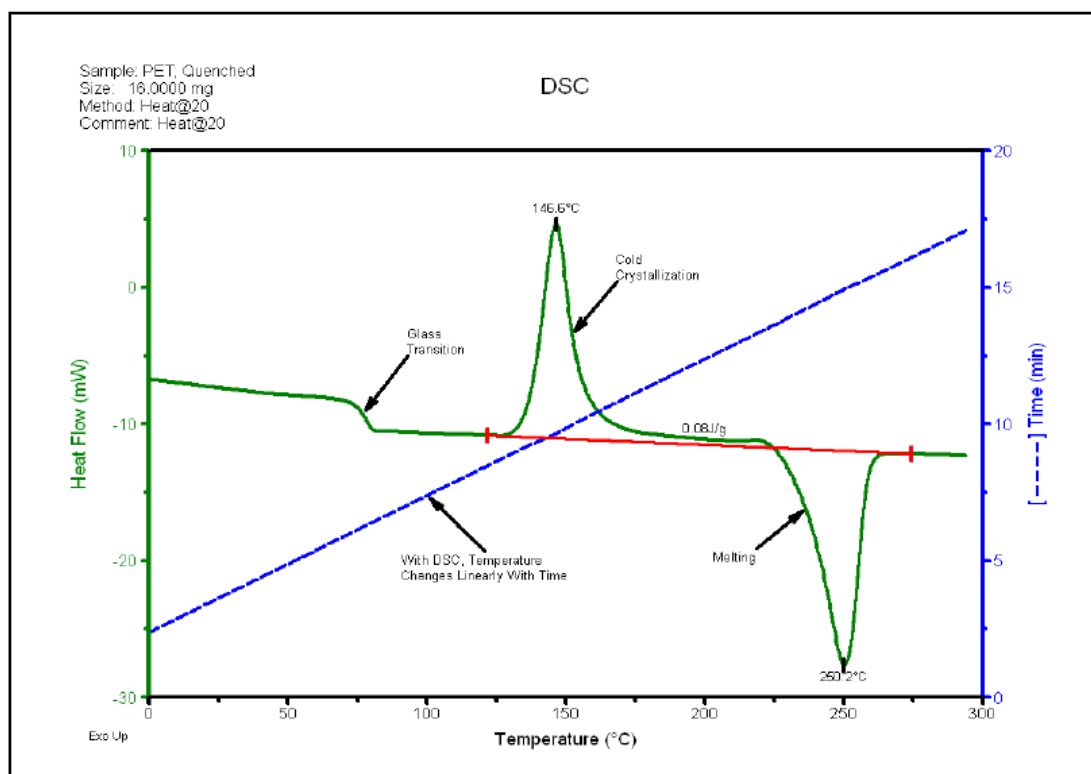
Figure 2.9. Representative curve of DSC. The y-axis shows the heat flow and the x-axis shows the temperature. As temperature increase, the sample PET undergoes glass transition, crystallization and melting. (ref.[100])

2.2.2 Advantages and Disadvantages of Standard DSC

The standard DSC is a relatively simple and fast technique. Samples are encapsulated in metal pans and taken to the heating/ cooling chamber by the auto-sampler. With a typical heating rate of 10°C/min, a measurement with temperature range of 200°C could be done in less than thirty minutes with isothermal steps. However, the standard DSC has limitations especially when the different processes overlap with each other or the transition is very small. It measures the total heat flow and cannot separate different processes if they overlap. Moreover, resolution will be sacrificed if the measurement is done with higher heating rate in order to amplify any low energy transitions.

2.2.3 Principles of Temperature Modulated-DSC

A more sophisticated technique with the name "modulated-DSC" has been developed based on the standard DSC.[100] In a standard DSC measurement, a single heating rate is applied to the pans. While in a Modulated DSC measurement, two simultaneous heating rates are applied to the pans. One of them is a linear heating rate which provides the same information as standard DSC, while the other is a sinusoidal (modulated) heating rate which can distinguish processes based on their different response on changing heating rate. The heat flow resulted from the linear heating rate is called the total heat flow, and heat flow obtained from the modulated heating rate is called the reversing heat flow. Heat flow that does not respond to the changing heating rate is determined by subtracting the reversing heat flow from the total heat flow, and is called non-reversing heat flow. The non-reversing heat flow includes information of kinetic processes such as crystallization.

The principle of modulated-DSC can be described by Eq. 2.32.

$$\frac{dH}{dt} = C_p \frac{dT}{dt} + f(T,t) \qquad (2.32)$$

in which $\frac{dH}{dt}$ is the total heat flow, C_p is the heat capacity, $\frac{dT}{dt}$ is the measured heating rate including the linear and modulated components, $C_p \frac{dT}{dt}$ is the reversing heat flow and $f(T,t)$ is the non-reversing heat flow.

The MDSC divides the total heat flow into two individual components, the reversing heat flow which contains information about processes such as glass transition, melting and the non-reversing heat flow which includes kinetic processes such as crystallization (Fig.2.10). Although a MDSC experiment takes longer time than a traditional DSC measurement, MDSC can distinguish processes which might overlap in a standard DSC measurement. The average heating rate in a MDSC measurement is usually smaller, typically in the range from 1 to 10 °C/min. The temperature modulation period is set between 30 and 100 seconds, and the temperature modulation amplitude is typically in the range of ± 0.1 to 2.0 °C.

2.3 Rheology

2.3.1 Principles of Rheology Measurement

Polymers are viscoelastic, i.e. they behave like viscous liquid or elastic solid depending on the time scale of the disturbing force. If the time for the deformation is short, the energy will be stored and recovered. In this case, the polymer can release the deformation, behaving like an elastic solid. If the deformation is carried out for an extended time, the
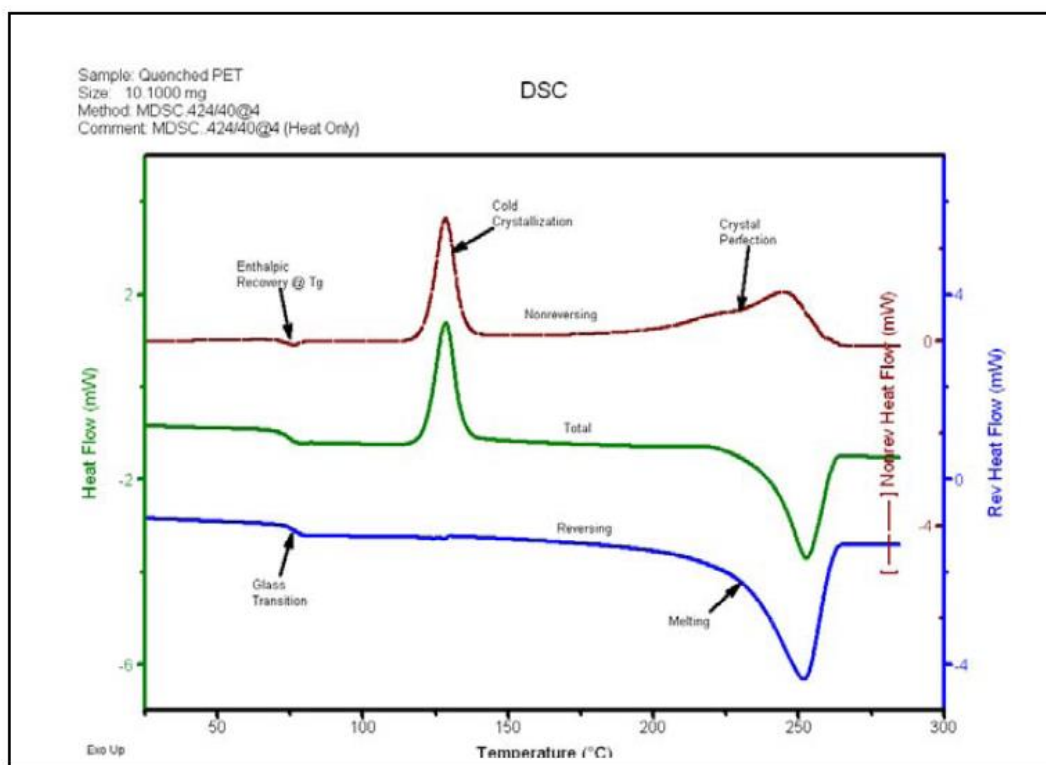
Figure 2.10. The total heat flow is shown in green which is equivalent to standard DSC. The reversing heat flow is shown in blue which contains information about glass transition and melting. Kinetic processes such as enthalpic recovery and crystallization, crystal perfection are presented in the brown curve which is the non-reversing heat flow. (ref.[100])

polymer will have enough time to fully release the initial stress/ strain and the energy is dissipated by friction. In this way, the polymer becomes a viscous liquid.

There are several experiments that have been commonly employed to study the viscoelasticity of polymers. In a creep test, a stress is applied and held constantly, the resulting strain is monitored as a function of time. According to the Maxwell model, in which an ideal Hookean spring is connected in series with an ideal Newtonian dashpot, the compliance of the system can be described as:

$$J(t) = \frac{\gamma(t)}{\sigma_0} = \frac{1}{\hat{G}} + \frac{1}{\hat{\eta}} t \tag{2.33}$$

in which $\gamma(t)$ is the strain, σ_0 is the stress, $\hat{G}$ is the spring constant, $\hat{\eta}$ is the viscosity of the dashpot.

In an oscillatory test, the sample is disturbed with a sinusoidal time-varying strain $\gamma^* = \gamma_0 \exp(i\omega t)$, resulting in a dynamic modulus G^*. The dynamic modulus G^* contains a storage modulus G' and a loss modulus G''.

The storage modulus reflects the polymer's elastic property and the loss modulus corresponds to the viscous property.

$$\frac{\sigma(t)}{\gamma_0} = = G' \sin \omega t + G'' \cos \omega t \tag{2.34}$$
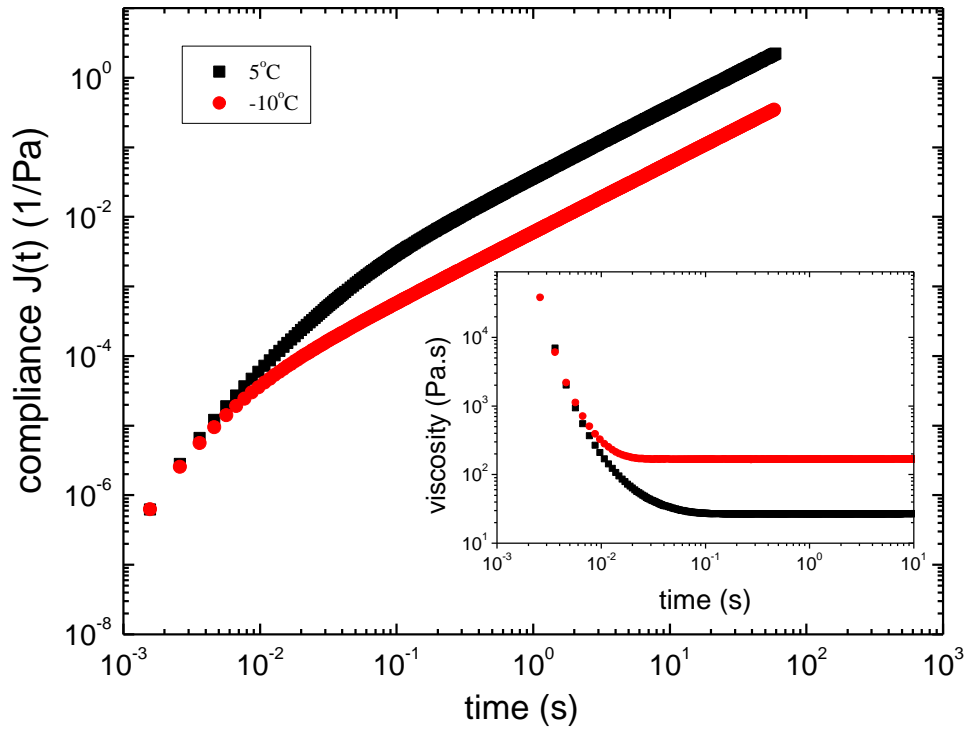
Figure 2.11. Compliance result of PPG-LiCF$_3$SO$_3$ (O:Li-30) at two temperatures 5°C, 10°C as a function of time. Inset: viscosity result as a function of time.

2.3.2 Time Temperature Superposition

In contrast to the broadband dielectric spectroscopy, normal rheometers only cover a relatively narrow frequency range, i.e. a range of three or four decades of frequency. It is desirable to extend the frequencies range studied by rheometers. This is achieved by applying the time-temperature superposition (TTS) principle.[101] TTS only works if all relaxation processes in the probed frequency range has the same temperature dependence. Generally, the dynamic modulus G′ and G″ or creep compliance J are measured at various temperatures. One

of these is taken as the reference temperature T, and all the other are shifted horizontally by the shift factor a_T and vertically by the shift factor b_T (usually equals unity) to overlap with data measured at adjacent temperatures. A master curve can be generated corresponding to the reference temperature which covers many decades of frequency. The data measured at the reference temperature are not shifted. The shift factor a_T should obey the empirical Williams-Landel-Ferry equation[102]:

$$\log a_T = -\frac{C_1(T - T_r)}{C_2 + (T - T_r)}$$ (2.35)

in which T is the reference temperature chosen to construct the master curve, and C_1 and C_2 are empirical constants.

In this way, the principle of TTS makes it possible to predict the behavior of a polymer at a wider frequency range. It offers a solution to study properties of a polymer at temperatures or time scales beyond the rheometer's capability. As mentioned earlier, the TTS only works if all relaxation processes in the probed time scale has the same temperature dependence. Failure of TTS analysis has been reported at some circumstances.[103, 104] For example, chain and segmental relaxation process are governed by different friction mechanisms, which has led to the failure of TTS in polystyrene.[103]
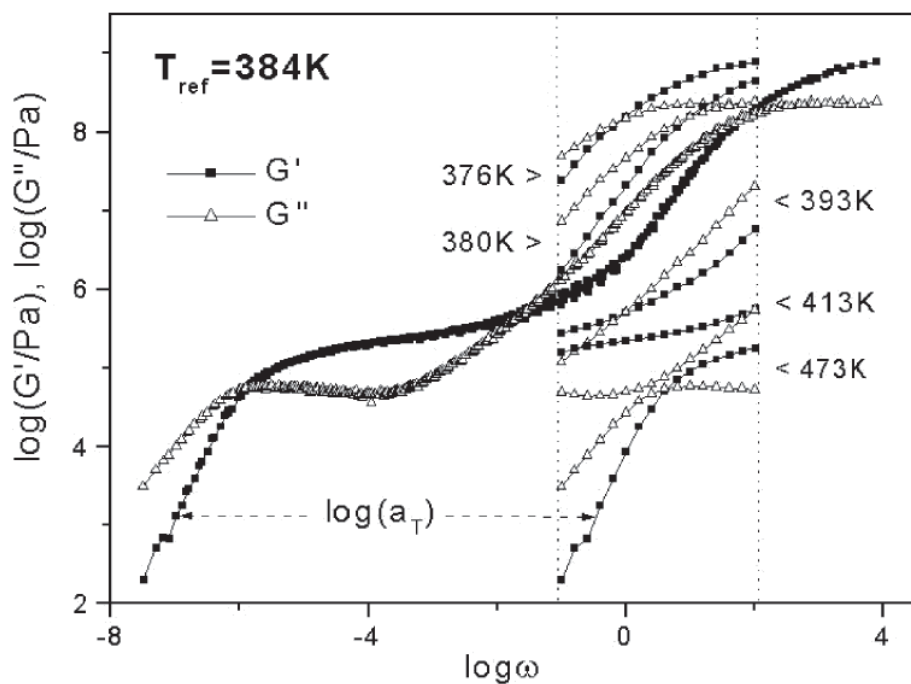
Figure 2.12 Illustration of a construction of a master frequency dependencies of **G′** and **G″** for a polystyrene melt (Mw = 200,000) taken as an example. (ref.[87])

2.3.3 Measurement Set-up

Experiments were performed at an AR2000ex rheometer from TA instrument. Two different types of measurements were carried out. They are creep and small amplitude oscillation shear measurements. A parallel plate geometry was employed. The diameter of the plates was varied according to the type of the measurement and sample properties. Fig.2.13 shows the geometry of a parallel plate system, in which two circular flat plates are in parallel, with the sample sandwiched between two plates. The correct filling of the sample requires a

flat surface of the sample in good contact with the plates and the edge of the sample should

flush with the rim of the plates.
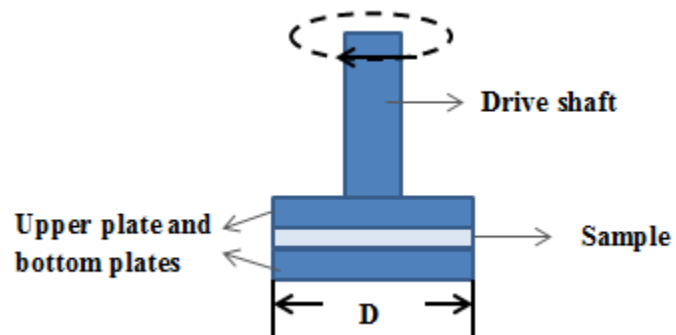
Figure 2.13. Parallel plate measuring system showing correct filling.

CHAPTER III

IONIC CONDUCTIVITY IN MODEL SYSTEM: POLY(PROPYLENE GLYCOL) AND LITHIUM PERCHLORATE MIXTURES

3.1 Introduction

Solid Polymer electrolytes have promising applications in energy storage and electrochemical devices. However, the highest conductivity achieved so far was around 10^{-5} S/cm at room temperature which is not enough for practical applications. Therefore, a complete and thorough understanding of the ion transport mechanism in the polymer electrolytes is highly desirable. It would help reveal the reason for the upper limit conductivity value, and guide the design of future polymer electrolytes to obtain required properties.

Poly(ethylene oxide) (PEO) and poly(propylene glycol) (PPG) were first recognized as promising candidates for polymer electrolytes in the 1970s,[105-107] and since then they have been studied intensively due to their high ability to solvate salts and low glass transition temperatures.[49, 108-117] PEO is prone to form crystalline phase with most of the salts, which makes it an unsatisfactory system for the study of ion transport mechanism.[118-120]

60

Low molecular weight PPGs are typically chosen as an alternative for polymer electrolytes related fundamental studies, since it stays amorphous at the salt concentration studied. Unfortunately, it has been shown, by several different experimental techniques, that the overall amorphous PPG-salt complexes exhibit micro-phase separation over a wide salt concentration range.[116, 121-123] Differential scanning calorimetry (DSC) studies from Vachon *et al.* showed two glass transition temperatures (*Tg*s) in several PPG-salt complexes.[121, 122] It was proposed that ion-rich and ion-depleted phases were formed as a result of the competition between the Li-O binding energy and the long-range Coulombic interactions. Additionally, two segmental relaxations were observed in the dielectric spectroscopy study of PPG-LiClO$_4$,[116] as well as the study of PPG-NaCF$_3$SO$_3$ by photon correlation spectroscopy.[123]

Furthermore, micro-phase separation has been found in several other polymer electrolytes. For example, Yoshida *et al.* reported a split of segmental relaxation in PEO-LiClO$_4$ in its amorphous phase.[114] Zhang and Runt also observed similar behavior in poly(vinyl methyl ether) (PVME)−LiClO$_4$.[89] All these findings suggest that micro-phase separation might widely exist in dry polymer electrolytes, and a systematic experimental study to clarify its physical origin and influence on the ionic transport, therefore, seems necessary. In addition, the molecular weight of many novel ionic conducting polymers is typically on the order of a few kilograms per mole.[28] In this limit, both molecular weight[124] and terminal groups[125, 126] may play an important role in the ionic transport properties of the polymer.

In neat PPG samples (no salts) with terminal −OH groups, Tg varies less than 1% as the molecular weight is reduced from 4000g/mol to 425g/mol. However, Tg dropped a lot

after substitution terminal –OH with –CH$_3$ groups.[127] It was proposed that the terminal OH groups form hydrogen bonding with each other and form "longer" chains. Furthermore, The terminal -OH groups has been reported to play an important role in the dissociation of ions in PPG mixed with Lithium salt. As proposed by Bernson et al.,[128] the cations prefer to coordinate with the end OH groups first rather than the ether oxygen. A series of work done by Ferry also suggested that the OH end groups contributed to the dissociation of ions.[129]

A thorough understanding of model polymer electrolytes can serve to better elucidate the effect of microphase separation, terminal groups on ion transport in solid polymer electrolytes in general.

Pressure is an important experimental variable that strongly influences the dynamics and thermodynamics of glass-forming liquids and polymers. While the dielectric behavior of neat PPG under high pressure has been extensively studied,[126, 130-134] much less attention has been given to PPG-based electrolytes, i.e., PPG-salt mixtures. The existing high-pressure studies are primarily focused on the conductivity aspect,[135-137] little is known about the influence of pressure on micro-phase separation and relaxation of PPG with salts.

A detailed analysis is presented in this chapter, which describes the dielectric behavior of PPG-based electrolytes, by systematically varying the experimental temperature, pressure, polymer molecular weight, and salt concentration. Micro-phase separation has been observed in some of the samples by both differential scanning calorimetry (PPG4000-LiClO$_4$, O:Li = 10, 15) and dielectric spectroscopy (PPG4000-LiClO$_4$, O:Li = 1000, 30, 15, 10); PPG1000-LiClO$_4$, O:Li = 30. The analysis indicates that both the polymer molecular weight and the number of terminal hydroxyl groups contribute to the different thermal and dielectric behavior

of PPG-LiClO$_4$. Using a modified Walden plot analysis, it is demonstrated that the ionic conductivity is controlled by the slow segmental relaxation in samples with micro-phase separation. Regardless of micro-phase separation, all the PPG data using (slow) segmental relaxation fall close to the "ideal" Walden line, exhibiting apparent similarity to other systems with ionic conductivity strongly coupled to structural relaxation, such as aprotic ionic liquids and salt aqueous solutions. In addition, dielectric spectroscopy measurements under high pressure have been performed. The degree of micro-phase separation is found to decrease with increase of pressure. Most importantly, the close relationship between ionic transport and segmental relaxation breaks down at sufficiently high pressure, where the sample (PPG4000-LiClO$_4$, O:Li = 30) starts to resemble superionic conductors.

3.2 Experimental Details

3.2.1 Differential Scanning Calorimetry (DSC)

The samples for DSC measurements were sealed in aluminum hermetic pans. A TA thermal instrument Q1000 was used to record the heat flow. The measurements were performed from 70°C and cooled to -90°C and then heated back to 70°C. The cooling and heating rate was 10°C/min. Each cooling and heating scan was repeated several times to make sure that the results were reproducible. In general, the glass transition temperature (Tg) was taken as the mid-point of the step in the heat flow in the cooling process. However, the cooling scan in our TA Q1000 differential scanning calorimeter typically had poorer sensitivity than the heating scan. As a result, the higher Tg in PPG4000-LiClO$_4$ (O:Li = 15)

and the lower Tg in PPG4000-LiClO$_4$ (O:Li = 10) could not be accurately obtained from the cooling scans and had to be determined from the heating scans.

3.2.2 Broadband Dielectric Spectroscopy (BDS)

Broadband dielectric measurements were performed in the frequency range of 10^{-2} – 10^7 Hz, using a Novocontrol Concept 80 system, which includes an Alpha-A impedance analyzer, a ZGS active sample cell interface, and a Quatro Cryosystem temperature control unit. The samples were placed between two gold-plated electrodes separated by a Teflon spacer. The experiments proceeded from high to low temperatures. The samples were equilibrated at each temperature for 10–20 minutes before the dielectric measurements.

The high-pressure dielectric measurements were carried out in a Unipress high pressure system with a parallel capacitor. The Alpha-A analyzer was connected to the dielectric cell through a ZG4 interface. The temperature was controlled by the PRESTO system from Julabo.

3.3 Results

Representative heat flow curves from DSC measurements are presented in Fig. 3.1. Only a single Tg can be observed at low and high salt concentrations, while two Tgs are found in PPG4000−LiClO4 at intermediate concentration (O:Li = 15 and 10). The observation of two Tgs in PPG4000−LiClO4 is consistent with the earlier DSC studies.[121, 138] For all three
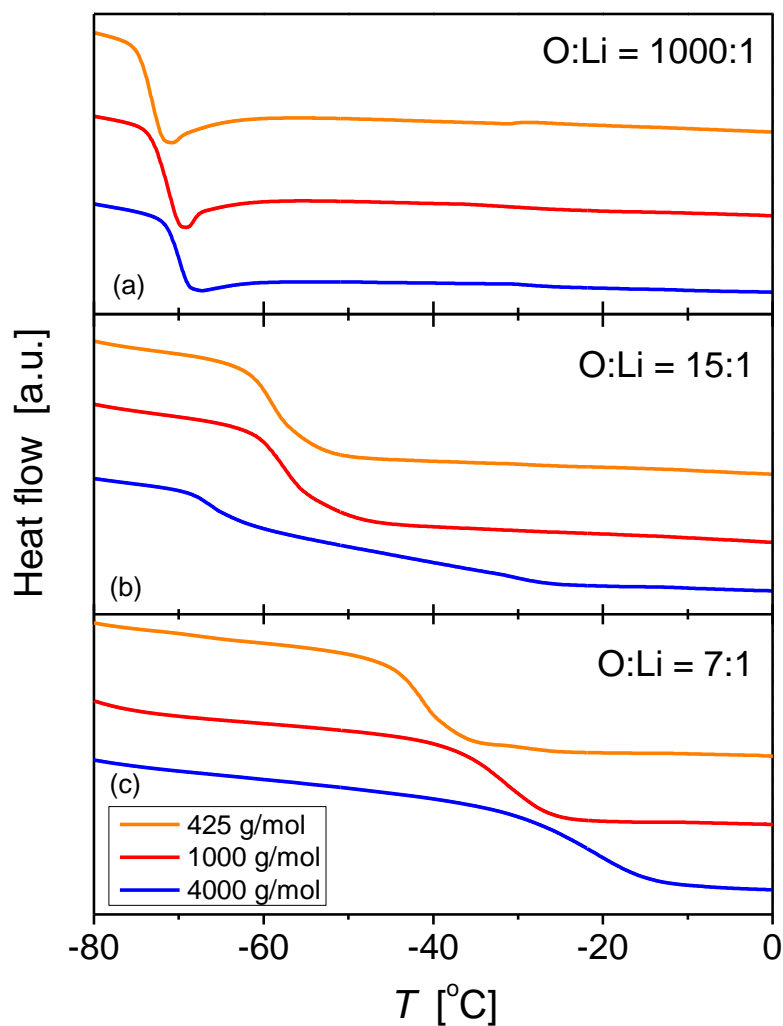
Figure 3.1. DSC curves recorded on heating of PPG/LiClO$_4$ complexes: (a) O:Li = 1000:1 (low concentration of LiClO$_4$), (b) O:Li = 15:1 (intermediate concentration), and (c) O:Li = 7:1 (high concentration). Orange (top), red (middle), and blue (bottom) curves stand for 425, 1000, and 4000 g/mol, respectively.

molecular weights, the glass transition temperature of PPG −LiClO$_4$ increases with the increase of salt concentration. For example, the Tgs of PPG425−LiClO4 at O:Li = 1000, 15, and 7 are 196 K, 212 and 229 K, respectively. It is worth noting that while the three neat PPGs (425, 1000, and 4000) have similar Tgs, the Tg of PPG−LiClO4 exhibits clear molecular weight dependence (e.g., Fig.3.1c). A complete summary of the concentration and molecular weight dependence of Tg in PPG−LiClO4 is presented in Fig.3.11.

3.3.1 Dielectric Spectra Analysis

Representative dielectric spectra of $\varepsilon'(f)$, $\varepsilon''(\omega)$ and derivative $\varepsilon''_{\mathrm{der}}(f)$ [$\varepsilon''_{\mathrm{der}} = (-\pi/2)\partial\varepsilon'/\partial\ln f$] of PPG-LiClO$_4$ are shown in Fig. 3.2. They consist of three major components: (1) slow and fast segmental relaxations in the high-frequency region; (2) dc conductivity in the mid-frequency region of $\varepsilon''(f)$; and (3) sharp increase of $\varepsilon'(f)$ and $\varepsilon''_{\mathrm{der}}(f)$ in the low-frequency region due to the electrode polarization (EP) effect. It should be emphasized that the purpose of presenting Fig. 3.2 is to demonstrate the general fitting procedure of the spectra, whereas the actual number of relaxation processes may vary, depending on the polymer molecular weight, salt concentration, temperature and pressure (see the discussions below).

As presented in Chapter 2, the complex permittivity spectra can be fit by the superposition of several functions, including Havriliak-Negami equations,[87] a dc conductivity term, and an electrode polarization term by Eq. 2.17. In this study, the frequency at ε''
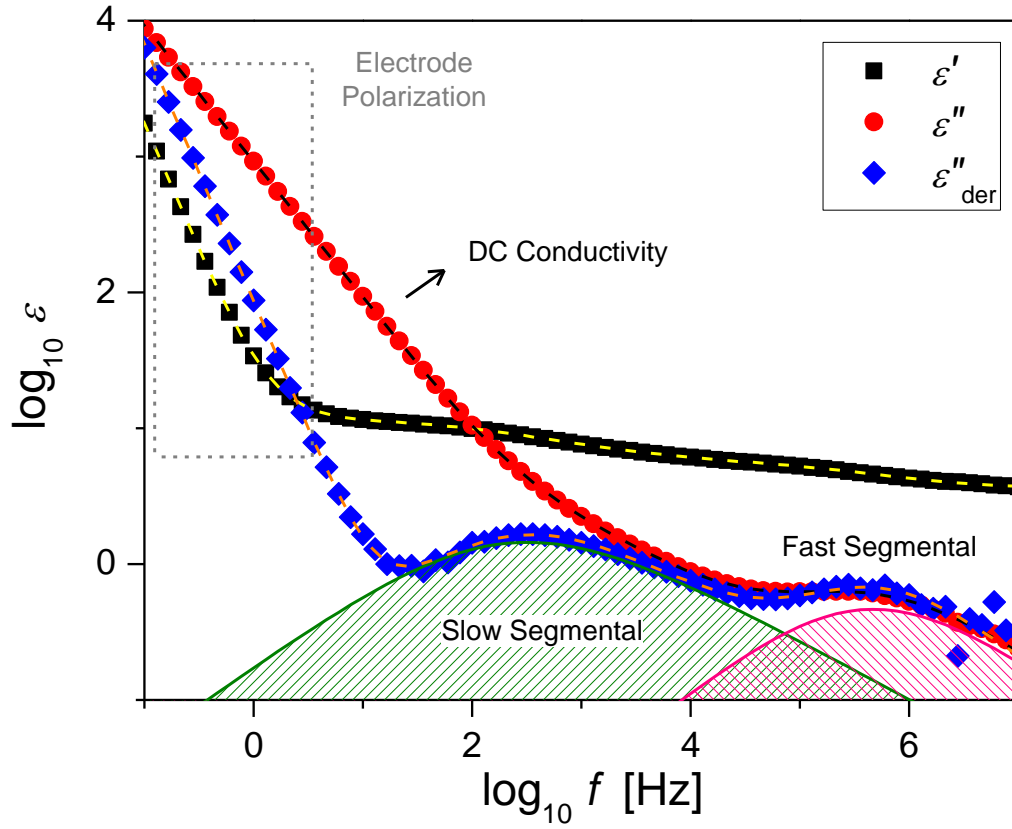
Figure 3.2. Dielectric spectrum of PPG4000/LiClO$_4$ (O:Li = 30) at -30°C. There are three major components: (1) split of the segmental relaxations (fast and slow) in the high-frequency region, (2) dc conductivity in the intermediate-frequency region of ε'', and (3) the sharp increase of ε' and ε''_{der} in the low-frequency region due to the electrode polarization effect. Solid symbols represent the experiment results and the dashed lines represent the fits.

maximum is used to calculate the relaxation time (τ_{max}). The τ_{max} is related to the Havriliak-Negami relaxation time τ_{HN}, and shape parameters α and β by Eq. 2.14:[87]

The analysis of the dielectric spectra of polymer electrolytes is often plagued by the high level of ionic conductivity. Multiple relaxation processes might be completely masked by the dc conductivity in $\varepsilon''(\omega)$. As briefly introduced in Chapter 2, the derivative spectra (e.g., Fig. 3.2, blue diamonds), $\varepsilon''_{der} = (-\pi/2)\partial\varepsilon'/\partial\ln\omega$, based on the Kramers-Kronig relations, is usually used to assist the data analysis.[88, 89] On the one hand, the derivative spectra are used to determine the number of relaxation processes and therefore the number of fitting terms in Eq. 2.17. On the other hand, they are used to check the quality of the fit of $\varepsilon'(\omega)$. In most cases, the use of derivative spectra significantly improves the accuracy of the analysis.

3.3.2 General Features of the Dielectric Spectra of PPG-LiClO₄

The dielectric spectra of all the neat PPGs and the PPG-LiClO$_4$ complexes are shown in Fig. 3.3. The dielectric relaxation in neat PPG has been the subject of many studies.[87, 124, 126, 130, 139-144] It is well known that two relaxations in general can be observed in PPG: a segmental relaxation at high frequencies, and a slower "normal mode" at low frequencies, which is due to the relaxation of the end-to-end vector of the entire polymer chain. In the neat PPG425 (Fig. 3.3a-c), only the segmental relaxation is visible, because of the relative short length of this polymer. In the neat PPG1000 (Fig. 3.3d-f), the normal mode appears as a weak
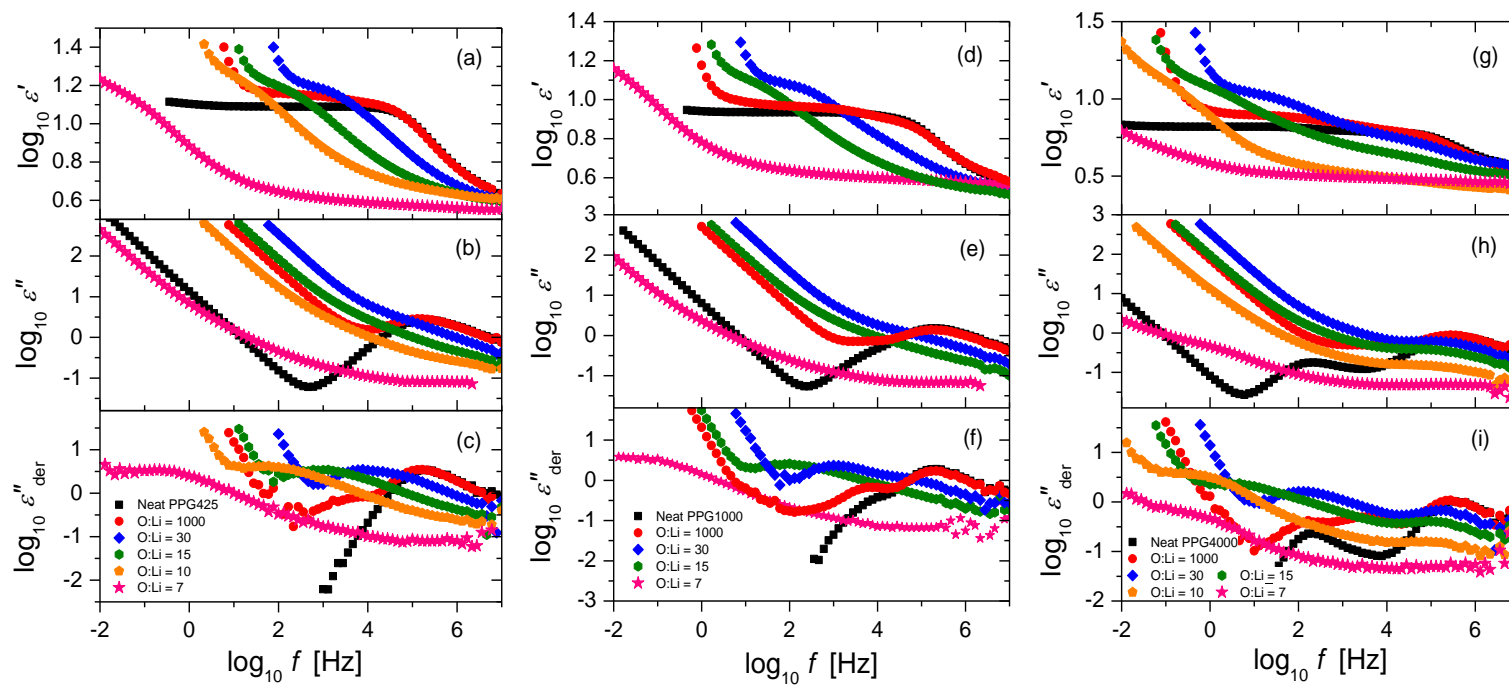
Figure 3.3. Comparison of the dielectric spectra of Neat PPG and PPG/LiClO$_4$ with different molecular weight: (a)-(c) - 425 g/mol at -36°C; (d)-(f) - 1000 g/mol at -35°C; (g)-(i) - 4000 g/mol at -34°C.

shoulder close to the segmental peak. In the neat PPG4000 (Fig. 3.3g-i), the normal mode becomes more separated from the segmental relaxation.

The addition of LiClO$_4$ salt shifts the segmental relaxation to lower frequencies (Fig. 3.3). At low salt concentration (O:Li = 1000), a new process ("ionic mode") appears in all three PPG-LiClO$_4$ complexes. In PPG4000-LiClO$_4$ (O:Li = 1000, 30, 15, 10) and PPG1000-LiClO$_4$ (O:Li = 30), a split of segmental relaxation into fast and slow processes can be observed. It can also be seen from Fig. 3.3 that with the addition of salt, the ionic conductivity starts to interfere with the polymer relaxation. Not only the segmental relaxation is eventually covered by ionic conductivity in $\varepsilon''(f)$, but also the EP starts to influence $\varepsilon'(f)$, at high salt concentrations.

3.3.2.1 Spectra at Low Salt Concentration

While only the segmental relaxation is visible in the neat PPG425, an additional relaxation shows up at low frequencies in PPG425-LiClO$_4$ (O:Li = 1000) due to the presence of LiClO$_4$ (Fig. 3a-c, Fig. 4a). Similar processes are also found in PPG1000-LiClO$_4$ (O:Li = 1000) (Fig. 3d-f) and PPG4000-LiClO$_4$ (O:Li = 1000) (Fig. 3.3g-i, Fig. 3.4b). This relaxation is assigned as "ionic mode".

In PPG4000-LiClO$_4$ (O:Li = 1000), a slow process appears at almost the same position as the normal mode in neat PPG4000 (Fig. 3.4b), although with increased relaxation strength. This mode is assigned as slow segmental relaxation (see discussions in Section 3.3.2.2). In PPG1000-LiClO$_4$ (O:Li = 1000), two processes are clearly observable (Fig. 3.3d-f). They are
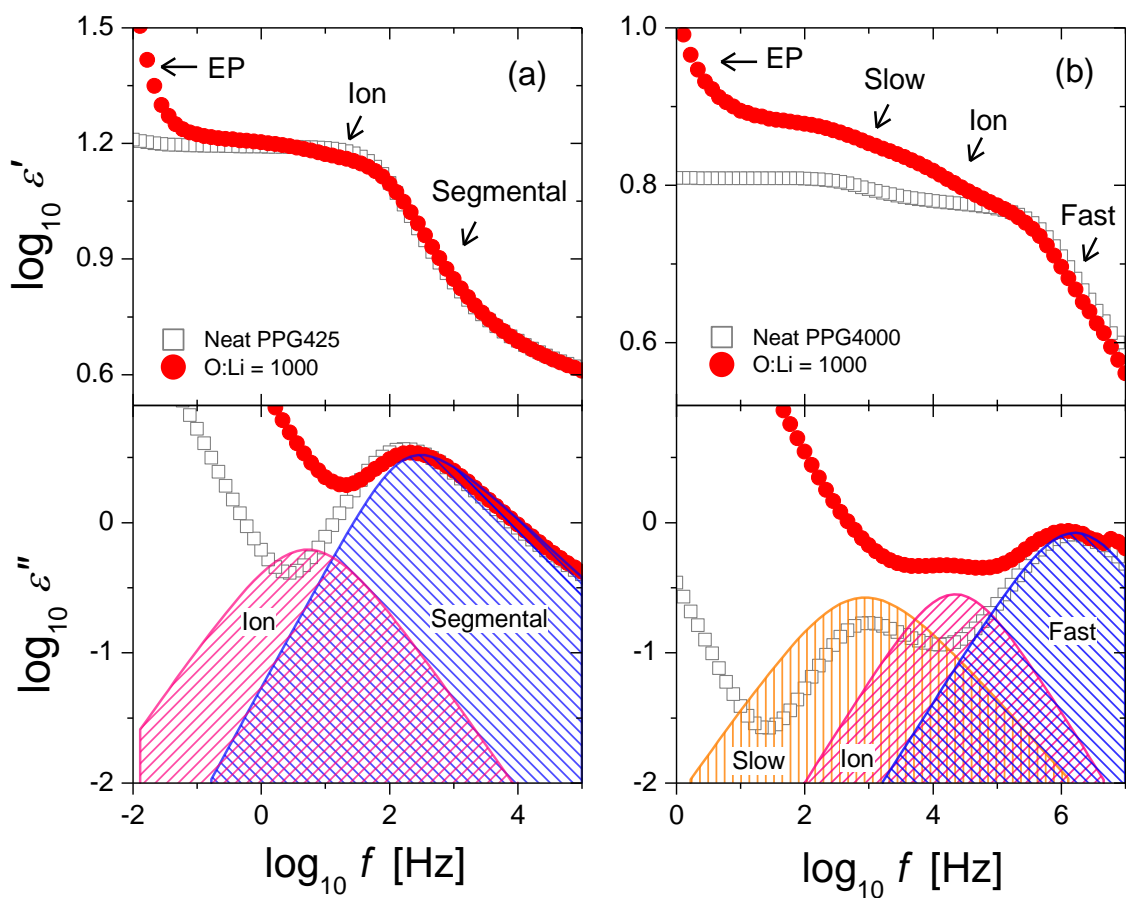
Figure 3.4. Comparison of the dielectric spectra of PPG (a) 425 and (b) 4000 g/mol at O:Li = 1000 (low salt concentration). The open squares present the spectra of neat polymers and the closed circles present the spectra of PPG/LiClO$_4$. The peaks represent different relaxation processes from the fitting of PPG/LiClO$_4$ spectra. The increase of ε' at low frequencies is due to the electrode polarization effect (EP).

ionic mode and fast segmental mode. Due to the presence of the ionic mode, it is hard to resolve the slow segmental peak from the spectrum. The fast segmental processes in PPG4000-LiClO$_4$, PPG1000-LiClO$_4$ at O:Li = 1000, as well as the only segmental process in PPG425-LiClO$_4$ at O:Li = 1000, do not differ much from the segmental peaks in the corresponding neat PPGs, in terms of both peak frequency and shape.

3.3.2.2 Spectra at Intermediate Salt Concentration

At intermediate salt concentration, the spectra PPG4000-LiClO$_4$ become considerably different from that of the neat PPG4000 (Fig. 3.3g-i). The split of segmental relaxation is much more pronounced (Fig. 3.5b). With the increase of salt concentration, the relaxation strength of the slow process increases, while the strength of the fast process is reduced, and becomes unobservable when O:Li = 7 (Fig. 3.6). It should be noted that the separation between slow and fast segmental relaxations also becomes larger with the increase of LiClO$_4$ concentration (Fig. 3.3g-i). It is also worth pointing out that the slow relaxation is qualitatively different from the low-frequency artifact that is frequently observed in viscous liquids.[145, 146] The presence of impurities such as air bubbles often leads to an ultra-slow Debye-like relaxation. In contrast, the slow (segmental) relaxation in PPG-LiClO$_4$ is much broader, especially at high salt concentrations. In addition, the agreement between the results of BDS and DSC clearly indicates that the origin of the slow dielectric peak is the segmental relaxation of the polymer in the ion-rich domain.
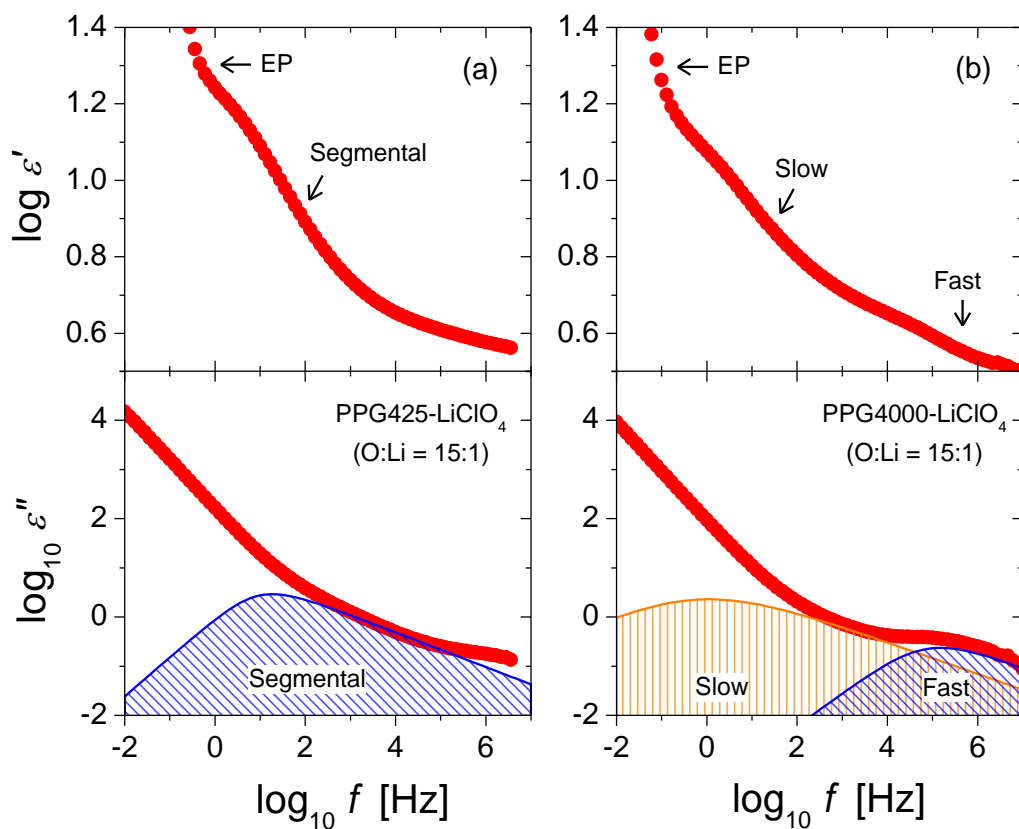
Figure 3.5. Comparison of the dielectric spectra of PPG-LiClO$_4$ with molecular weight (a) 425 and (b) 4000 g/mol at O:Li = 15:1 (intermediate salt concentration). The peaks represent different relaxation processes from the fitting of the spectra.

In PPG1000-LiClO$_4$, as the salt content increases to O:Li = 30, the ionic mode is no longer observable and the segmental relaxation splits into two separate processes (Figure 3.3d-f), similar to the behavior of PPG4000-LiClO$_4$. The fast segmental relaxation becomes unobservable when O:Li ≤ 15. In PPG425-LiClO$_4$, with the increase in salt concentration the segmental relaxation process is shifted to lower frequencies (Figure 3.3a-c, 3.5a). No splitting of segmental process is observed in the concentration range studied.

3.3.2.3 Spectra at High Salt Concentration

At high salt concentration (O:Li = 7), only a single segmental relaxation peak, with shape much broader than the original segmental peak in the neat PPG, is observed in all three PPG-LiClO$_4$ complexes (Fig. 3.3 and 3.6). This result is consistent with the DSC measurement where only one Tg is detected at O:Li = 7.
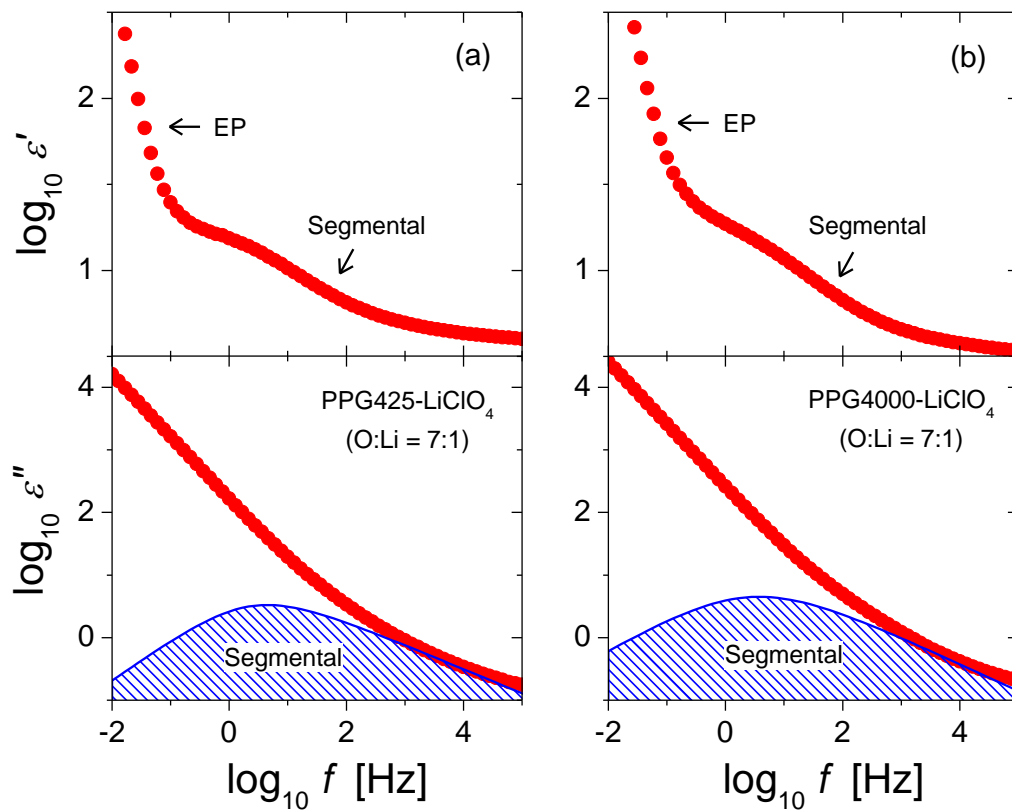
Figure 3.6. Comparison of the dielectric spectra of PPG-LiClO$_4$ with molecular weight (a) 425 and (b) 4000 g/mol at O:Li = 7:1 (high salt concentration).

3.4 Discussion

3.4.1 Nature of the Ionic Mode

3.4.1.1 Molecular Weight, Temperature, and Concentration Dependence

At O:Li = 1000, a new relaxation process appears on the low-frequency side of the (fast) segmental relaxation in PPG-LiClO$_4$ of all three molecular weights (Fig. 3.3 and 3.4). This mode becomes unobservable when O:Li $\leq$ 30. The relaxation strength and relaxation time of this new mode and segmental mode are presented as a function of 1000/T in Fig. 3.7. It can be seen that in the entire temperature range of this study, (1) the relaxation strength of the new (ionic) mode is nearly independent of the molecular weight of PPG while the relaxation strength of the segmental mode decreases with increase of the molecular weight of PPG; (2) the relaxation time of both the new (ionic) mode and segmental mode is almost independent of the molecular weight of PPG. The same additional relaxation (ionic mode) was also observed in PPG-LiClO$_4$ by Furukawa *et al.*[116, 117] They showed that the strength of this mode increased with increasing salt concentration in the range of $100 \leq O: Li \leq 1000$. Furthermore, the inset of Fig. 3.7 indicates that the ionic mode closely follows the (fast) segmental relaxation, i.e., they have similar temperature dependence. Runt *et al.* observed a similar ionic mode in PEO-based single-ion conductors.[147] Interestingly, in both PPG- and PEO-based electrolytes, the ionic mode is about 100 times slower than the (fast) segmental relaxation.
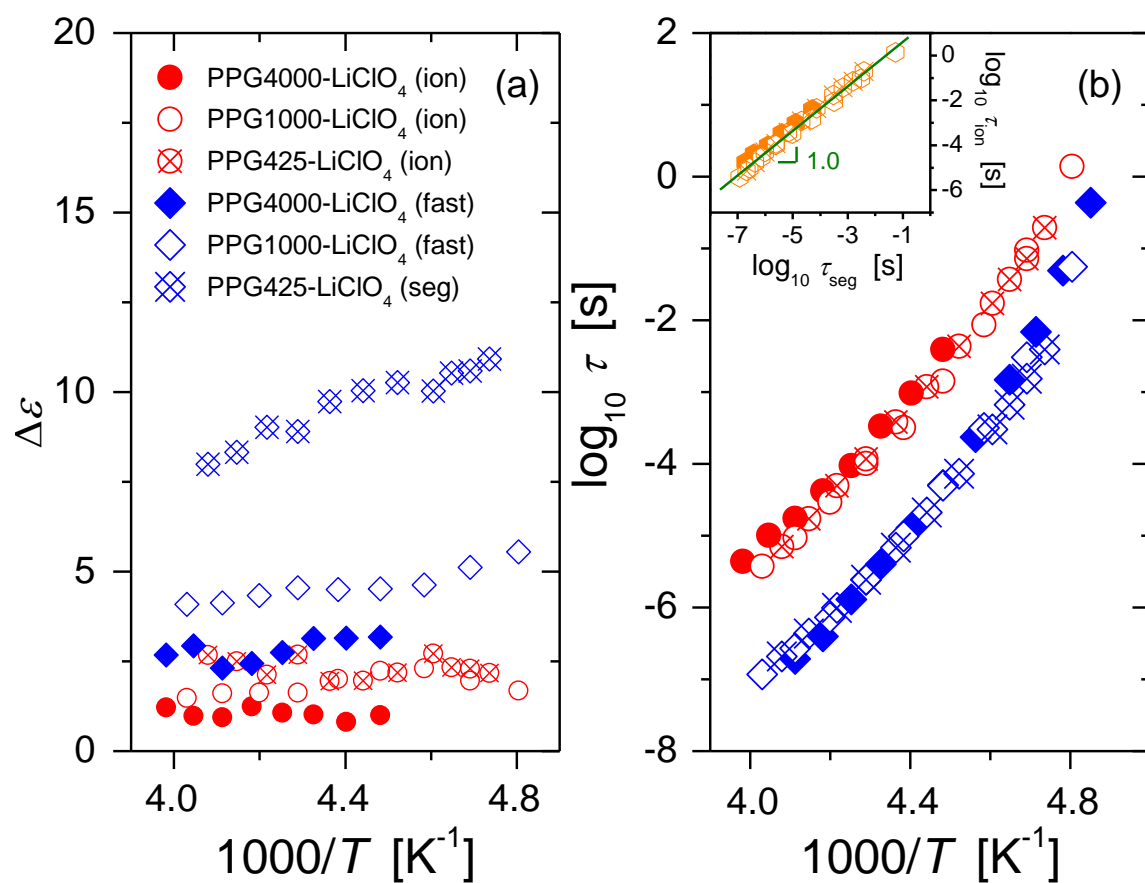
Figure 3.7. Temperature dependence of (a) the relaxation strength and (b) relaxation time for the fast segmental and ion modes. The red circles and blue diamonds represent the ionic mode and segmental mode, respectively. Inset: relation between the ionic and segmental relaxation times. The filled, open, and crossed symbols correspond to PPG4000, PPG1000, and PPG425, respectively.

3.4.1.2 Ionic Mode under High Pressure

The dielectric spectra of PPG425-LiClO$_4$ (O:Li = 1000) at ambient and high pressure
(551 MPa) are shown in Fig. 3.8.
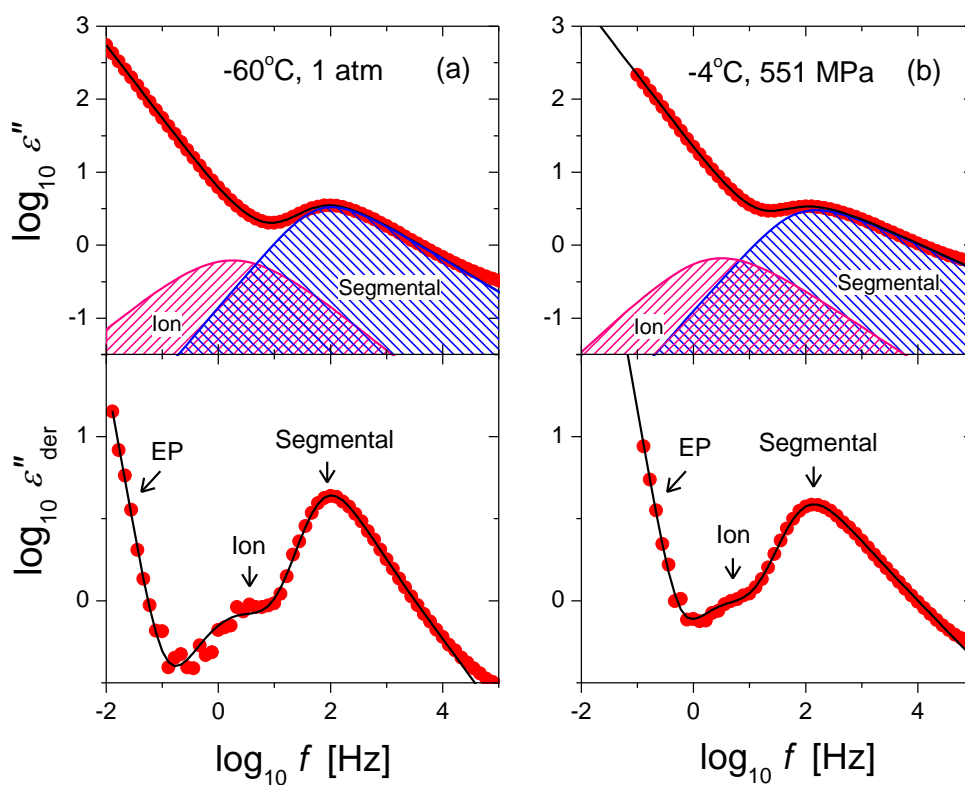
Figure 3.8. Comparison of the spectra of PPG425-LiClO$_4$ (O:Li = 1000) at (a) ambient
pressure (1 atm) and (b) high pressure (551 MPa).

The strength and shape of the ionic and segmental relaxation at the two pressures are almost identical, despite a slight decoupling of ionic conductivity from the segmental relaxation at high pressure. The relaxation times of the ionic and segmental modes are presented as a function of pressure in Fig. 3.9. Similar to the effect of decrease of temperature, the increase of pressure shifts the ionic and segmental modes to lower frequencies. The inset shows the relation of the ionic relaxation to the segmental relaxation under both isothermal and isobaric conditions. The data fall onto the same line of a slope of one, indicating that the ionic and segmental modes are affected in a very similar fashion by pressure and temperature. Moreover, the inset suggests that these two modes are well coupled at the studied pressure and temperature range.

3.4.2 Origin of the Slow and Fast Relaxations

3.4.2.1 Correlation between BDS and DSC

Two (segmental) relaxations (slow and fast) are observed in PPG4000-LiClO$_4$ (O:Li = 1000, 30, 15, 10) and PPG1000-LiClO$_4$ (O:Li = 30). This is presumably related to the well-known micro-phase separation behavior in PPG-based electrolytes.[116, 121-123] However, the results of dynamic and calorimetric measurements have never been directly compared. In our dielectric spectroscopy (BDS) measurements, the temperature dependence of segmental relaxation time (τ) across the temperature range of study can be well described by the Vogel-Fulcher-Tammann (VFT) equation (eq.2.12) (Fig.3.10). The glass transition temperature can be defined as the temperature where $\tau = 100s$. In samples (PPG1000-LiClO$_4$, O:Li = 30 and
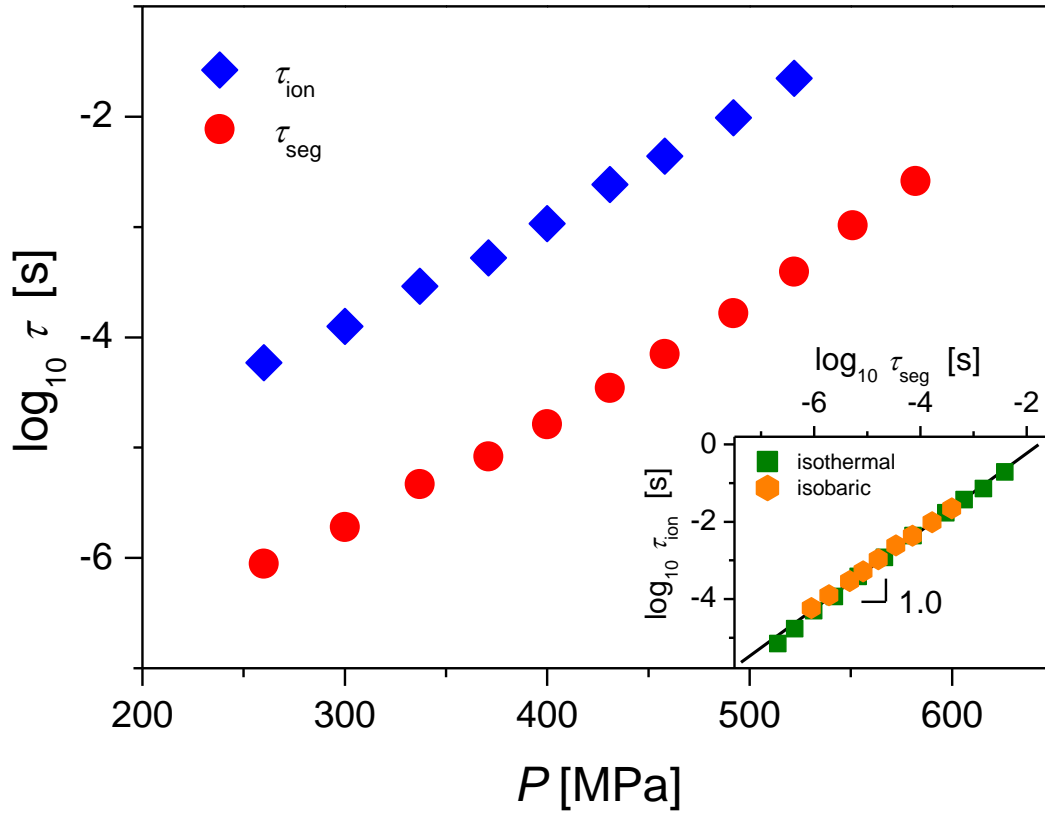
Figure 3.9. The relaxation time as a function of pressure for both ion mode (diamonds) and segmental mode (circles). The inset shows the relationship between the relaxation time of the ion mode and the segmental mode in isothermal (squares) and isobaric (hexagons) experiments.
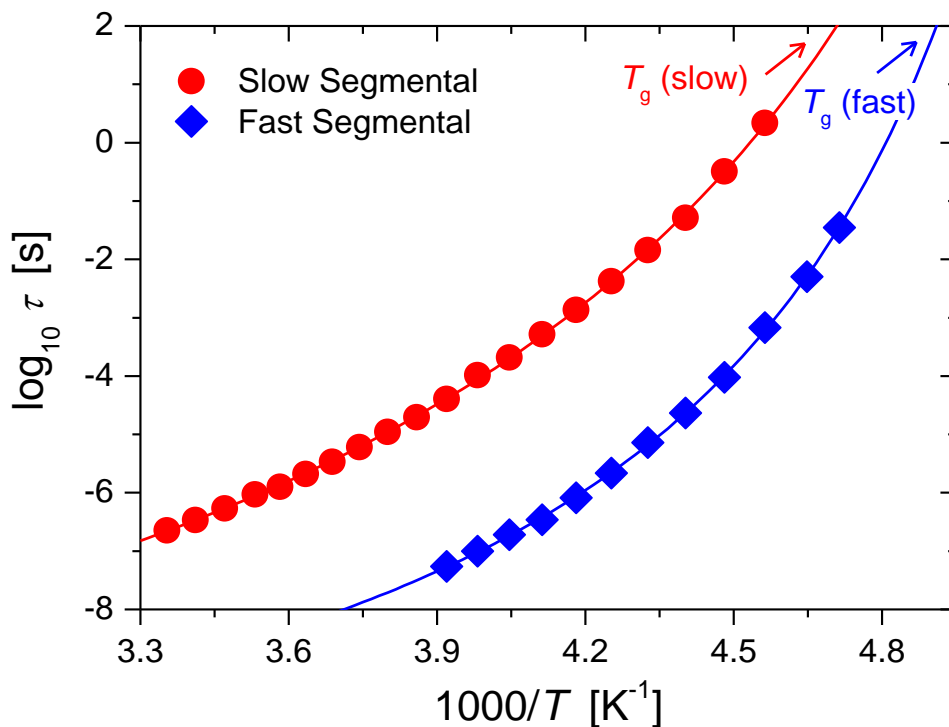
Figure 3.10. Temperature dependence of the slow and fast segmental relaxation times in PPG4000-LiClO$_4$ (O:Li = 30). The solid lines are the fits by VFT equation.

PPG4000-LiClO$_4$, O:Li = 1000, 30, 15, 10) with the splitting feature, two glass transition temperatures can be obtained using this method (Fig. 3.11). The VFT fit parameters for all the samples are summarized in Table 1-3. On the other hand, the glass transition temperature can be determined from DSC by taking the mid-point of the change of the heat flow.

Fig. 3.11 shows that glass transition temperatures from DSC and BDS are in reasonable agreement with each other. In both cases, (1) Tg increases with the increase of salt concentration; and (2) two Tgs are found at intermediate concentrations O:Li = 15-10 for PPG4000-LiClO$_4$. However, since DSC is not as sensitive as broadband dielectric
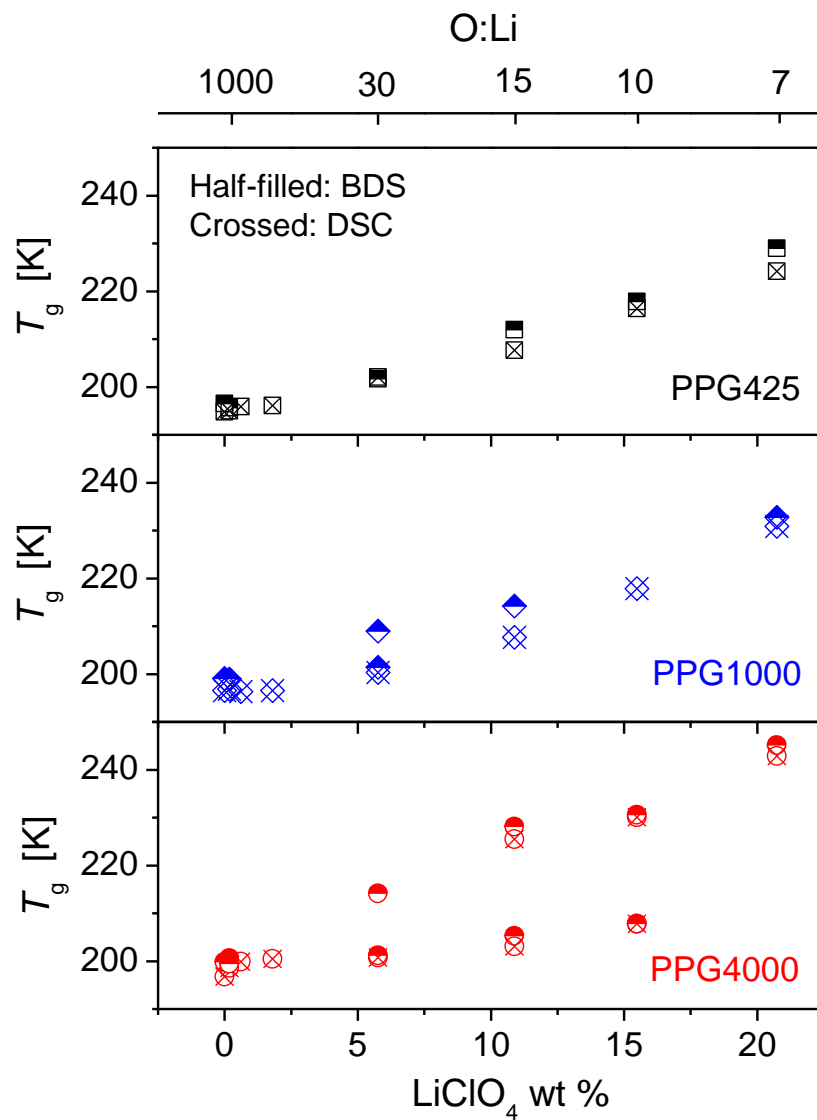
Figure 3.11. Comparison of the Tgs determined from DSC (crossed symbols) and broadband dielectric spectroscopy (BDS) (half-filled symbols) measurements for the neat PPG and PPG-LiClO$_4$ at various O:Li ratios. The higher Tg for PPG4000-LiClO$_4$ (O:Li = 15) and the lower Tg for PPG4000-LiClO$_4$ (O:Li = 10) are determined from the heating scans. This is because the Tgs cannot be accurately determined from the cooling processes due to very small change of heat flow.

spectroscopy, only one Tg is found in PPG4000-LiClO$_4$ (O:Li = 1000, 30) and PPG1000-LiClO$_4$ (O:Li = 30), whereas two Tgs are obtained from dielectric analysis. Nevertheless, good agreement has been found for DSC and BDS Tgs, wherever a direct comparison is possible. This result confirms that slow and fast relaxations indeed come from the polymer segmental motions in different micro-domains. Since it is expected that the ion-polymer interaction would slow down the segmental relaxation, the fast and slow segmental relaxations should correspond to the motions in the ion-depleted and ion-rich domains, respectively.

3.4.2.2 Effects of Molecular Weight and Terminal Groups

Both DSC and BDS measurements indicate that the glass transition temperature (of either ion-rich or ion-depleted domain) of PPG-LiClO$_4$ increases monotonically with the increase of salt concentration. This is because the transient "crosslinking" between lithium cations and ether oxygens slows down the segmental dynamics of the polymer matrix. The effect of salt on Tg is relatively small at low salt concentration. However, the *Tg* of PPG-LiClO$_4$ with high salt content is considerably higher than that of the neat PPG. It has been demonstrated that the terminal -OH groups forms hydrogen bonding between chains which reduces the segmental mobility of the polymer.[126, 148] For example, Tg of hydroxyl-terminated PPG varies less than 1%, in the molecular weight range 425 – 4000 g/mol, while the Tg of methyl-terminated PPG strongly depends on the molecular weight.[148] When LiClO$_4$ is added to PPG, the lithium cations prefer to coordinate with the terminal OH groups first,[149] and thus

Table 3.1 VFT Fit Parameters for PPG4000-Based Samples

	PPG4000		O:Li = 1000			O:Li = 30		O:Li = 15		O:Li = 10		O:Li = 7
	Chain	segmental	slow	ion	fast	slow	fast	slow	fast	slow	fast	slow
τ_0 [ps]	113	104	119	22.4	0.0291	4.14	1.20	9.05×10^{-5}	4.32	6.52×10^{-3}	0.311	6.35×10^{-8}
B [K]	1206	1079	1211	964.8	1210	1444	827.7	2995	716.2	2950	937.9	5228
T_0 [K]	162.5	168.6	162.8	172.3	166.2	165.5	177.8	156.1	182.1	151.4	179.7	134.1

Table 3.2 VFT Fit Parameters for PPG1000-Based Samples

	PPG1000		O:Li = 1000		O:Li = 30		O:Li = 15	O:Li = 7
	chain	segmental	ion	fast	slow	fast	Slow	slow
τ_0 [ps]	0.816	0.199	3.40	0.107	30.4	0.231	1.57×10^{-3}	8.95×10^{-6}
B [K]	1362	1058	1175	1142	960.5	1138	2699	3290
T_0 [K]	157.4	167.9	164.2	165.8	175.6	167.6	148.4	158.6

Table 3.3 VFT Fit Parameters for PPG425-Based Samples

	PPG425		O:Li = 1000	O:Li = 30	O:Li = 15	O:Li = 10	O:Li = 7
	segmental	ion	segmental	segmental	segmental	segmental	segmental
τ_0 [ps]	0.0129	7.46×10^{-5}	0.0314	0.183	1.56	0.0228	1.54×10^{-3}
B [K]	1527	3011	1387	1424	1103	1689	2306
T_0 [K]	154.3	126.1	156.8	159.8	177.3	170.9	169.4

break up the hydrogen bonding between polymer chains. At low salt concentration, there are many unbroken hydrogen bonds, which still strongly influence the glass transition behavior of the samples. The increase of salt content leads to a decrease of hydrogen bonds and an increase of coordination between the OH groups and cations, causing a stronger dependence of Tg on the molecular weight of PPG. Since the number density of end OH groups increases from PPG4000 to PPG425, the Tg of (the ion-rich domains in) PPG4000-LiClO$_4$ experiences the largest change, whereas the Tg of PPG425-LiClO$_4$ has the smallest change in the studied concentration range.

No micro-phase separation has been observed in PPG425-LiClO$_4$. In contrast, clear indications of micro-phase separation are found in PPG4000-LiClO$_4$ (O:Li = 1000, 30, 15, 10) in both DSC and BDS measurements. The polymer molecular weight affects the micro-phase separation behavior in two ways: (1) the number of repeating units per polymer chain, and (2) the number density of terminal hydroxyl groups. Because the mixing entropy $\Delta S \sim k_B[(1-\phi)\ln(1-\phi) + (\phi/N)\ln\phi]$,[150] with ϕ being the polymer volume fraction and N the number repeating units per chain, the mixtures become less likely to form a homogeneous solution as N increases. In addition, the terminal hydroxyl groups favor the solvation of ions.[125, 149] Among the three PPGs in this study, PPG425 has the smallest molecular weight and thus the highest number density of terminal OH groups. As a result, there is no indication of micro-phase separation for PPG425-LiClO$_4$ in either DSC or BDS measurement. On the other hand, while the split of segmental relaxation is only observed at O:Li = 30 for PPG1000-LiClO$_4$, micro-phase separation occurs in a much wider concentration range for PPG4000-LiClO$_4$ (O:Li = 1000-10 in BDS; O:Li = 15, 10 in DSC). It is perhaps useful to point out an

interesting fact: The fast process in PPG4000-LiClO$_4$ disappears at O:Li = 7, indicating no micro-phase separation. This O:Li number is the average number of repeating unit in PPG425, in which no micro-phase separation has been observed at any salt concentration.

3.4.2.3 Behavior under High Pressure

Pressure is another important parameter that strongly influences the dynamics of polymer electrolytes. As a demonstration, the result of high-pressure dielectric measurement of PPG4000-LiClO$_4$ (O:Li = 30) is shown in Fig. 3.12b, together with the result of isobaric experiments (Fig. 3.12a).

With the decrease of temperature or increase of pressure, both slow and fast segmental modes shift to lower frequencies. However, in the isothermal experiments, the two segmental relaxations exhibit different pressure sensitivity. The fast mode shifts quicker than the slow mode does, and eventually merges into the slow mode as pressure increases, while in the isobaric experiments, both segmental processes show similar sensitivity to the change of temperature. Alternatively, one may interpret this as suppression of micro-phase separation under high pressure. Because the ion-rich domain might have higher efficiency of packing, the tendency of forming ion-depleted domain decreases under high pressure.
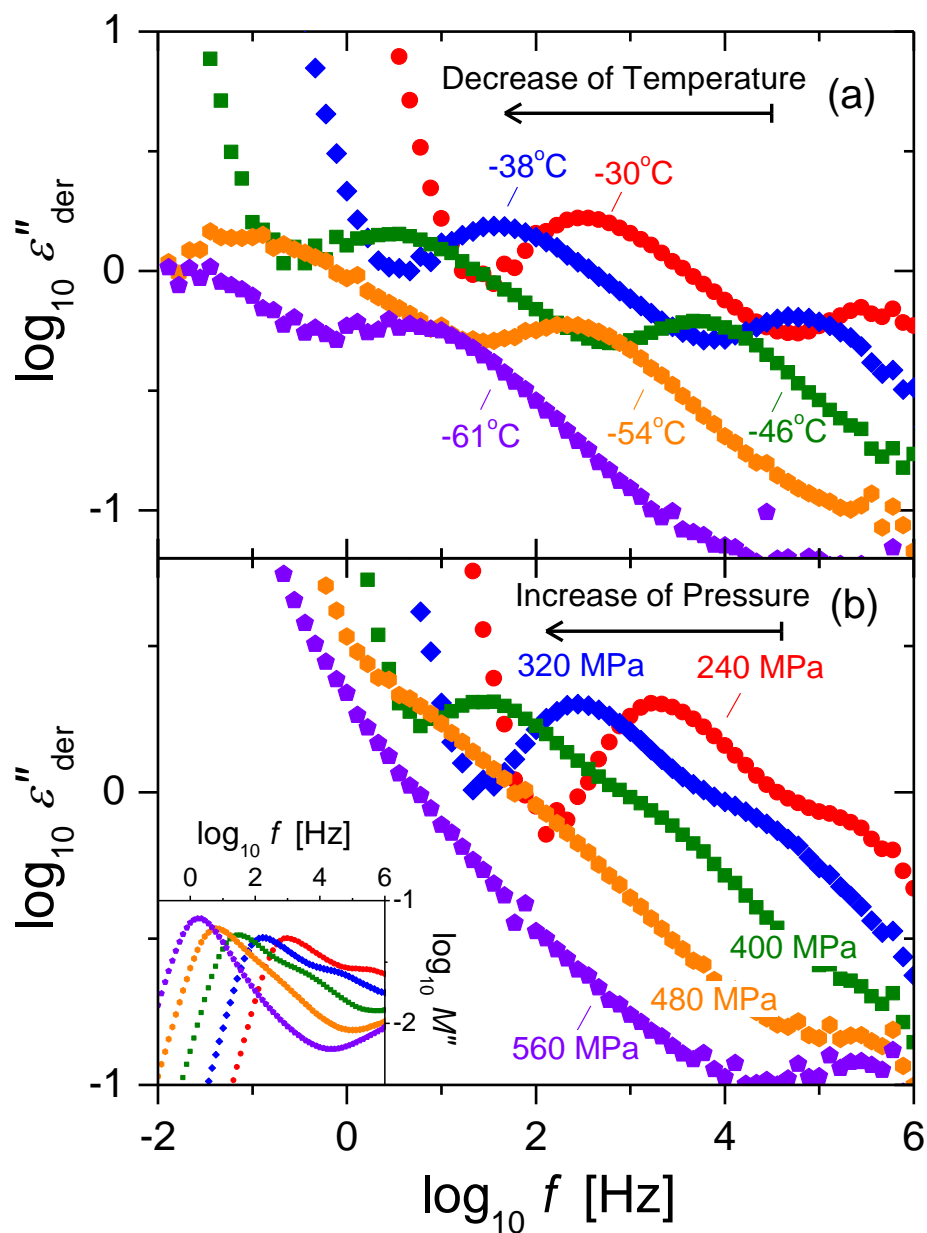
Figure 3.12. Comparison of the derivative spectra of PPG4000-LiClO$_4$ (O:Li = 30) at (a) various temperatures and (b) pressures. The isobaric measurements (top) were carried out at 1 atm, whereas the isothermal measurements were performed at 10.4°C. Inset: corresponding modulus spectra at high pressures.

3.4.3 Relation of Ionic Transport to Segmental Relaxation

3.4.3.1 Walden Plot at Ambient Pressure

The classical Walden rule has been introduced in Chapter 1. In polymer electrolytes, the ionic motions are directly related to the local segmental relaxation while macroscopic viscosity is controlled by the chain relaxation. Therefore, to apply the Walden plot analysis to polymers, the fluidity must be substituted by the rate of structural (segmental) relaxation $(1/\tau_\alpha)$, which is a more relevant quantity for ionic transport in polymers.

The Walden plot for PPG-LiClO$_4$ is shown in Fig. 3.13, which is constructed by using the τ_α of the segmental relaxation (both slow and fast segmental relaxation if micro-phase separation was observed). Here, it is assumed that all ions are fully dissociated. The dilute LiClO$_4$ aqueous solution is chosen as the reference for constructing the "ideal" Walden line. In PPG425-LiClO$_4$ (Fig. 3.13a), only a single segmental relaxation was observed, and the data of all concentrations fall onto the "ideal" line. In samples with the two segmental modes, PPG1000-LiClO$_4$ (O:Li = 30) (Fig.3.13b) and PPG4000-LiClO$_4$ (O:Li = 1000, 30, 15, 10) (Fig. 3.13c), the points plotted using the slow segmental relaxation fall close to the "ideal" Walden line, whereas the points plotted using the fast segmental relaxation stay below the "ideal" line. In the rest of the PPG1000-LiClO$_4$ and PPG4000-LiClO$_4$ samples where only a single segmental relaxation is observed, all points fall very close to the "ideal" Walden line as well.

The above Walden plot analysis leads to a clear conclusion: the (slow) segmental relaxation controls the macroscopic ionic conductivity in all the three PPGs regardless of their
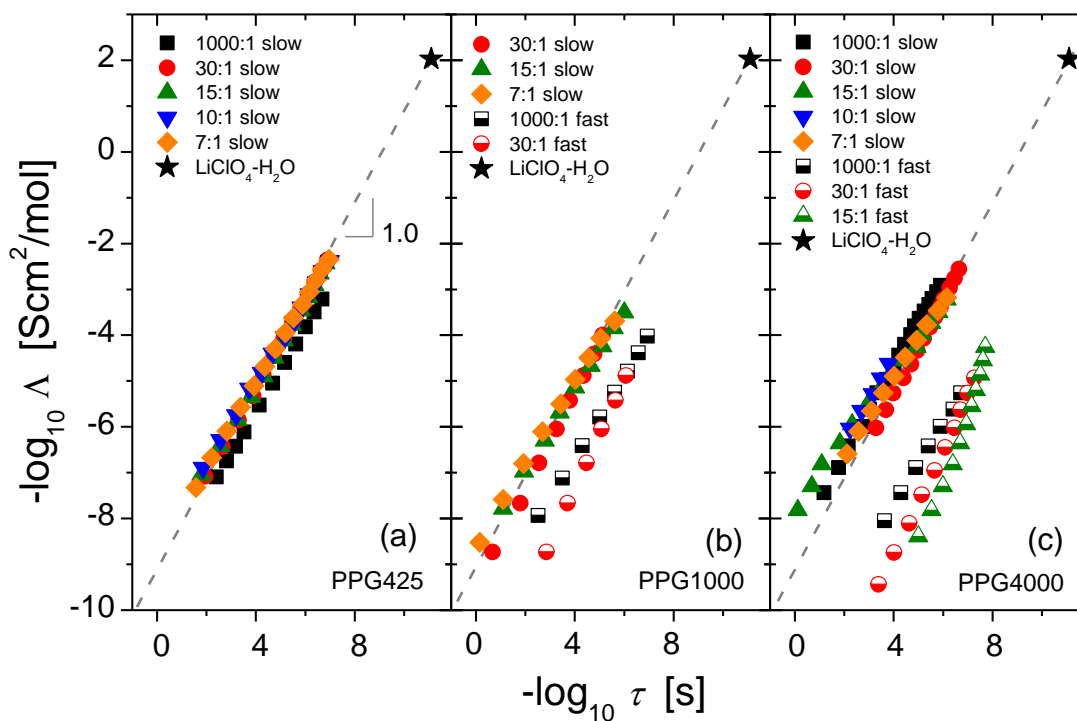
Figure 3.13. Walden plots for (a) PPG425-LiClO$_4$, (b) PPG1000-LiClO$_4$, and (c) PPG4000-LiClO$_4$. Here, dilute LiClO$_4$ aqueous solution is used as a reference. The dashed line with slope 1.0 is the "ideal" Walden line. For samples with the micro-phase separation, two groups of data are presented. They are data from the slow segmental mode (closed symbols), and data from the fast segmental mode (semi-open symbols).

molecular weight, i.e., the ionic transport in PPG is closely coupled to the (slow) segmental relaxation. In addition, the Walden plot analysis reveals that the ionic mobility of PPG-based electrolytes is very similar to that of the dilute aqueous solutions, which will be discussed in more details in the next Chapter. The relatively low ionic mobility in PPG at ambient temperature is caused by the slow segmental dynamics, which is additionally slowed down due to the interactions with ions.

3.4.3.2 Behavior under High Pressure

While the ionic transport in PPG is strongly coupled to the segmental relaxation under ambient pressure, our analysis reveals a different picture at elevated pressures (Fig. 3.14). In PPG4000-LiClO$_4$ (O:Li = 30), the points presented using the slow segmental relaxation fall on the "ideal" Walden line at low pressures ($p < 400$ MPa), but move into the superionic regime (above the ideal line) when the pressure exceeds 400 MPa. This indicates that at high pressure the ionic motions are decoupled from the segmental relaxation of the polymer. In another words, densification of PPG slows down its segmental dynamics significantly stronger than dynamics of ions. This observation suggests that the close relation between ionic transport and segmental relaxation only holds in a certain pressure range. Because of the asymmetry in size, small ions may require much smaller activation volume for diffusive motion than do the polymer segments. Here, it is important to note that although the electrode polarization (EP) effect interferes the fitting of the dielectric relaxation at high pressures and the obtained segmental relaxation times might be subject to certain error, the overlapping of electrode polarization and segmental relaxation itself is a manifestation of decoupling. This is

89
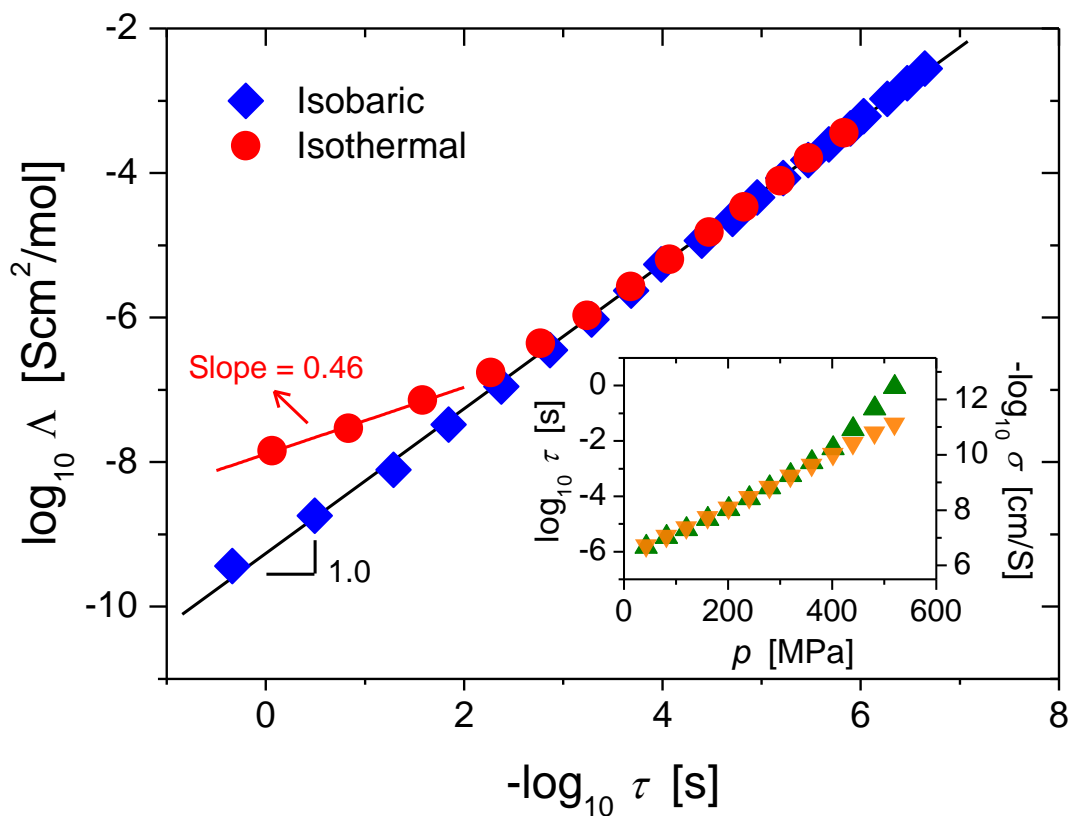
Figure 3.14 Effects of temperature and pressure on the relationship between ionic transport and (slow) segmental relaxation in PPG4000-LiClO$_4$ (O:Li = 30). The isobaric data (blue diamonds) were obtained by varying temperature at 1 atm. The isothermal data (red circles) were obtained by varying pressure at 10.4°C. Inset: dependence of the slow segmental relaxation time (green up triangle) and resistivity ($1/\sigma$) (yellow down triangle) on pressure.

because EP is controlled by ionic conductivity. If the ionic transport is closely coupled to the segmental relaxation, then the high-frequency tail of EP should move hand in hand with the segmental relaxation peak when the pressure is changed. Since the high-frequency tail of EP and segmental relaxation are well separated at low pressures but strongly overlap at high pressures, the ionic transport and segmental relaxation must be decoupled under high pressure.

3.5 Conclusion

Although PPG-based electrolytes have been the subject of many investigations, the present study demonstrates that a complete understanding of these materials cannot be obtained, unless the temperature, pressure, polymer molecular weight, and salt concentration are varied in a systematic manner. Because of the mediocre solvating power of PPG, complex micro-phase separation behavior shows up in PPGs with relatively high molecular weight. At low salt concentration (O:Li = 1000), an ionic mode has been observed in PPGs of all three molecular weight (425, 1000, and 4000 g/mol). The strength and shape of this ionic relaxation are insensitive to the change of temperature and pressure. Micro-phase separation is found in PPG4000-LiClO$_4$ (O:Li = 1000, 30, 15, 10) and PPG1000-LiClO$_4$ (O:Li = 30). The Tgs determined for the ion-rich and ion-depleted domains from BDS and DSC are consistent with each other.

In contrast to the ionic mode, the micro-phase separation is strongly suppressed under high pressure. The Walden plot analysis shows that the ionic transport at ambient pressure in

PPG-LiClO$_4$ is controlled by the (slow) segmental relaxation, and all the PPG data fall close to the "ideal" Walden line. These results emphasize the strong coupling of ionic transport to segmental dynamics in PPG-based polymer electrolytes. The reason might be the strong coordination of lithium ions to oxygen atoms in the polymer backbone. However, this close relation between ionic transport and segmental relaxation breaks down at high pressure.

CHAPTER IV

CAN WE MAKE POLYMER ELECTROLYTES SUPERIONIC?

4.1 Introduction

As discussed in Chapter 1, the ion mobility in traditional liquid electrolytes is controlled by the macroscopic viscosity of the solvent molecule, which is proportional to the rate of structural rearrangement of the solvent molecules. Therefore, the ion transport in traditional liquid electrolytes is determined by the structural relaxation of the solvent molecules: $\mu \sim \tau_s^{-1}$. In the case of polymer electrolytes, the size of ion is much smaller than that of solvent molecule (polymer). Therefore, it is generally accepted that in polymer electrolytes,[151, 152] the charge transport is controlled by the local "microscopic" viscosity η_{micro} rather than the macroscopic viscosity. Since η_{micro} is determined by the polymer segmental (structural) motion, i.e., $\eta_{\text{micro}} = G_g \tau_S$, the same equation can be derived: $\mu \sim \tau_s^{-1}$ in polymer electrolytes. In Chapter 3, the conductivity mechanism in low molecular weight PPG was discussed. The ionic transport is strongly coupled to the segmental relaxation of the polymers, or the slow segmental relaxation corresponding to the ion-rich domain in samples where micro-phase separation was observed. Following this guideline, extensive efforts have been put into making polymers electrolytes with low Tg, where a faster segmental relaxation would

lead to a higher conductivity. However, the reality is that the highest conductivity achieved so far was around 10^{-5} S/cm at room temperature which is not enough for practical applications.

Clearly, our understanding of the relation between ionic transport and polymer segmental relaxation is far from complete and an in-depth analysis seems necessary. The derivation of $\mu \sim \tau_s^{-1}$, for polymer electrolytes is based on several assumptions which may not necessarily hold. For example, the Stokes–Einstein relation may breakdown for guest molecule diffusion in polymers, especially in the vicinity of glass transition. Moreover, even if the electrical mobility can be related to microscopic viscosity, it is not obvious whether η_{micro} will be defined by segmental relaxation.

The concept of decoupling has been introduced in Chapter 1. It states that in some fast ion conductors, the ionic migration and structural/segmental relaxation have different temperature dependence. The decoupling phenomenon has been reported in several types of fast ion conductors. More importantly, it has been found that in relatively rigid (fragile) polymers their ionic conductivity can be decoupled from segmental relaxation.[78, 153-155]

In this chapter, three categories of polymer electrolytes were studied. They are polycarbonate based, polystyrene based and polyether based polymer electrolytes. The ion transport mechanism was investigated in those samples and compared with small molecule electrolytes. Surprisingly, there is a fundamental difference between the ionic transport in polymers and small molecules. Our analysis reveals that at the same structural relaxation rate, the ionic mobility in polymers can be orders of magnitude higher than in small-molecular electrolytes. More importantly, in contrast to the traditional view, it is demonstrated that many polymers fall into the category of "superionic" conductors, due to strong decoupling of ionic

motion from structural relaxation. These findings highlight the importance of decoupling ionic transport from structural relaxation for future design of solid polymer electrolytes.

4.2 Materials and Methods

The ionic liquids (ILs) 1-butyl-3-methyl-imidazolium hexafluorophosphate ([BMIM][PF$_6$]), was purchased from Sigma–Aldrich and used as received.

Five polymers were synthesized using conventional free radical (co)polymerization and anionic polymerization: poly(vinyl ethylene carbonate)-*co*-poly(vinyl acetate) (PVEC-PVAc), poly(vinyl ethylene carbonate)-*co*-poly(methoxyethylacrylate) (PVEC-PMEA), poly(vinyl carbonate)-*co*-poly[poly(ethylene glycol methyl ether methacrylate)] (PVC-PPEGMEMA), poly[4-(2-methoxyethoxy)methyl styrene] (PMOEOMSt), and poly[poly(ethylene oxide styrene)]-*co*-polystyrene (PPEOSt-PSt). The first three polymers, PVEC-PVAc, PVEC-PMEA, and PVC-PPEGMEMA, were based on the carbonate structure, whereas the last two polymers, PMOEOMSt and PPEOSt-PSt, were based on the polystyrene backbone.[28, 156] Those polymers were kindly provided by Tomonori Saito, Jun Yang, Xiang Yu, Kunlun Hong and Jimmy Mays. Polypropylene oxide (PPO) with M_w of 425 g/mol was purchased from Sigma-Aldrich. The lithium salts included lithium perchlorate (LiClO$_4$) (from Alfa Aesar) and lithium bis(trifluoromethane) sulfonimide (LiTFSI) (from Sigma-Aldrich). The polymer electrolytes were prepared by dissolving polymers and lithium salts in appropriate organic solvents (tetrahydrofuran, methanol, or acetone), and subsequently removing the solvent in a vacuum oven at room temperature. For polymers with relatively

high glass transition temperatures, the mixtures were further dried at elevated temperatures to completely remove the residual solvents. The data of polyethylene oxide (PEO) was taken from ref. [114]. Detailed information about their chemical structures and molecular characteristics can be found in Table 4.1.

Broadband dielectric spectroscopy measurements of our polymer electrolytes were carried out on the same instrument used for PPG/LiClO$_4$ study presented in last Chapter. The polymer electrolyte sample under test was sandwiched between gold-plated electrodes (10 and 20 mm) with a Teflon spacer of 0.054 mm. The applied voltage was 0.1 V to avoid any non-linear effects. The samples were annealed at the highest experimental temperature for approximately 30 min prior to the dielectric measurement. All the samples were thermally stable over the temperature range of our experiments.

4.3 Results

Fig.4.1 gives the representative spectra of the examined polymer electrolytes. The spectrum consists of three major components: (1) polymer segmental (structural) relaxation in the high-frequency region, (2) dc conductivity in the mid- frequency region, and (3) pronounced increase of ε' in the low-frequency region due to the electrode polarization (EP) effect.

Table 4.1. Structural Information for the Polymer Electrolytes
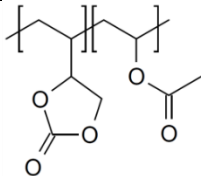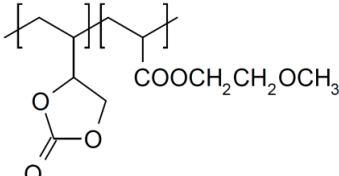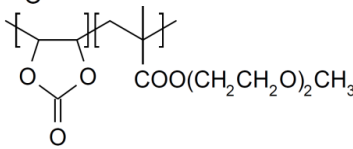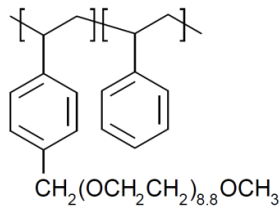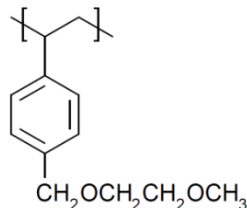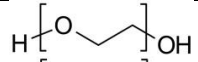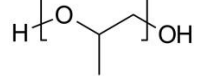
Sample Name	Abbreviation	Chemical Structure	M_w [kg/mol]	PDI	Composition
Poly(vinyl ethylene carbonate)-*co*-Poly(vinyl acetate)	PVEC-PVAc		32.4	1.95	VEC (39 mol%)
Poly(vinyl ethylene carbonate)-*co*-Poly(methoxyethylacrylate)	PVEC-PMEA	$COOCH_2CH_2OCH_3$	22.3	1.83	VEC (63 mol%)
Poly(vinyl carbonate)-*co*-Poly[poly(ethylene glycol methyl ether methacrylate)]	PVC-PPEGMEMA	$COO(CH_2CH_2O)_2CH_3$	31.2	1.98	VC (53 mol%)
Poly(polyethylene oxide styrene)-*co*-Polystyrene	PPEOSt-PSt	$CH_2(OCH_2CH_2)_{8.8}OCH_3$	11.4	1.26	PEOSt (21 mol%)
Poly[4-(2-methoxyethoxy)methyl styrene]	PMOEOMSt	$CH_2OCH_2CH_2OCH_3$	5.8	1.22	homopolymer

Table 4.1 (Continued)

Sample Name	Abbreviation	Chemical Structure	M_w [kg/mol]	PDI	Composition
Polyethylene oxide	PEO		2.0	-	homopolymer
Polypropylene oxide	PPO		0.425	-	homopolymer
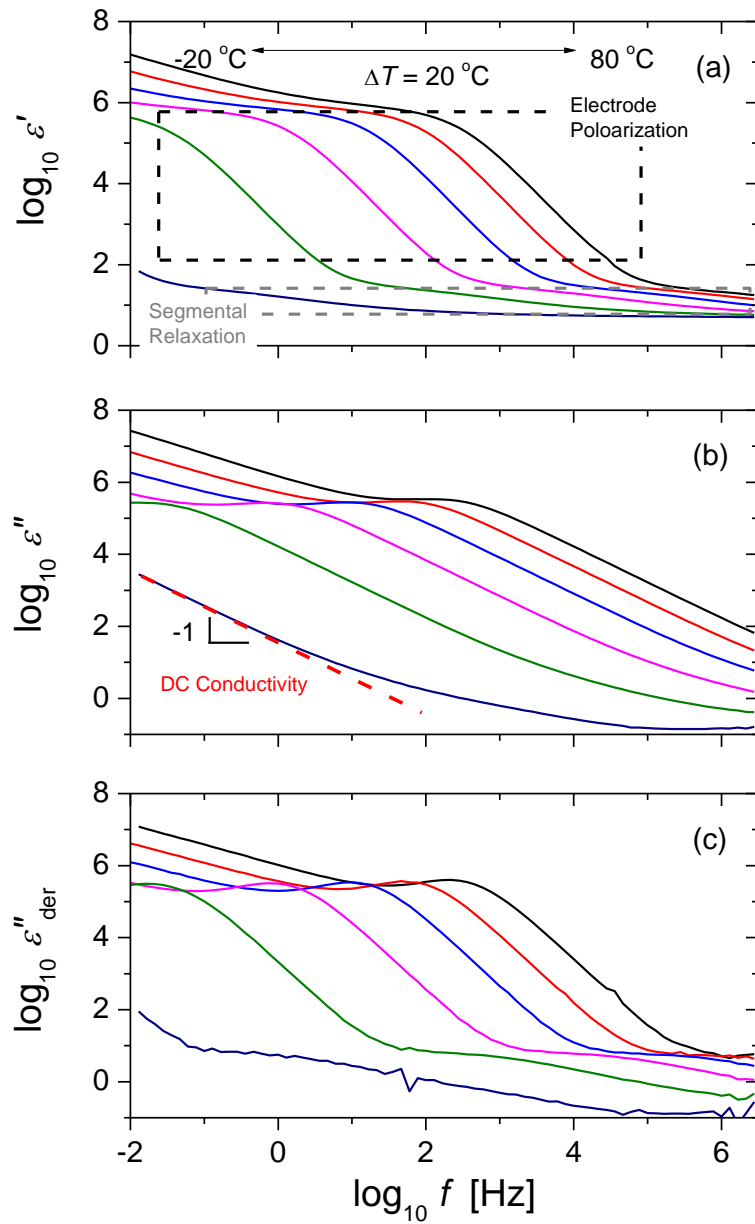
Figure 4.1. Representative spectra of PVC-PPEOMEMA/LiTFSI (3 wt%). (a) Frequency dependence of the real part of dielectric permittivity ε'. The electrical response due to electrode polarization and segmental relaxation are highlighted by black and gray rectangles, respectively. (b) Frequency dependence of the imaginary part of dielectric permittivity ε''. The red dashed line indicates the contribution due to dc conductivity. (c) The corresponding derivative spectra.

As being demonstrated in Chapter 2 and 3, information about ionic conductivity and segmental relaxation in these polymer electrolytes can be obtained simultaneously from the dielectric spectroscopy measurements. The complex permittivity spectra was modeled by Eq.2.17. The relaxation time τ_{max} is related to the Havriliak-Negami relaxation time τ_{HN}, the shape parameters α and β by Eq.2.14.[87] Because the segmental loss peak is typically covered by conductivity, the structural relaxation time τ_S is estimated from the maximum in the derivative of the real part of permittivity ε'. The (apparent) molar conductivity (Λ) can be calculated from the total salt concentration c_{tot} assuming complete dissociation): $\Lambda = \sigma/c_{tot}$.

The ionic conductivity and polymer segmental relaxation time of these samples follow Vogel–Fulcher–Tammann (VFT) type temperature dependence. Temperature dependence of the segmental relaxation time and ionic conductivity is given in Fig.4.2. It can be seen clearly that in samples PPEOSt-PSt/LiClO$_4$ (0.3%), PMOEOMSt/LiClO$_4$ (0.3%) (Fig.4.2d and 4.2e), segmental relaxation time and conductivity have very different temperature dependence. On the other hand, in the rest of the samples PVEC-PVAc/LiTFSI (50%) (Fig. 4.2a) PVEC-PMEA/LiTFSI (30%) (Fig. 4.2b) PVC-PPEOMEMA/LiTFSI (3 wt%) (Fig.4.2c), the segmental relaxation time and conductivity have same temperature dependence. The solid (red) curves are the fits of experimental data using the VFT equation. According to the convention, at the glass transition temperature (Tg), the structural relaxation time $\tau_S = 100$ s. (black arrows in Fig.4.2a-e) Tg from DSC measurement agrees well with the extrapolated VFT fit of the dielectric relaxation time. This agreement supports the assignment of the primary dielectric

100
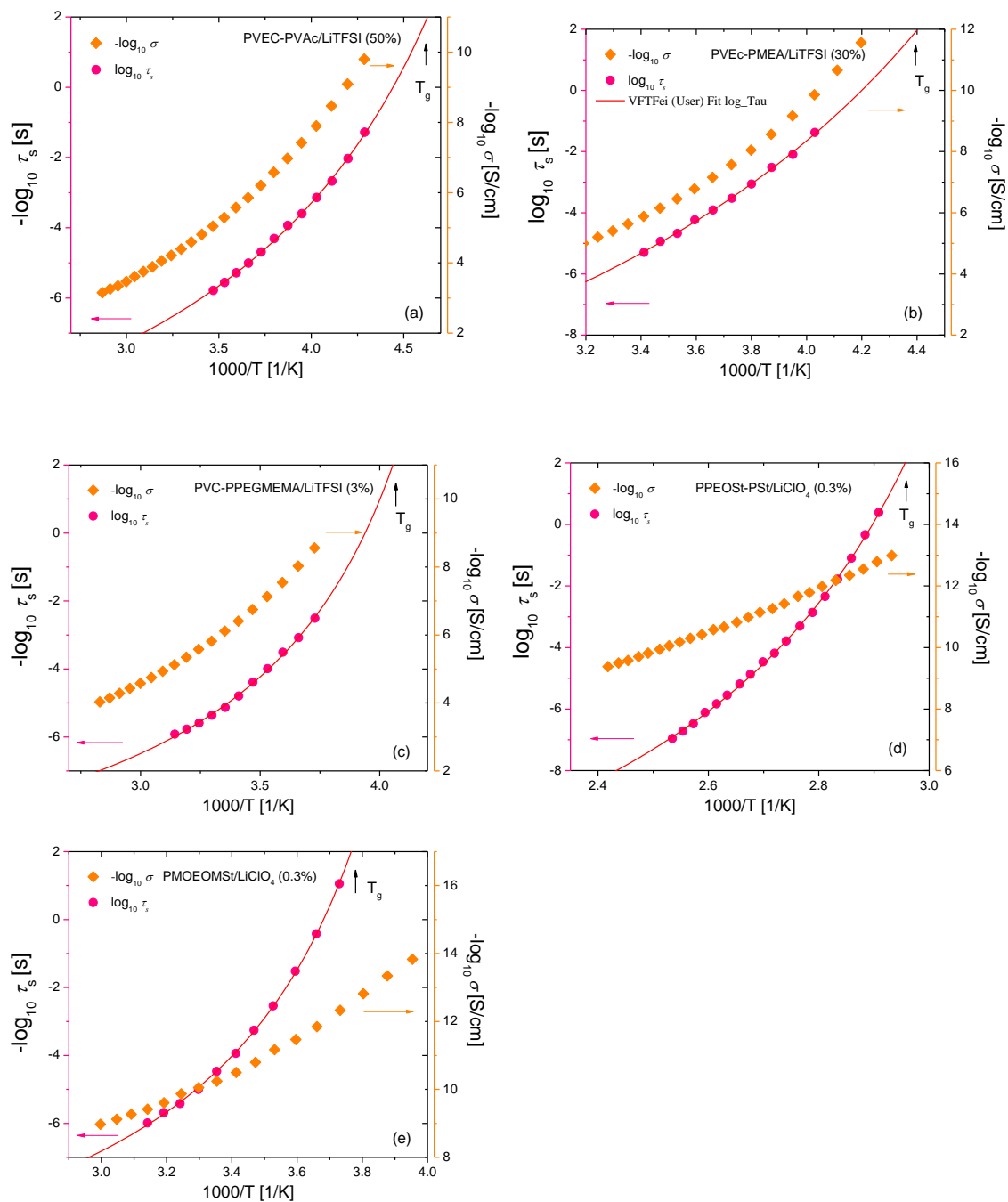
Figure 4.2. Temperature dependence of the segmental relaxation time and ionic conductivity in (a) PVEC-PVAc/LiTFSI (50%) (b) PVEC-PMEA/LiTFSI (30%) (c) PVC-PPEOMEMA/LiTFSI (3 wt%). (d) PPEOSt-PSt/LiClO₄ (0.3%) (e) PMOEOMSt/LiClO₄ (0.3%) The solid (red) curves are the fits of experimental data using the VFT equation: and. The black arrows point at the Tg value obtained from the BDS, where the structural relaxation time equals100s

relaxation as the polymer segmental (structural) relaxation. In the next chapter, it will be shown that this is not always the case that the main dielectric relaxation peak might be originated from conductivity relaxation.

The two quantities, molar conductivity (Λ) and segmental relaxation time (τ_S), determined by the dielectric spectroscopy, will serve as the basis for the analysis of ionic transport in polymer electrolytes in this Chapter.

4.4 Discussion

4.4.1 The Classic Walden plot analysis

In this section, the relation between the (apparent) molar conductivity (Λ) and structural relaxation time (viscosity for small molecules) in small molecules will be investigated using the concept of Walden rule.[26, 157] (Details of Classic Walden rule see Chapter 1.) In this work, dilute LiCl aqueous solution is used as the reference. Since the limiting molar conductivity in water does not vary significantly from one ion to another, the choice of reference is not critical for our analysis. For example, the limiting molar conductivities at infinite dilution of LiCl and KCl are 114.97 and 149.79 $Scm^2\ mol^{-1}$, respectively.[158] On the scale of a Walden plot, which typically covers more than 10 orders of magnitude on both horizontal and vertical axes, such a small difference is not important. Fig. 4.3 describes the relation between molar conductivity to fluidity for various ionic conductors. The inorganic glass $(AgI)_{0.5}(AgPO_3)_{0.5}$ appears in the top-left corner of the Walden plot,
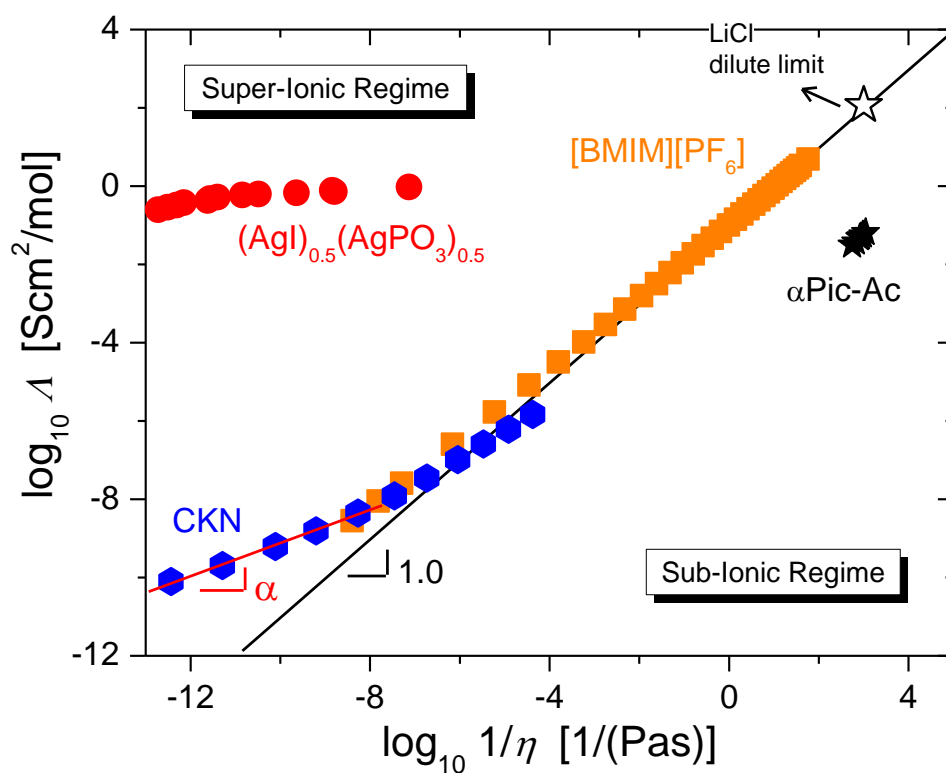
Figure 4.3. Relation of molar conductivity (Λ) to fluidity ($1/\eta$) for various ionic conductors. CKN stands for the ionic glass former $[Ca(NO_3)_2]_{0.4}[KNO_3]_{0.6}$.[159] αPic-Ac stands for α-picolinium acetate.[25] The data of $(AgI)_{0.5}(AgPO_3)_{0.5}$ is from ref. [160] and [161]. The open black star represents the dilute LiCl aqueous solution at room temperature,[162] and is used as the reference for ideal Walden line.

exhibiting superionic behavior. In contrast, the protic ionic liquids α-picolinium acetate (αPic-Ac) fall into the subionic regime, due to their low ionicity (low free-ion concentration).[25] Ionic melt $[Ca(NO_3)_2]_{0.4}[KNO_3]_{0.6}$ (CKN) stays on the ideal line at high temperatures (high fluidities), but moves into the superionic regime in the vicinity of the glass transition, due to the well-known decoupling between ionic conductivity and structural relaxation in CKN.

The slope α is related to the degree of decoupling ε though equation: $\varepsilon = 1 - \alpha$. "Good" electrolyte, ionic liquids [BMIM][PF$_6$] falls very close to the ideal line of the Walden plot, exhibiting a universal behavior. This means that the ionic transport in these samples is closely connected to their fluidity, and the relation $\mu \sim \eta^{-1}$ holds.

4.4.2 The Modified Walden Plot Analysis

Since according to the classical theory, $\mu \sim \tau_s^{-1}$ should be valid for both small molecule and polymeric electrolytes, we can use this relation as the basis for extending the Walden plot analysis to polymers, and this modification makes it possible to directly compare the molar conductivities of the studied polymer electrolytes to those of other well-known ionic conductors. Moreover, since $\sigma = pq\mu$, we can arrive at $\Lambda/q = \sigma/pq = \mu$. This equation implies a simple fact that the molar conductivity of free ion is directly related to the electrical mobility. In other words, Λ and μ_q only differ by a constant, which is the amount of charges carried by an ion (q). Combining with the Walden rule, it is clear that the question becomes what the relation is between the ion mobility (μ) and the rate at which the polymer matrix rearranges its local structure ($1/\tau_S$) in small molecules and polymer electrolytes.

Fig. 4.4 presents the relationship of apparent molar conductivity (Λ) to structural relaxation rate ($1/\tau_S$) for various electrolytes (modified Walden plots), including aprotic ionic liquids (ILs) [BMIM][PF$_6$], [BMIM][TFA][163], aqueous LiCl solution (24%)[164], and the molten salt CKN[165]. Because of the Maxwell relation ($\eta=G_g\tau_S$), the behavior of these electrolytes in the modified Walden plot (Fig. 4.4) is very similar to that in the traditional Walden plot (Fig. 4.3).

The ILs and LiCl/H$_2$O fall close to the ideal line of the Walden plot, because of their strong coupling between ionic transport and structural relaxation.[166, 167] CKN also follows the ideal line at high temperatures (short τ_S), but deviates near the glass transition, showing the well-known superionic behavior. Similar to ILs, the flexible polymers PEO and PPO lie almost perfectly on the ideal line, indicating a strong coupling of ionic transport to structural relaxation and good ion solvation. Although only two samples are shown here, this is in fact a universal behavior for all PEO and PPO based electrolytes, regardless of polymer molecular weight and salt concentration.[168, 169] In the case of polyethers, the Walden plot provides a simple estimate for the rate of segmental relaxation required to achieve conductivity $\sim 10^{-3}$ S/cm.

Lithium content in PEO even at 50 wt% of salt LiTFSI is only ~ 1.2 wt%. Thus the required molar conductivity to reach $\sigma = 10^{-3}$ S/cm should be ~ 0.6 Scm^2/mol, even if we assume that all salts are completely dissociated. In polymers like PEO and PPO this is possible only when segmental relaxation is faster than $\sim 10^{-8}$ s (Fig. 4.4), which can be achieved only at temperatures much higher than ambient temperature.
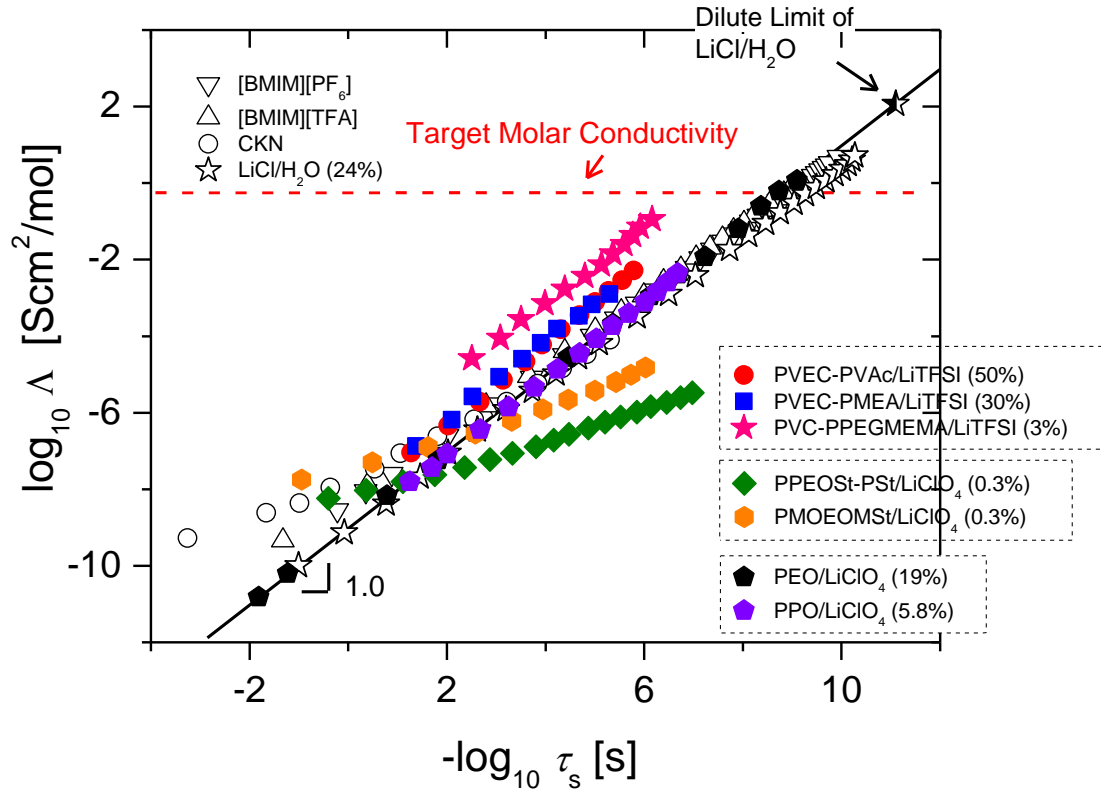
Figure 4.4. Relationship of apparent molar conductivity (Λ) to structural relaxation rate ($1/\tau_S$) for various electrolytes (modified Walden plots). The PEO data are taken from Ref. [114]. The horizontal dashed line indicates the target molar conductivity required to achieve $\sigma = 10^{-3}$ S/cm in PEO/LiTFSI system. The calculation is based on a polymer electrolyte with 50 wt% of LiTFSI, assuming the density is 1.0 g/cm^3 and complete salt dissociation.

In contrast to the behavior of PEO and PPO, strong decoupling of ionic conductivity from segmental dynamics is found in the rigid (fragile) polymers PMOEOMSt and PPEOSt-PSt. In these samples, the relation between Λ and τ_S can be described by a fractional Walden's rule: $\Lambda(\tau_s)^{\alpha}$=const. where $\alpha < 1$. This implies that the ionic conductivity is much less sensitive to the temperature change than the structural relaxation. As a result, PMOEOMSt

and PPEOSt-PSt appear in the superionic regime in the vicinity of the glass transition. The most surprising results come from carbonate-based polymers: they stay well above the ideal line, exhibiting superionic behavior over the entire studied temperature range. In particular, PVC-PPEGMEMA/LiTFSI (3%) has a molar conductivity two orders above the ideal line. This result reveals that the rate of ionic motion in these polymers is much faster than the rate of structural relaxation. The molar conductivity in these polymers is significantly higher than in the traditional polymer electrolyte PEO at the same τ_S. While the slope α for styrene-based polymers is significantly smaller than 1.0, α in carbonate-based polymer is close to 1.0. This suggests that the interaction between ions and the polymer matrix may play an important role in determining the coupling between ionic transport and structural relaxation (in terms of temperature dependence). The weak interaction between the ions and the polymer matrix might be the cause for different temperature dependence of conductivity and segmental relaxation in PPEOSt-PSt and PMOEOMSt.

4.4.3 Consideration of True Free Ion Concentration

The Walden plot analysis in Fig.4.4 is carried out under the assumption of complete salt dissociation. In reality, only a small fraction of ions exists as "free ions", due to the mediocre solvating power of polymers. The use of apparent molar conductivity (Λ) thus underestimates the true mobility of free ions. In order to estimate the true molar conductivity of free ions (Λ_{True}), we adopt an empirical method based on the analysis of the electrode polarization (EP) effect in dielectric spectroscopy. This method is based on the Macdonald-

Trukhan model of electrode polarization,[97, 98, 170-174] Fig. 4.5 presents the temperature

dependence of (a) free-ion number density n evaluated from the electrode polarization effect

using the Macdonald-Trukhan model. Solid lines denote Arrhenius fits. $n = n_0 \exp(-E_{dis}/$

$k_B T)$ (b) the temperature dependence of free-ion fraction n/n_{tot}, the fraction of free ion

number density in total ion number density, where the Arrhenius fits are extrapolated to

infinitely high temperature, i.e., 1000/ T = 0. The horizontal dashed line indicates the limit of

100 % dissociation. (Fig.4.5b)

The total ion number density n_{tot} is calculated from the total amount of salt in the

solution, under the assumption of complete dissociation, density equals 1g cm^{-3}:

$$n_{tot} = density \times salt\ wt\%/salt\ MW \times 2 \times N_A \qquad (4.1)$$

in which, salt wt% is the salt weight percentage, salt MW is the formula weight of the salt, N_A

is the Avogadro's number. Thus, the apparent salt concentration can be written as:

$$c_{tot} = n_{tot}/(2 \times N_A) \qquad (4.2)$$

If the electrode polarization analysis could indeed quantitatively capture the free-ion

concentration, one would expect $\log 10(n/n_{tot})$ should be zero at 1000/ $T = 0$.

However, Fig. 4.5b shows different scenarios. For the three polycarbonate based

polymer electrolytes, PPO/LiClO$_4$, and LiCl/H$_2$O, the extrapolations of all five samples fall

much below the ideal dissociation line. For the two polystyrene based polymer electrolytes,

PPEOSt-PSt/LiClO$_4$ shows an extrapolation a little above the ideal dissociation line while

PMOEOMSt shows an extrapolation more or less agrees with the idea assumption.
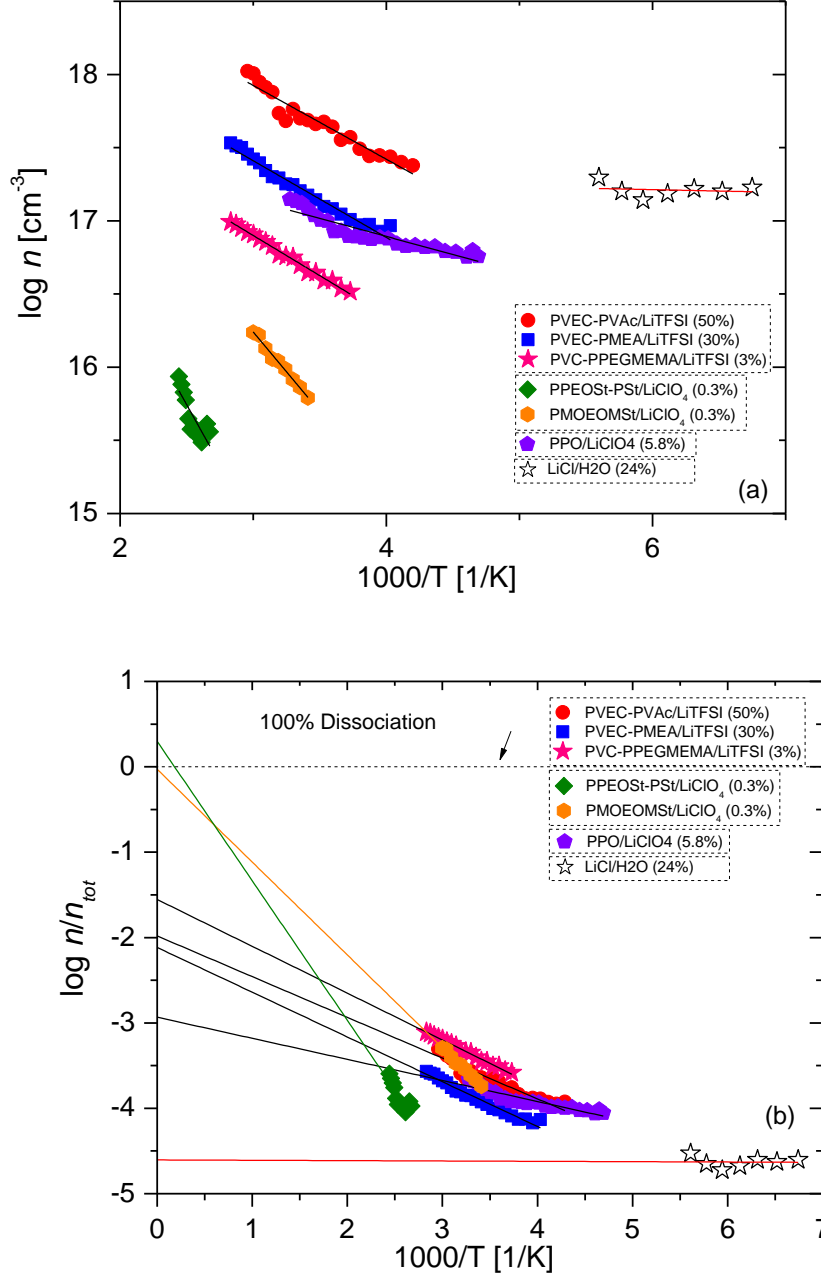
Figure 4.5 Temperature dependence of (a) free-ion number density n evaluated from the electrode polarization effect using the Macdonald-Trukhan model. (b) the temperature dependence of free-ion fraction n/n_{tot}, the fraction of free ion number density in total ion number density, where the Arrhenius fits are extrapolated to infinitely high temperature, i.e., $1000/T = 0$. Solid lines denote Arrhenius fits. The horizontal dashed line indicates the limit of 100 % dissociation.

Therefore, additional corrections are introduced in order to account for the failure of the Macdonald-Trukhan model at high salt concentration (either above idea dissociation line or below). (Details of analysis can be found in Chapter 2) Fig. 4.6 shows the temperature dependence of the calculated free-ion number density before and after the correction for sample PVEC-PVAc/LiTFSI (50%). Inset: calculated diffusivity before and after correction. As it is seen from Fig. 4.6, the free ion density of sample PVEC-PVAc/LiTFSI was elevated after correction. The fitting parameters n_0, E_{dis}, n_{tot} and the corresponding correction factor of all samples are presented in Table 4.2.

Thus, the (true) molar conductivity Λ_{true} ($\Lambda_{true} = \sigma/c_{true}$) can be calculated from the true salt concentration c_{true} with the corrected free ion density dissociation $\tilde{n}$:

$$c_{true} = \tilde{n}/(2 \times N_A) \tag{4.1}$$

After correction, the the true molar conductivities estimated using this approach for all the polymer electrolytes appear in the superionic regime (Fig. 4.7). Even PPO is slightly above the ideal line.

It should be stressed that the analysis of the apparent molar conductivity in Fig. 4.4 is model independent, whereas the analysis in Fig. 4.7 clearly depends on the validity of the EP model. Thus the general trend depicted in Fig. 4.7 should be regarded only as qualitative, i.e., the true molar conductivities of many polymer electrolytes are indeed in the superionic regime. These results demonstrate a strong decoupling of the rate of charge transport from the rate of structural relaxation in polymers. The largest decoupling is found in
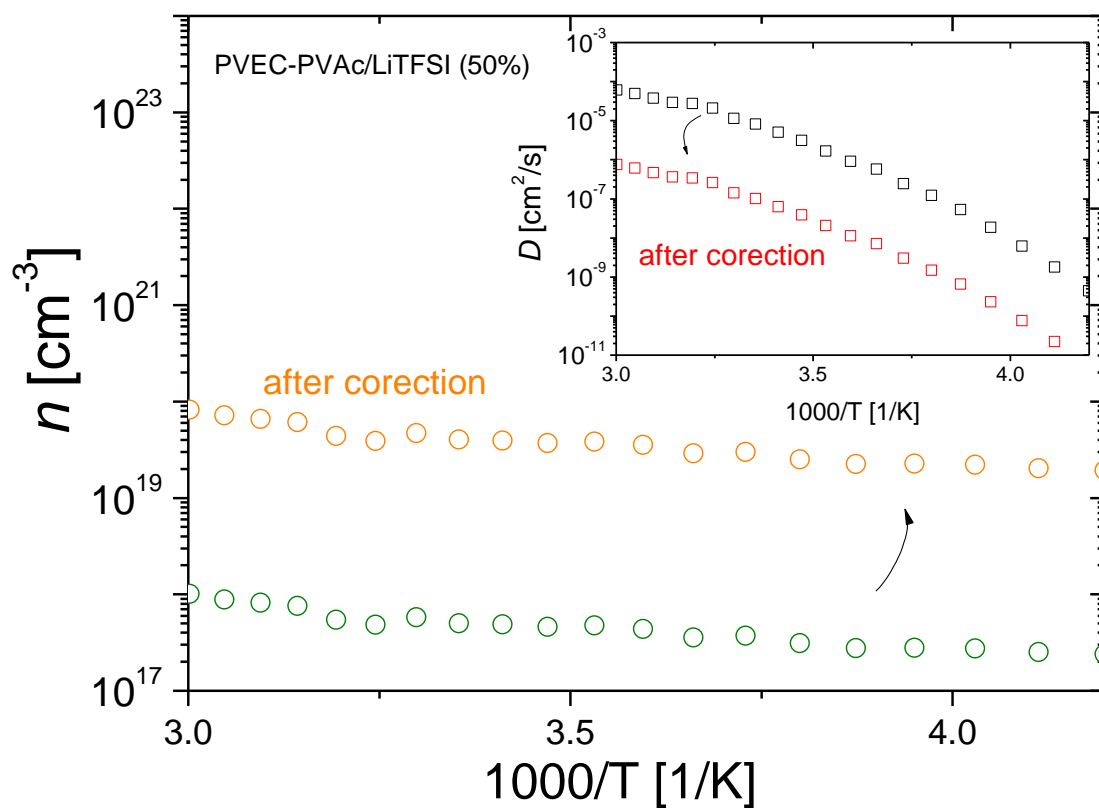
Figure 4.6. The temperature dependence of the calculated free-ion number density before and after the correction for sample PVEC-PVAc/LiTFSI (50%). Inset: calculated diffusivity before and after correction.

PMOEOMSt/LiClO$_4$ near Tg, where the true molar conductivity of the sample is more than

six orders of magnitude higher than that in the "ideal" LiClO$_4$ dilute solution at the same rate

of structural relaxation.
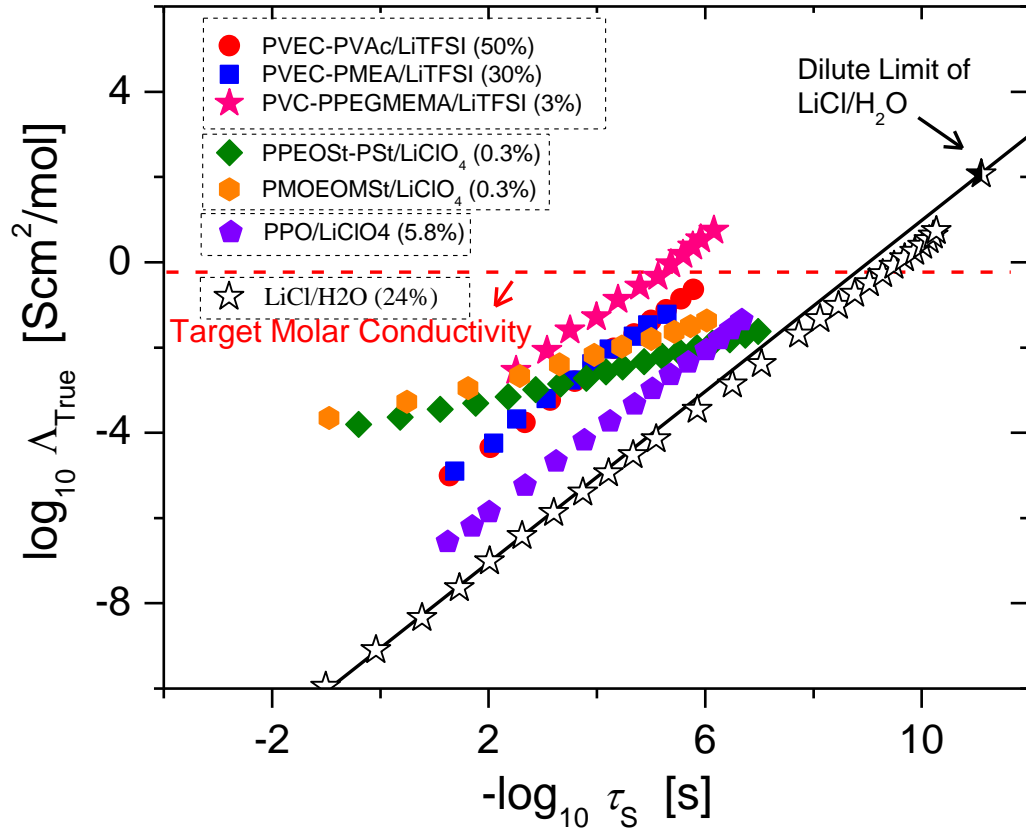
Figure 4.7. Relationship of true molar conductivity (Λ_{True}) to structural relaxation rate ($1/\tau_S$) for various electrolytes. The open stars: LiCl/H$_2$O (24%).

Table 4.2 Summary of Samples

Sample Abbreviation	Salt (weight percentage%)	n_0 (cm^{-3})	n_{tot} (cm^{-3})	E_{dis} (eV)	$\dfrac{n_{tot}}{n_0}$
PVEC-PVAc	50	2.74×10^{19}	2.22×10^{21}	0.10	80.9
PVEC-PMEA	30	9.64×10^{18}	1.26×10^{21}	0.10	130.5
PVC-PPEGMEMA	3	3.51×10^{18}	1.26×10^{20}	0.11	35.9
PPEOSt-PSt	0.3	6.75×10^{19}	3.4×10^{19}	0.32	0.5
PMOEOMSt	0.3	3.17×10^{19}	3.4×10^{19}	0.21	1.07
PPO	5.8	7.59×10^{17}	6.51×10^{20}	0.04	858.7

4.4.4 Comparison with Small Molecule Electrolytes

Previous studies have shown that most of the liquid electrolytes, including aqueous and non-aqueous solutions, protic and aprotic ionic liquids, fall either very close to or below the "ideal" Walden line (Fig. 4.4 [BMIM][PF$_6$], [BMIM][TFA], aqueous LiCl solution (24%)[164]).[25, 37, 175] Additionally, liquid electrolytes typically exhibit a slope of ~1.0 on the Walden plot, because of strongly coupled ionic conductivity.

On the other hand, as revealed by the Walden plot analysis in Fig. 4.4 and Fig. 4.7, the intrinsic relationship between ionic transport and structural relaxation in polymer electrolytes can be fundamentally different from that in small-molecule liquid electrolytes. First, the ionic transport in polymers can be much less sensitive to the change of temperature. This is demonstrated by the fractional Walden rule behavior of the styrene-based polymers. Second, at a given structural relaxation rate, the ionic transport in polymers can be much faster than in

small-molecule liquid electrolytes, making polymers appear in the superionic regime of the modified Walden plot.

As was discussed in Chapter 1, in small molecule liquid electrolytes, the size of the transporting ions are comparable to that of the solvating molecules. Moreover, ions transport together with the solvation shell. As a result, ion migration is strongly coupled to the structural relaxation of the medium. On the other hand, the size of the polymer segments are relatively large than the solvated ion. Therefore, ions might be able to "hop" to available sites without complete segments reorientation. (Fig. 4.8) Besides, unlike the situation in liquid electrolytes, the polymer segments ("solvation shell") do not transport with the ion migration.

Thus, it is reasonable that after correction polymer electrolytes appear in the superionic regime of the modified Walden plot. Moreover, the Walden plot analysis also reveals that polymers with relatively rigid backbones provide stronger decoupling of ionic conductivity and higher true molar conductivity than flexible polymers such as PEO. According to the general entropy theory proposed by Dudowicz [17, 19, 21] et al. and other recent experimental works[176], rigid polymer backbones cannot pack tightly, leaving extra space ("free volume") for diffusion of small ions even when segmental dynamics are very slow. As a result, the rate of ionic diffusion is significantly faster than the rate of segmental relaxation (Fig. 4.7). Moreover, in some polymers the ionic motion is much less sensitive to temperature than the segmental dynamics. The polymers with relatively rigid backbones therefore exhibit true superionic behavior. Flexible polymers are able to form tightly packed structures[19, 176] and in this case ionic diffusion is possible only when segments are moving. In addition,
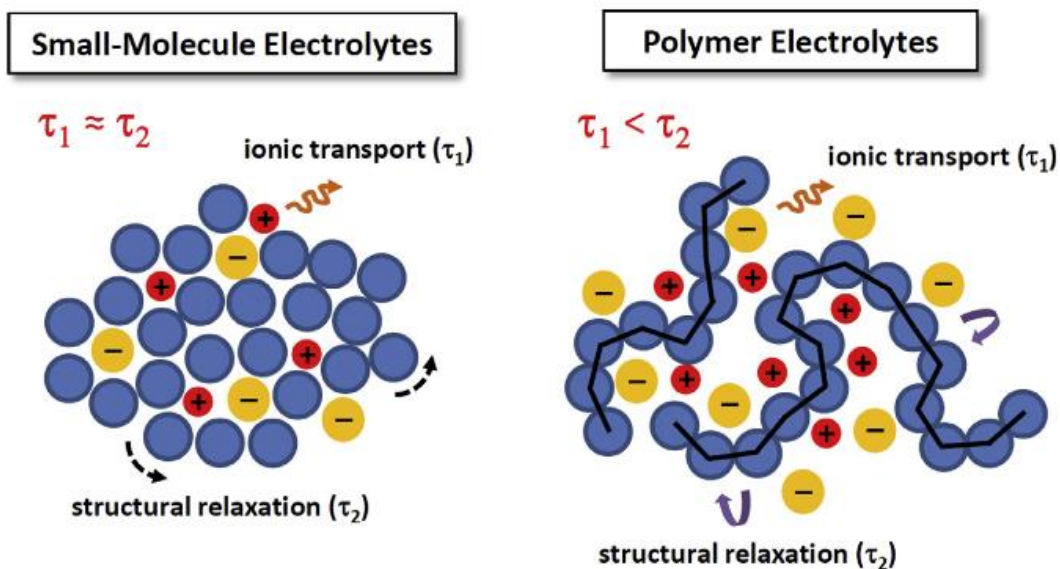
Figure 4.8. Illustration of the qualitative difference between the ion transport mechanisms in small molecules and polymers. In small molecules, the characteristic time scales for ionic transport ($\tau 1$) and structural relaxation ($\tau 2$) are comparable. In contrast, fast ion transport can occur in polymer electrolytes.

lithium ions are coordinated with the oxygen atoms in the backbone of PEO and PPO. All these factors lead to strong coupling of ionic conductivity to segmental dynamics in such polymers. Reaching the desired level of ionic conductivity in these types of polymers requires very fast segmental dynamics (Fig. 4.4).

Although the Λ_{True} of PPEOSt-PSt and PMOEOMSt shows very desirable "superionic" feature, the actual ionic conductivities in these polymers are still relatively low, due to their low free ion concentrations and relatively high T_gs. These finding have important implications for the design of solid polymer electrolytes. By improving solvating properties of

these polymers it might be possible to achieve the desired level of ionic conductivity at segmental relaxation time $\tau_S \sim 10^{-4}$ s (Fig. 4.7) or even slower. In this case, properly balancing decoupling with ion solvation would be critical for the future success.

4.4.5 Comparison with Benchmarks in the Literature

Fig.4.9 shows the temperature dependence of the ionic conductivity of three representative polymer electrolytes in our study, together with those of other representative electrolytes used in lithium batteries[177, 178]. Relatively high ionic conductivity has been achieved in the carbonate-based polymer electrolytes, i.e., PVEC-PVAc/LiTFSI (50 wt%), PVEC-PMEA/LiTFSI (30 wt%), PVC-PPEGMEMA/LiTFSI (50 wt%)]. At high temperatures, the ionic conductivity of PVEC-PVAc/LiTFSI (50 wt%) is similar to that of PEO/LiTFSI (45 wt%)[179], which is one of the best traditional dry polymer electrolytes. At low temperatures, PVEC-PVAc/LiTFSI (50 wt%) is even slightly better than PEO/LiTFSI (45 wt%), partially due to the decoupling. At 60 °C, the conductivity of PVEC-PVAc/LiTFSI (50 wt%) is approximately 20 times higher than that of P(STFSILi)-*b*-PEO-*b*-P(STFSILi)[178], which represents the state of the art for single-ion polymeric lithium conductors.

Nevertheless, the ionic conductivity of PVEC-PVAc/LiTFSI (50 wt%) reaches the level required for many applications (10^{-3} S/cm)[70] only at high temperatures. Although the Walden plot analysis (Fig. 4.4 and Fig. 4.6) reveals that PVC-PPEGMEMA exhibits the highest degree of decoupling in terms of the relation between Λ (Λ_{True}) and τ_S, the electrolyte

116

based on PVEC-PVAc actually gives the highest level of conductivity (inset of Fig. 8). This is

due to the fact that the Tg of PVEC-PVAc/LiTFSI (50 wt%) is much lower than that of PVC-

PPEGMEMA/LiTFSI (50 wt%) (Tg = 216 K for the former, and 243 K for the later).

Achieving high ionic conductivity at a given temperature requires both a high degree of

decoupling and a relatively low glass transition temperature (short τ_S). It should also be noted

that carbonate-based polymers are generally not stable under high voltage. Although as a

model system, the carbonate-based polymers in this study have provided invaluable insights,

more stable chemical structures such as sulfone- and sulfolane might be considered in the

future design of superionic polymers[180-182].

4.5 Conclusion

In conclusion, the analysis of the relation between ionic transport and structural

relaxation has revealed a fundamental difference between the ion transport mechanisms in

polymers and small-molecule liquid electrolytes. Motion of ions is usually coupled to

structural relaxation in small-molecule electrolytes and high ionic conductivity is possible due

to very short structural relaxation time. In contrast, the ionic transport in polymer electrolytes

can be strongly decoupled from structural relaxation, especially in polymers with relatively

rigid structures. This result clearly demonstrates that decoupling of ionic conductivity from

the segmental dynamics should be the key target property for polymer electrolytes. Ions may

utilize the loose local packing structure of long chains, which is not available in small

molecules, and diffuse through the polymer matrix even when segmental dynamics are slow
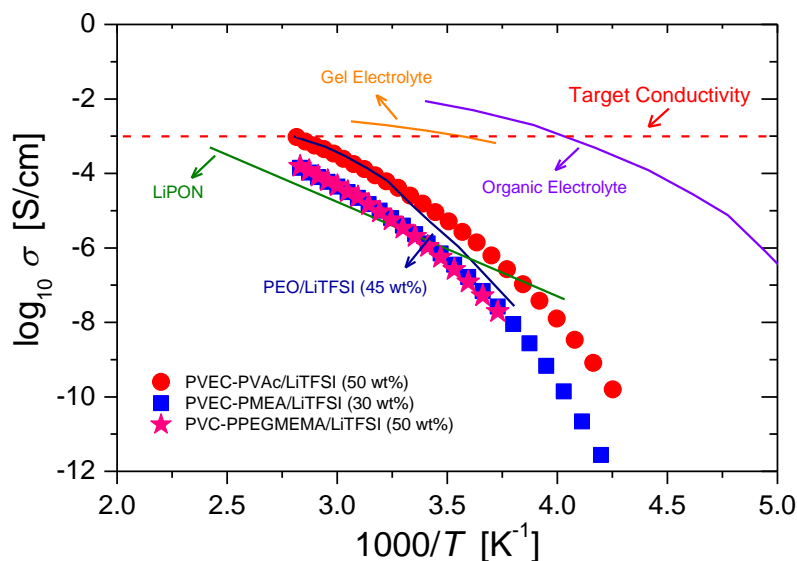
Figure 4.9. Temperature dependence of ionic conductivity of three representative polymer electrolytes, together with those of other lithium conductors.[183] LiPON stands for the lithium phosphorous oxynitride electrolyte. The gel electrolyte is 1M LiPF6/EC-PC (50:50 vol%) in 10 wt% of polyvinylidene difluoride-hexafluoropropylene.[184] The organic electrolyte is 1M LiPF6/EC-PC (50:50 vol%).[185] The PVEC-PVAc/LiTFSI (50 wt%) sample out-performs the conventional PEO/LiTFSI (45 wt%) electrolyte[186] in the studied temperature range. The dashed line presents the target value of conductivity $\sigma = 10^{-3}$ S/cm that is important for many applications.[15]

or frozen. This behavior is analogous to superionic conductors such as AgI, where the smaller silver ions can "slip" through the quasi-lattice of the larger iodide ions. Combined with strong ion solvating properties, the decoupling concept may lead to the design of a new class of superionic polymer electrolytes with desired level of ionic conductivity at ambient temperature.

CHAPTER V

ION CONDUCTION IN POLYMERIZED IONIC LIQUIDS WITH DIFFERENT PENDANT GROUPS

5.1 Introduction

In Chapter 3 and 4, different Li^+ salts are dissolved in various polymers. In this chapter, a new type of materials called "polymerized ionic liquids" (PolyILs) is studied. The structure of ionic liquids is incorporated into the backbone or the side chain of the polymer, forming this new type of polymer. In this case, either cation or anion is imbedded in the polymer.

Ionic liquids (ILs) are molten salts at room temperature composed mostly of organic ions. ILs have received great attention in recent years due to their unique electrochemical behavior and distinct properties such as high conductivity, negligible vapor pressure, non-flammability and high thermal stability.[187-191]

To utilize the unique properties of ILs for polymer electrolytes purpose, we can either physically blend ILs with the polymer or to chemically bond them. The former could be achieved by either using ILs as the main conducting medium supported in a polymer matrix or using ILs as plasticizers in polymer electrolytes. The latter, as mentioned in the beginning, is

to incorporate ILs structure into either the backbone or side groups of polymers, resulting the so-called polymerized ionic liquids (PolyILs).[192-195] PolyILs were first synthesized in the 1970s.[196] PolyILs present an opportunity to combine the intrinsic high ionic conductivity of ILs and superior mechanical properties of polymers. Moreover, concentration polarization has always been a problem in the battery field. Due to the difference in ion diffusivity, the transference numbers of cation and anion are not equal. As a result, a concentration gradient would build up. Single ion conductors in which either the cation or anion is bonded to the polymer, i.e. only the untethered ion can transport, can solve the problem. As for PolyILs, either cation or anion is incorporated into the polymer, thus only the counterion can transport in the polymer electrolyte, making the transference number of the untethered ions close to unity. This advantage, together with those properties mentioned above make PolyILs promising candidates as solid polymer electrolytes for energy storage and electrochemical device applications.[39, 197] By modifying the structures of the polymer and pairing the polymer with different organic cations or anions, a seemingly endless list of PolyILs can be synthesized. Therefore, it is of utmost importance to have a clear understanding of the structure-property relationships in PolyILs to guide the design of their structures to achieve desired properties.

Extensive efforts have been put into the development of PolyILs with high ionic conductivities. But so far there has been no clear understanding on how structural parameters control ionic conductivity in PolyILs. In the majority of aprotic ILs, the ion transport and structural dynamics are closely coupled.[198-200] A line with slope of 1 is formed between dc conductivity, σ_0, versus the characteristic frequency, ω_c. (Fig. 5.1) It indicates that the ion

transport has the same temperature dependence as the structural dynamics. The decoupling in aprotic ILs is significantly weaker than that observed in other glass-forming liquids with similar fragility.[36]
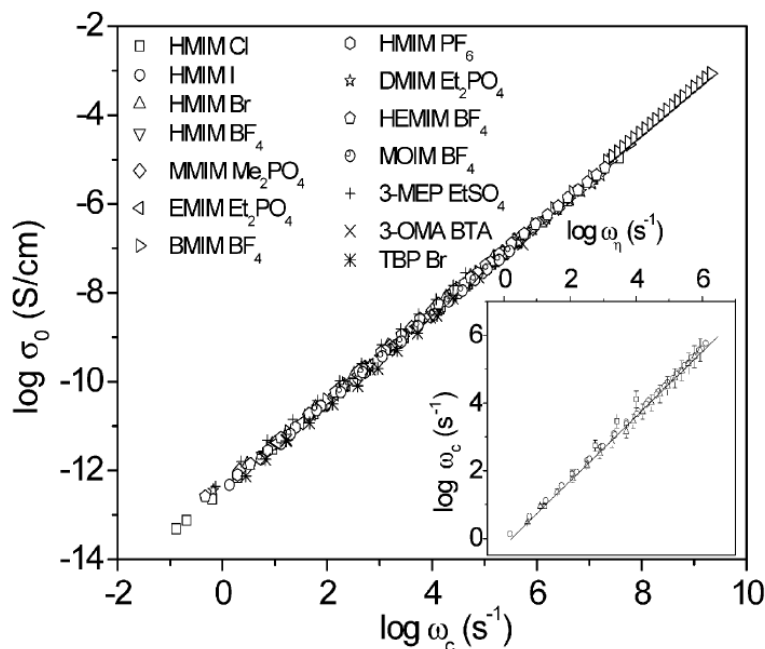
Figure 5.1. DC conductivity, σ_0, versus the characteristic frequency, ω_c, for different liquids as indicated. This plot experimentally demonstrates the universality of charge transport in ionic liquids. Inset: correlation of $\omega_c(T)$ with the characteristic frequency, ω_η (T), corresponding to structural relaxation time obtained from viscosity by applying the Maxwell relation (ref [198]).

Ohno and co-workers have been developing PolyILs for fast ion conductors since 1998.[201-207] They prepared a series of vinylimidazole based PolyILs[203-205, 207, 208] in which the

charged end was distanced from the main chain with ether groups. They suggested that the flexibility of the charged site controlled the ion transport. Colby and co-workers[209, 210] studied the influence of the different pendant groups attached to imidazolium cation on conductivity. It was reported that samples with shorter alkyl chain, despite their higher Tgs, showed slightly higher conductivity than samples with a longer alkyl tail, and replacing the alkyl tail on the imidazolium cation with diethyleneoxy units led to even higher ionic conductivity. The latter might be due to the higher mobility of the ether tail. Cation structures have also been varied to study their effect on ionic conductivity of PolyILs.[211] Imidazolium-type cation was found to be the best among those being studied. A recent study by Colby and co-workers[212] proposed that the molecular volume of the repeating unit for the prepared PolyILs governs Tg and the dielectric constant and therefore the ionic conductivity.

As discussed in Chapter 3, the classical theory predicts that the ionic transport in polymers is controlled by the structural (segmental) dynamics of the polymer matrix.[152, 213] Our study of PPG mixed with $LiClO_4$ agrees with this coupling relation. Long and co-workers[214] found that the absolute ionic conductivity among several alkyl-substituted vinylimidazolium-based PolyILs with different alkyl chain length and counter ion size showed an inverse dependence on Tg. Neutral monomers have been copolymerized with PolyILs to suppress Tg, which resulted in higher ionic conductivity in work done by Elabd and co-workers.[215]

Since structural relaxation in dry polymer electrolytes at ambient temperature is much slower than in traditional liquid molecular electrolytes (including ILs), strong coupling between ion conductivity and segmental (structural) dynamics severely limits the ion

conductivity in polymer electrolytes. In Chapter 4, we have demonstrated that decoupling of the ionic conductivity from segmental relaxation was observed in several polymers electrolytes, and higher degree of decoupling might be obtained in polymers with higher fragility due to stronger packing frustration.

Indeed, several works have shown that the ion transport in PolyILs might be different from the traditional polymer electrolytes. In work by Nakamura et al.,[216, 217] conductivity of poly(1-ethyl-3-vinylimidazolium)-based PolyILs displayed Vogel-Fulcher-Tammann (VFT) type of temperature dependence at high temperatures and crossed over to an Arrhenius type as the temperature decreased. They proposed that the ionic conductivity was modulated by ion pair formation and dissociation process, which was faster than the segmental relaxation of the polymer. The Arrhenius feature is typical for superionic conductors, in which the ionic transport and structural relaxation are decoupled.[218] The deviation of temperature dependence of conductivity from VFT to Arrhenius was also reported in recent work by Colby and co-workers[219] and by Sangoro et al.[220] The latter work proposed that the ionic transport mechanism in vinyl-3-pentyl imidazolium based PolyIL is different from that in the corresponding monomer. While the ion transport and structural dynamics are closely coupled in the monomer IL in Sangoro et al.'s study, they found that the ion transport was strongly decoupled from the structural dynamics after polymerization of the monomer.[220]

Since PolyILs are made of IL structures incorporated in polymer repeating units, it is not clear whether decoupling in PolyILs will follow the change of fragility, as it is in polymers doped with salts, or the decoupling will be weak as in regular aprotic ILs. An

improved understanding of the relationship between chemical structure and ion transport in PolyILs on the molecular-level is therefore highly desirable.

In this chapter, a systematic study of PolyILs using broadband dielectric spectroscopy (BDS), together with rheology and differential scanning calorimetry (DSC) is performed. All samples have the same degree of polymerization, same backbone structure, and same anion (TFSI⁻), and the only different part is the pendant groups attached onto the charged site. The variation of pendant groups alters the dielectric, mechanical and thermal properties of our samples. The analysis reveals that in contrast to the coupled mechanism found in aprotic ionic liquids, the ionic transport in our samples is decoupled from the segmental dynamics. Fragility indexes of our samples were extracted from dynamic mechanical measurements, and change in the pendant group structures resulted in a range of fragility from 84 to 134. Combining the data from Chapter 4 and literatures, we found that the degree of decoupling increases with increasing fragility. We suggest that the correlation between the degree of decoupling and fragility is related to the polymer packing efficiency.

5.2 Materials and Methods

Materials. 2-(Dimethylamino) ethylacrylate ($> 97\%$, TCI) was deinhibited via passing through activated alumina column. Ethylacetate (Fischer Scientific), bromomethyl methyl ether (COC, Oakwood Chemical), 2-bromoethyl methyl ether (C_2OC, Oakwood Chemical), 1-bromo-4-methoxy butane (C_4OC, Matrix Scientific), bromo-2-(2-methoxyethoxy) ethane (C_2OC_2OC, Alfa Aesar), dimethylformamide (DMF, anhydrous, Alfa Aesar), hexanes (BDH),

tetrahydrofuran (THF, BDH), bis(trifluoromethane)sulfonimide lithium salt (LiTFSI, Aldrich, >99%) were used as received. 2,2-azobis(isobutyronitrile) (AIBN, 99%, Aldrich,) was purified by recrystallization prior to use.
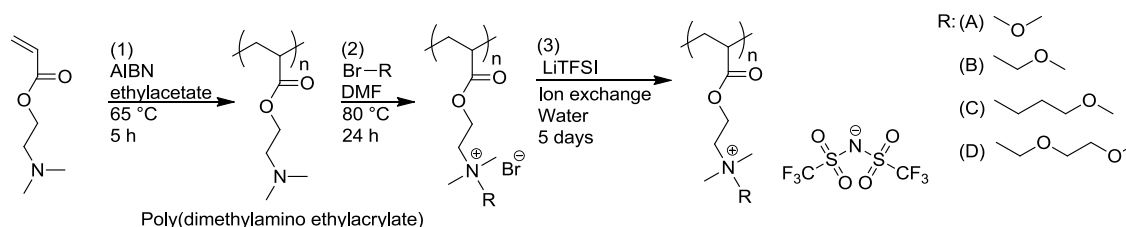
Scheme 5.1 Synthesis of polymerized ionic liquids with different pendant groups

Synthesis of Quaternary Ammonium Ionic Liquid Polymers. 2-(Dimethylamino) ethylacrylate (113 g, 120 mL) and AIBN (0.2 wt%, 226.3 mg) were dissolved in ethyl acetate (190 mL). Argon was bubbled through the solution for 20 min. The reaction proceeded for 5 h at 65 °C (Scheme 1, (1)). The resulting poly(dimethylamino ethylacrylate) was precipitated into hexanes for 5 times. The precipitated polymer was dried at 40 °C in vacuum for 24 h and the isolated yield was 52% (58 g). ^{1}H NMR (400 MHz, D$_2$O, δ) Poly(dimethylamino ethylacrylate): 1.3-2.0 ppm (br,-CH_2CH-), 2.1-2.2 ppm (br,-N(CH_3)$_2$), 2.2-2.4 ppm (br,-CH$_2$CH-), 2.4-2.8 ppm (br,-CH$_2$CH_2N(CH$_3$)$_2$), 3.8-4.3 ppm (br,-CH_2CH$_2$N(CH$_3$)$_2$)

Quaternization of poly(dimethylamino ethylacrylate) was performed via reaction with alkyl ether bromide (COC, C$_2$OC, C$_4$OC, C$_2$OC$_2$OC, Scheme 1 (2)). All the quaternization reactions were performed with 1.1 equimolar of alkyl ether bromide in anhydrous DMF at 80 °C for 24 h. The resulting quaternized poly(dimethylamino ethylacrylate) bromide was washed with THF several times. The isolated polymer was dried at 40 °C in vacuum for 24 h. All the ^{1}H NMR spectra for the synthesized quaternary ammonium bromide ionic liquid polymers showed quantitative shifting of a dimethyl amine peak (δ 2.1-2.2 ppm) to N,N'-dimethyl ammonium peak (δ 3.0-3.2 ppm), confirming the quantitative quaternization.

^{1}H NMR (400 MHz, D$_2$O, δ):

Poly[(2-(acryloyloxy)ethyl)-N,N'-dimethyl-N-methoxy methyl-ammonium bromide] 1.5-2.1 ppm (2H, br, -CH_2CH-), 2.2-2.7 ppm (1H, br, -CH$_2$CH-), 2.7-3.1 ppm (6H, br, -N(CH_3)$_2$-), 3.1-3.5 ppm (3H, br, -N(CH$_3$)$_2$CH$_2$OCH_3), 3.5-3.8 ppm (2H, br, -OCH$_2$CH_2N(CH$_3$)$_2$-), 4.2-4.6 ppm (2H, br, -OCH_2CH$_2$N(CH$_3$)$_2$-), 4.6-4.8 ppm (2H, br, -N(CH$_3$)$_2$CH_2OCH$_3$)

Poly[(2-(acryloyloxy)ethyl)-N,N'-dimethyl-N-methoxy ethyl-ammonium bromide], 1.5-2.1 ppm (2H, br, -CH_2CH-), 2.2-2.7 ppm (1H, br, -CH$_2$CH-), 3.0-3.2 ppm (6H, br, -N(CH_3)$_2$-), 3.2-3.4 ppm (3H, br, -N(CH$_3$)$_2$CH$_2$CH$_2$OCH_3), 3.5-3.6 ppm (2H, br, -N(CH$_3$)$_2$CH_2CH$_2$OCH$_3$), 3.7 ppm (2H, br, -OCH$_2$CH_2N(CH$_3$)$_2$-), 3.7-3.9 ppm (2H, br, -N(CH$_3$)$_2$CH$_2$CH_2OCH$_3$), 4.3-4.6 ppm (2H, br, -OCH_2CH$_2$N(CH$_3$)$_2$-)

Poly[(2-(acryloyloxy)ethyl)-N,N'-dimethyl-N-methoxy butyl-ammonium bromide], 1.4-1.6 ppm (2H, br, -N(CH$_3$)$_2$CH$_2$CH$_2$CH_2CH$_2$OCH$_3$), 1.5-2.0 ppm (2H, br, -CH_2CH-), 1.7-

1.8 ppm (2H, br, -N(CH$_3$)$_2$CH$_2$C*H$_2$CH$_2$CH$_2$OCH$_3$), 2.2-2.7 ppm (1H, br, -CH$_2$C*H*-), 3.0-3.2 ppm (6H, br, -N(C*H$_3$*)$_2$-), 3.2-3.3 ppm (3H, br, -N(CH$_3$)$_2$CH$_2$CH$_2$CH$_2$CH$_2$OC*H$_3$*), 3.3-3.6 ppm (4H, br, -N(CH$_3$)$_2$C*H$_2$*CH$_2$CH$_2$C*H$_2$*OCH$_3$), 3.6-3.8 ppm (2H, br, -OCH$_2$C*H$_2$*N(CH$_3$)$_2$-), 4.2-4.6 ppm (2H, br, -OC*H$_2$*CH$_2$N(CH$_3$)$_2$-)

Poly[(2-(acryloyloxy)ethyl)-N,N'-dimethyl-N-(methoxy ethoxy) ethyl-ammonium bromide], 1.5-2.0 ppm (2H, br, -C*H$_2$*CH-), 2.2-2.7 ppm (1H, br, -CH$_2$C*H*-), 3.0-3.2 ppm (6H, br, -N(C*H$_3$*)$_2$-), 3.2-3.3 ppm (3H, br, -N(CH$_3$)$_2$CH$_2$CH$_2$OCH$_2$CH$_2$OC*H$_3$*), 3.4-3.6 ppm (2H, br, -N(CH$_3$)$_2$C*H$_2$*CH$_2$OCH$_2$CH$_2$OCH$_3$), 3.6-3.7 ppm (4H, br, -N(CH$_3$)$_2$CH$_2$CH$_2$OC*H$_2$*C*H$_2$*OCH$_3$), 3.7-3.8 ppm (2H, br, -OCH$_2$C*H$_2$*N(CH$_3$)$_2$-), 3.8-4.0 ppm (2H, br, -N(CH$_3$)$_2$CH$_2$C*H$_2$*OCH$_2$CH$_2$OCH$_3$), 4.3-4.6 ppm (2H, br, -OC*H$_2$*CH$_2$N(CH$_3$)$_2$-)

The ion-exchange reaction from bromide ion to bis(trifluoromethane)sulfonimide (TFSI) ion was performed using 1.2 equivalent of LiTFSI in water for 5 days (Scheme 1 (3)). The TFSI‾ exchanged ionic liquid polymers include poly[(2-(acryloyloxy)ethyl)-N,N'-dimethyl-N-methoxy methyl-ammonium TFSI] (A), poly[(2-(acryloyloxy)ethyl)-N,N'-dimethyl-N-methoxy ethyl-ammonium TFSI] (B), poly[(2-(acryloyloxy)ethyl)-N,N'-dimethyl-N-methoxy butyl-ammonium TFSI] (C), poly[(2-(acryloyloxy)ethyl)-N,N'-dimethyl-N-(methoxy ethoxy) ethyl-ammonium TFSI] (D). The isolated yield indicated nearly quantitative ion exchange with TFSI‾ (89-97%). Considering some loss during separation of the resulting polymer, the isolated yields suggest the nearly quantitative exchange with TFSI‾.

Polymer Characterization. Size exclusion chromatography (SEC) measurements were performed in THF/5% triethylamine mobile phase at 40 °C at flow rate of 1 mL/min

using a Polymer Labs GPC-120 size exclusion chromatography. The GPC-120 is equipped

with Polymer Laboratories PLgel; 7.5x300 mm; 10 μm; 500, 10^3, 10^5, and 10^6 Å, a Precision

Detector PD2040 (two angle static light scattering), Precision Detector PD2000DLS (dynamic

light scattering), Viscotek 220 differential viscometer, and a Polymer Labs refractometer

calibrated with narrow polydispersity polystyrene standards. The RI increment (dn/dc) was

calculated online. The resulting poly(dimethylamino ethylacrylate) showed M_n 22300 g/mol,

M_w 39600 g/mol, PDI 1.78 (absolute molecular weight from LS detector) and Tg = -46 °C

(DSC). Elemental analysis for carbon, nitrogen, hydrogen, and sulfur were performed by

Galbraith Laboratories, Inc. (Knoxville, TN) and the elemental analysis results further

confirmed the nearly quantitative TFSI exchange within error range for all the resulting

polymers.
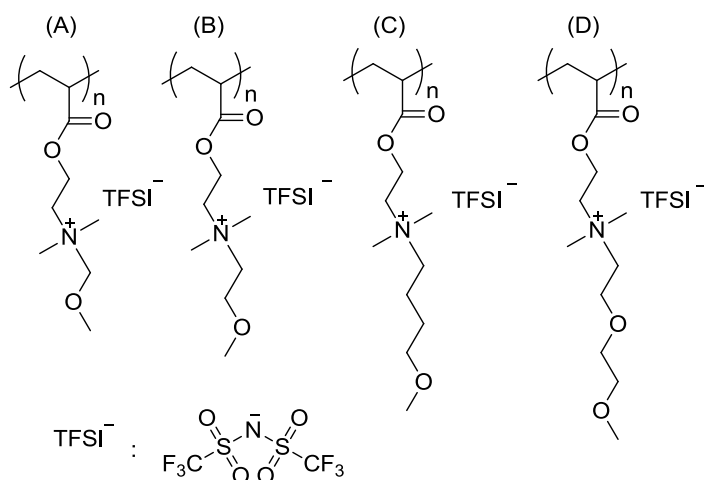
Figure 5.2. Chemical Structures of polymerized ionic liquids with different pendant groups.

Differential Scanning Calorimetry (DSC). Samples were dried in vacuum oven for a week at room temperature and then at 80 °C for at least 1 day until DSC results showed no difference in Tg. The samples for DSC measurements were loaded in aluminum hermetic pans and dried in vacuum oven at 60 °C overnight before pans being sealed. A TA thermal instrument Q2000 was used to record the heat flow. Temperature-modulated DSC (TMDSC) measurements were performed using the following procedure: equilibrate at 80 °C, isothermal for 5 min, and then cool to -60°C at 3 °C/min with a modulation of ±1 °C /min and heat back to 80 °C. In general, Tg was taken as the mid-point of the step in the heating process in the reversing heat flow signals. By using TMDSC instead of traditional DSC, we were able to accurately determine the glass transition temperature.

Broadband Dielectric Spectroscopy (BDS). Broadband dielectric measurements were performed in the frequency range of $10^{-2} – 10^{7}$ Hz, using a Novocontrol Concept 80 system, which includes an Alpha-A impedance analyzer, a ZGS active sample cell interface, and a Quatro Cryosystem temperature control unit. Samples were placed between two gold-plated electrodes separated by a Teflon spacer. Samples were dried in the same way as described above. Before measurements, each sample was loaded within the spacer on the bottom electrode and dried under vacuum at 80°C to remove bubbles. The experiments proceeded from high to low temperatures. The samples were equilibrated at the highest temperature (80 °C) for at least 3 h and the measurement results were reproducible, indicating that the samples didn't degrade and there was no residual solvent. The samples were equilibrated at each temperature for 20 minutes before the dielectric measurements.

Rheology. Small-amplitude oscillatory shear (SAOS) measurements of PolyILs were performed on an AR2000ex rheometer. Samples were dried in the same way as described in the DSC measurements. The experiments were performed in parallel plate geometry using 3 mm plates. The measurements near the glass transition temperature were also repeated with 4 mm plates and we confirmed that these experiments were free from the effect of instrument compliance.[221] The temperature was controlled by an environmental test chamber with nitrogen as the gas source. Strain sweep measurement was done before SAOS measurement to make sure the SAOS response was within the linear region.

5.3 Results

5.3.1 Dielectric Spectra

Representative dielectric spectra of sample B at T = 270.15 K are shown in Fig. 5.3. There are three major components: (1) a dielectric relaxation process around the first crossover point of ε' and ε'' (2) dc conductivity in the intermediate-frequency region of ε'', and (3) the sharp increase in the low-frequency region due to the electrode polarization (EP) effect.

The complex permittivity spectra can be modeled by the superposition of one Havriliak-Negami (HN) function, corresponding to the relaxation peak,[87] a dc conductivity term and an EP term (Fig. 5.3a) by eq.2.17.The conductivity obtained from the fitting procedure is essentially identical to that from the direct reading of $\sigma'(\omega)$ in the dc plateau
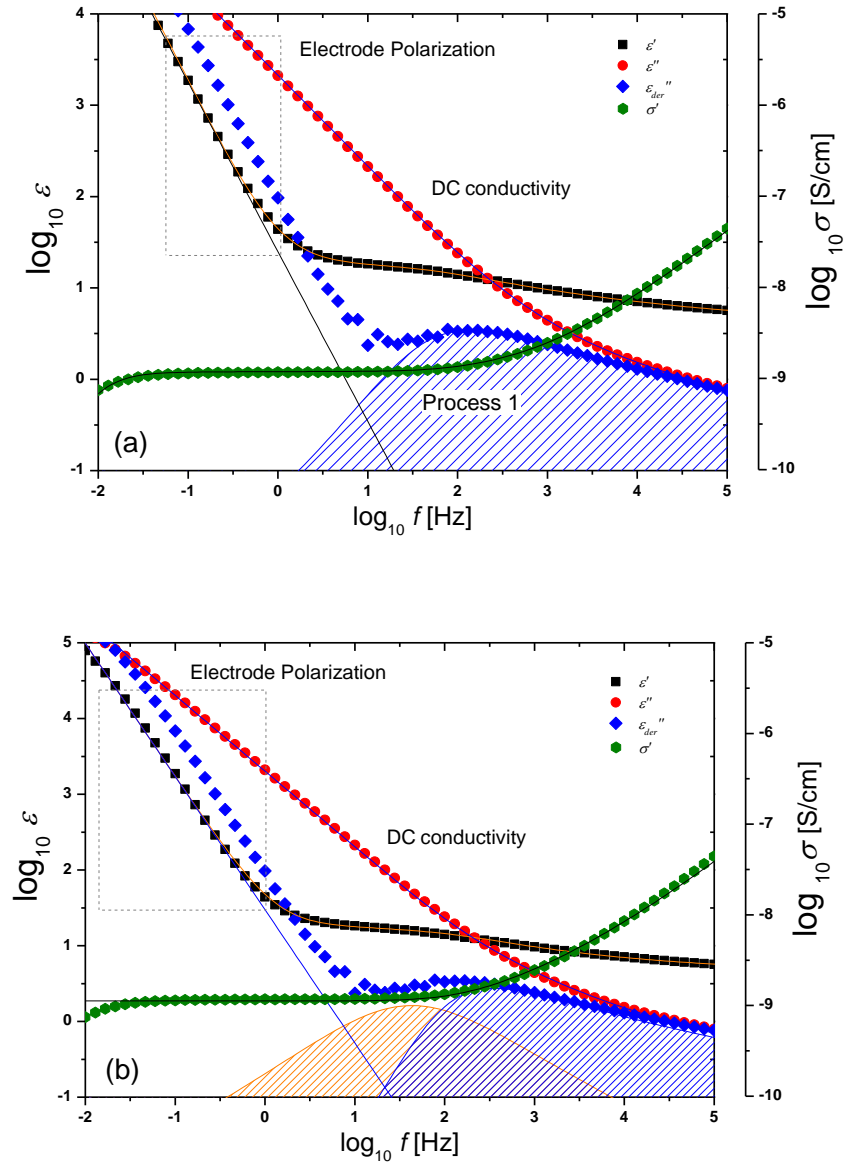
Figure 5.3. Dielectric spectra of sample B at T = 270.15 K (solid symbols). There are three major components: (1) a dielectric relaxation peak around the first crossover point of ε' and ε'', marked as "process 1" in the derivative spectrum; (2) DC conductivity in the intermediate-frequency region of ε'', and (3) the electrode polarization effect that appears as the sharp increase of ε' and ε''_{der} in the low-frequency region. (a) Lines show the fit of the dielectric spectrum by HN model with one relaxation process. (b) Lines show the fit of the dielectric spectrum by Dyre model and two relaxation processes are used to achieve a good fit.

region (Fig.5.3a). The relaxation time τ_{max} is related to the Havriliak-Negami relaxation time τ_{HN}, the shape parameters α and β by eq.2.14.[87]

As demonstrated in Chapter 2, 3, 4, relaxation peaks in $\varepsilon''(\omega)$ might be completely hidden by the conductivity in dielectric spectra of materials with high dc conductivity. The derivative spectra was used to assist the data analysis.[88, 89] A pronounced relaxation process is revealed in the derivative spectrum (blue diamonds in Fig. 5.3a). ε' and ε'' were fitted using eq.2.17, while the position of the peak maximum in the derivative spectra were used to determine the initial fitting parameters. Fitting curves are showing as solid lines in Fig. 5.3.

It should be noted that another function, which is usually applied for ILs studies,[36] can also be used to fit the dielectric spectrum (Fig. 5.3b). To differentiate the two methods, we name the first one as "HN model" and the second one as "Dyre model" in this paper. In the Dyre model, the dielectric response is analyzed in terms of complex conductivity $\sigma^*(\omega) = i\omega\varepsilon_0\varepsilon^*(\omega)$, which includes the first term for ion transport (blue peak in Fig. 5.3b), and $A\omega^{-n}$ is added to fit the EP effect. The derivative spectrum clearly shows that the one term "Dyre model" is not enough to fit the spectrum. Another term which is fitted to a Havriliak-Negami relaxation function in conductivity notation has to be added to provide good fit of the data (orange peak in Fig. 5.3b). The complete function then has the form:

$$\sigma^*(\omega) = \sigma_0 \left(\frac{i\omega\tau_e}{\ln(1 + i\omega\tau_e)} \right) + i\omega\varepsilon_0 \left(\varepsilon_\infty + \frac{\Delta\varepsilon}{[1 + (i\omega\tau_{HN})^\alpha]^\beta} + A\omega^{-n} \right) \qquad (5.1)$$

where τ_e is the characteristic hopping time of an ion, τ_{HN} is the relaxation time from the Havriliak-Negami relaxation function.The HN model can describe the data in the entire

frequency range very well with less fitting parameters than the Dyre model. Thus, the HN model was used consistently throughout this Chapter.

5.3.2 Rheological Behavior

Small amplitude shear oscillation experiments were performed to verify the effect introduced by the different pendant groups on the viscoelasticity of our samples. Fig. 5.4 shows the master curves of the storage moduli b_{TG}' and the loss moduli b_{TG}'' constructed using the time−temperature superposition (tTS) principle, referenced to the labeled temperatures respectively. The tTS have been demonstrated to work well for PolyILs in the current molecular weight range.[20, 222] It worked for all our samples within the temperature range studied as demonstrated by the master plot of tan(delta) (see Supporting Information). In the terminal relaxation region, the characteristic slopes of terminal relaxation of viscoelastic liquids are observed, with $G' \sim \omega^2$ and $G'' \sim \omega$.

The segmental relaxation time at the referenced temperature is defined as $\tau_s = 1/\omega_0$ where ω_0 is the frequency at the cross point of G' and G'' ($G' = G''$) at high frequencies. ω_0 is sometimes determined at the frequency where the loss modulus has a maximum in the glassy region.[20, 223] However, since the loss modulus is strongly stretched at high frequencies, and the peak maximum is thus ambiguous, the cross point is chosen to represent the segmental relaxation time of all samples. It is well known that chain and segmental relaxations generally have different temperature dependencies, i.e. the shift factor is dominated by chain dynamics at high temperatures and controlled by segmental dynamics at low temperatures, thus giving
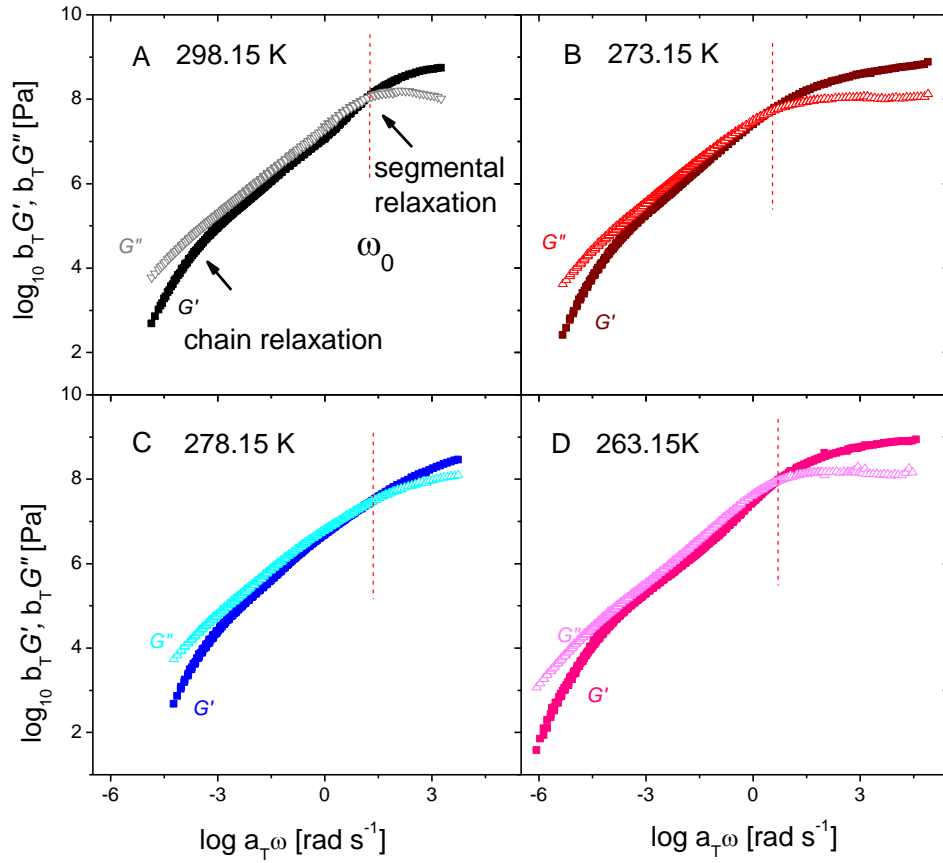
Figure 5.4. Storage and loss moduli (labeled as G′ and G″ near each curve) for all the samples. Master curves are constructed by using time-temperature superposition, referenced to the labeled temperatures respectively. The reference temperatures are Rheology-Tg + 13.1 K for A, Rheology-Tg + 11.8 K for B; Rheology-Tg + 21.7 K for C and Rheology-Tg + 13.2 K for D. (Rheology-Tgs are summarized in Table. 3.) It is generally accepted that chain relaxation governs the response at low frequencies while segmental dynamics dominate the response at high frequencies. The segmental relaxation time at the reference temperature is defined as τ_s $=1/\omega_0$ where ω_0 is the frequency at the point of G′ crossing G″ at high frequencies.

rise to the failure of tTS. While such a failure is not discernable in our oscillatory

measurement over a relatively narrow frequency range, it might nevertheless manifest itself

when we construct the temperature dependence of segmental relaxation time. Therefore,

although we expect our method of determining τ_s to be accurate near Tg, it might overestimate

τ_s at high temperatures. It is important to keep this fact in mind when we come to the

discussion of the relation between ionic transport and polymer segmental dynamics in section

5.4.2.

5.4 Discussions

5.4.1 Origin of the Main Dielectric Relaxation Peak

According to the linear response theory, the dielectric spectrum can be described in

terms of complex electric modulus $M^*(\omega)$, in addition to $\varepsilon^*(\omega)$, and $\sigma^*(\omega)$.[224, 225] The three

quantities are related by the following equations:

$$M^*(\omega) = 1/\varepsilon^*(\omega) = i\omega\varepsilon_0/\sigma^*(\omega)$$

(5.2)

To investigate the origin of the main dielectric relaxation peak, the dielectric spectra

of σ', ε', ε'', M'' are plotted together in Fig. 5.5.

A relaxation peak is clearly visible in the electric loss modulus $M''(\omega)$ (orange

symbols in Fig. 5.5). The frequency corresponding to the peak maximum gives the

conductivity relaxation time. Since the dielectric relaxation process is usually covered by the

dc conductivity in ε'', the derivative spectrum had to be used (green symbols in Fig. 5.5) to
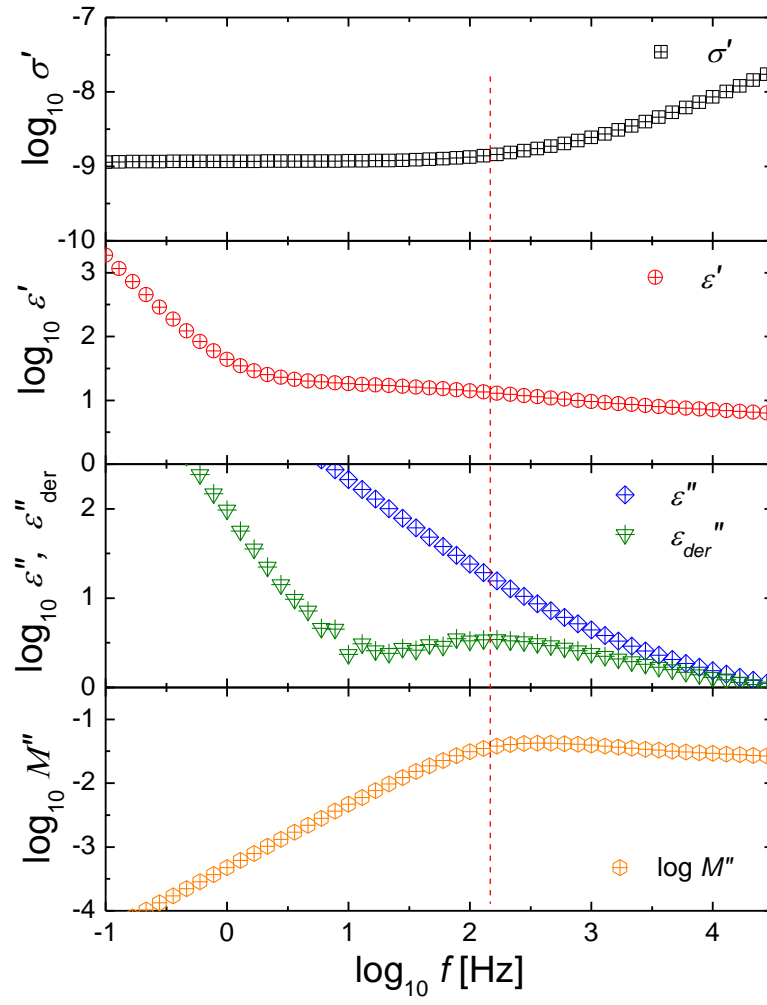
Figure 5.5. Conductivity, permittivity and electric modulus of sample B at T = 270.15 K. The red dashed line is a guide for the eye, indicating the position of the peak maximum revealed by the derivative spectrum (green). This frequency is close to the plateau region onset in σ' and to the frequency maximum of the electric modulus loss.

discriminate the relaxation process. The frequency maximum of the main relaxation process in ε''_{der} (indicated by the red dashed line) is close to the frequency of the plateau region onset in σ' and the peak maximum in the electric modulus loss, both of which are signs for the onset of conductivity relaxation. The conductivity relaxation time obtained from $M^*(\omega)$ is generally shorter than that read from ε''_{der}, which is also the case in our study in the temperature range studied.[226, 227]

The temperature dependence of the relaxation time of the main dielectric process τ_{max} determined from the HN model is presented in Fig. 5.6. Within the temperature range of study, τ_{max} shows Vogel-Fulcher-Tammann (VFT) type temperature dependence at high temperatures (eq.1.11).The temperature dependence of τ_{max} crosses over to an Arrhenius-type behavior at lower temperatures (eq. 1.12).

The glass transition temperature is usually defined as the temperature where the segmental (structural) relaxation time $\tau = 100$ or 1000 s. By extrapolating the VFT curves to $\tau = 100$ s, a glass transition temperature can be estimated. However, Tg determined from this method (under label Tg-VFT) falls far below the Tg obtained from the DSC (under label Tg-DSC) measurements (Fig. 5.6). This difference indicates that the primary dielectric relaxation peak does not correspond to the segmental relaxation of the polymer. It has been observed in several polymerized aprotic ionic liquids[18, 20, 23] and one polymerized protic ionic liquids[226] that the temperture dependence of conductivity or conducting ion related process usually exhibit a crossover from VFT to Arrhenius type of behavior around their glass transition temperature. This deviation of temperature dependence is similar to the behavior of the
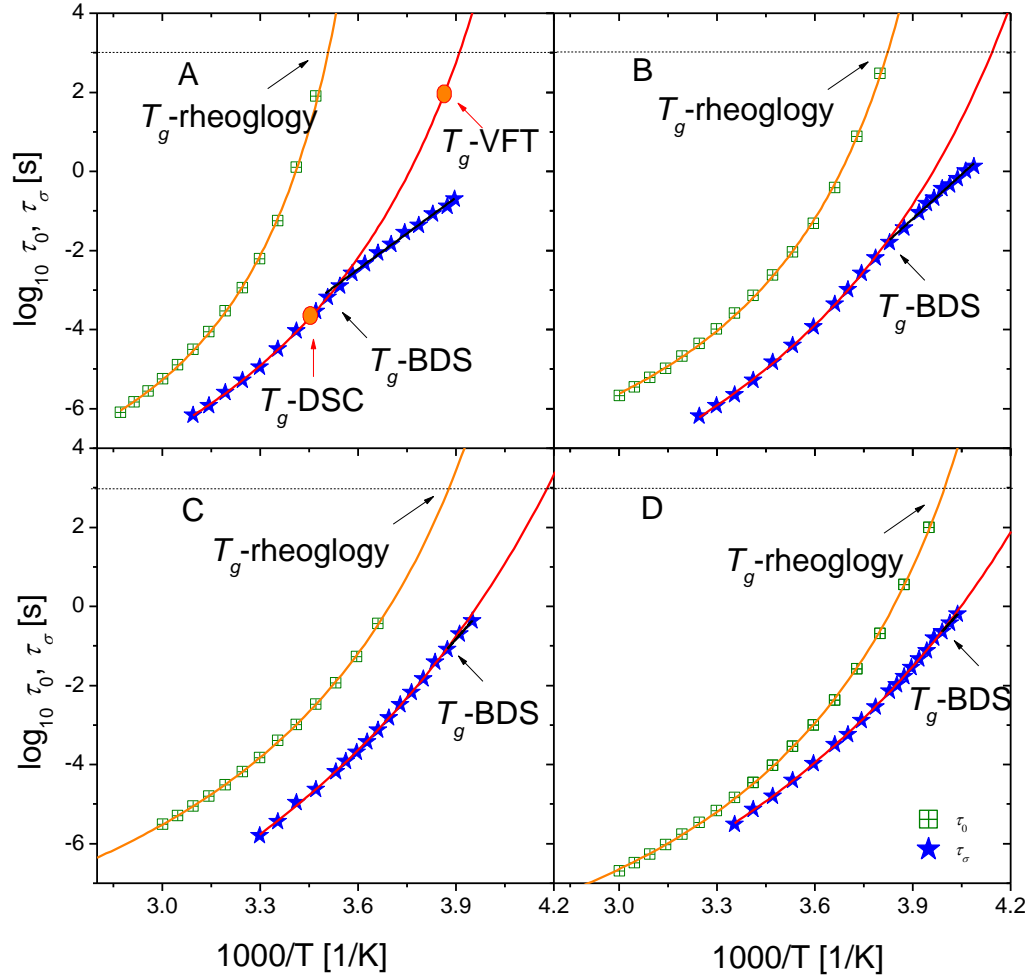
Figure 5.6. Temperature dependence of segmental relaxation time τ_0 measured by mechanical relaxation (squares) and the dielectric relaxation time τ_σ (stars). Solid lines are fits to the VFT and Arrhenius equations. The glass transition temperature from mechanical measurements (Tg-rheology) is determined at $\tau_s = 1000s$. The glass transition temperature from the dielectric measurements (Tg-BDS) is determined at the temperature where the crossover from VFT-type to Arrhenius-type occurred. DSC measurements were also performed and the glass transition temperatures obtained are listed in Table 3. Tgs acquired from those three different methods are in good agreement with each other. The two orange dots were used to represent the big difference between Tg from DSC (Tg-DSC) and the false Tg (Tg-VFT) determined by VFT extrapolation of the dielectric time to $\tau_\sigma = 100s$. These results clearly demonstrate that the main dielectric relaxation is not the segmental relaxation process.

primary dielectric process observed in our study. Thus, we ascribe the main dielectric

relaxation process to the conductivity relaxation rather than to the segmental relaxation.

Indeed, the VFT-to-Arrhenius crossover temperature agrees with the Tg obtained from the

DSC measurements (Fig. 5.6) and we assign the crossover temperature to Tg-BDS (Table

5.3). The VFT fitting parameters for the conductivity relaxation are presented in Table 5.1.

5.4.2 Decoupling of Ion Transport from Segmental Dynamics

According to the tradtional view, diffusion coefficient of a molecule/ion through a

liquid is determined by the structual relaxation time of the medium, τ_α, which is rationalized

by the Stokes-Einstein relation: $D \propto 1/\tau_\alpha$. In aprotic ILs, the ion transport is indeed found to

be strongly controlled by the structural dynamics.[198] The Stokes-Einstein relation is also

found to be valid for ion transport in poly(ethylene oxide),[114, 116] poly(propylen glycol)[228] and

other similar polymer electrolytes. It means that in these polymers ionic transport is

determined by the segmental relaxation.[152, 213, 228, 229] However, deviation from this

relationship, i.e. decoupling of the ion transport from the structural relaxation, has been found

in many ion conducting systems. For example, the ionic transport in protic ILs and protic

ionic conductors has been reported to be decoupled from the structural dynamics.[230, 231] The

decoupling behavior has also been observed in various polymer electrolytes with relatively

rigid structures.[78, 153]

Table 5.1 VFT Fit Parameters for the Temperature Dependence of τ_σ above Tg-BDS

	A	B	C	D
$\log \tau_0$	-13.2	-13.6	-13.9	-13.1
B	2071.3	2171.8	2307.3	2124.4
T_0	194.9	181.6	180.5	176.6

To investigate whether the ionic transport mechanism in PolyILs is the same as it is in their small molecule analogues, a comparison between the response from the dielectric measurement and the master curve constructed from mechanical measurement of sample B is presented in Fig. 5.7.

The conductivity relaxation time is determined as the reciprocal frequency ω_σ at the peak maximum of the loss electric modulus at high frequencies. The reciprocal frequency ω_0 at $G' = G''$ in the master curves provides estimates of the segmental relaxation time. The difference between ω_σ and ω_0 (indicated by the black dashed lines) is more than two orders, which clearly shows that the conductivity relaxation is significantly faster than the segmental relaxation at this temperature.
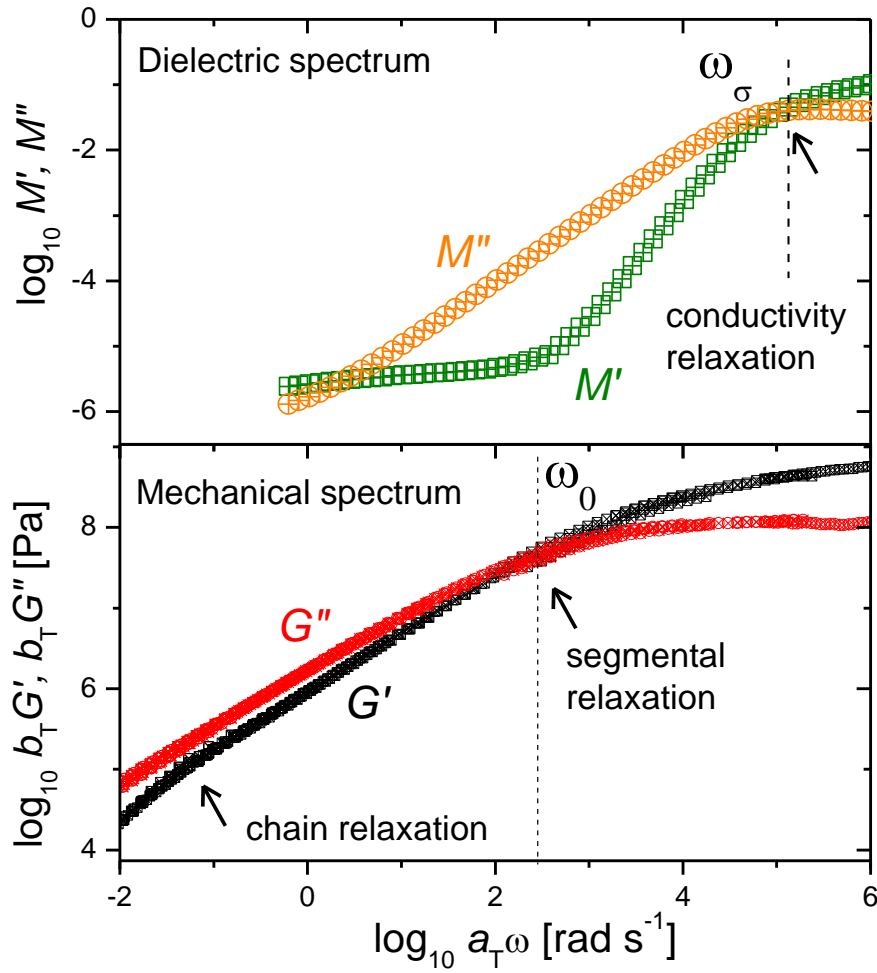
Figure 5.7. Comparison between the electrical modulus from the dielectric measurement and the master curves constructed from mechanical measurement of sample B at T = 288.15 K. The reciprocal frequency (labeled as ω_σ) at the peak maximum in the loss electric modulus gives the conductivity relaxation time. The reciprocal frequency at the crossing point of storage and loss modulus (G′ = G″) (labeled as ω_0) gives the estimation of segmental relaxation time. The difference between ω_σ and ω_0 is more than 2 orders.

The temperature dependencies of conductivity and segmental relaxation time are presented together in Fig. 5.6 for comparison. In the entire temperature range studied here, τ_s obtained from mechanical measurement follows VFT-type temperature dependence. The VFT fitting parameters are summarized in Table 5.2. The glass transition temperature, Tg-rheology, determined at temperature where $\tau_s = 1000$ s is listed in Table 5.3. The glass transition temperatures obtained from rheology, dielectric measurement (crossover temperature) and DSC are in good agreement with each other. The conductivity relaxation time τ_σ, as mentioned earlier, follows the VFT equation and deviates to the Arrhenius equation at the glass transition temperature. It is obvious (Fig. 5.3) that the conductivity relaxation time is shorter than the segmental relaxation time, indicating that the rate of ions diffusion is faster than the structual dynamics of the polymer matrix. The difference between the conductivity relaxation and the segmental relaxation becomes larger as temperature approaches the glass transtion temperature.

Table 5.2 VFT Fit Parameters for The Temperature Dependence of τ_s

	A	B	C	D
$\log \tau_0$	-10.0	-9.4	-11.1	-11.0
B	829.0	914.7	1608.0	1196.1
T_0	257.4	229.7	206.7	213.0

If the ion transport is completely coupled to the structural relaxation, the DC conductivity in ionic conductors should be on the order of 10^{-15} S/cm at the glass transition temperature.[232, 233] The conductivities of all our samples at their Tgs are much higher than 10^{-15} S/cm (Fig. 5.8), indicating that the conductivity is indeed decoupled from the segmental relaxation of the polymer in the vicinity of the glass transition temperature in our study.
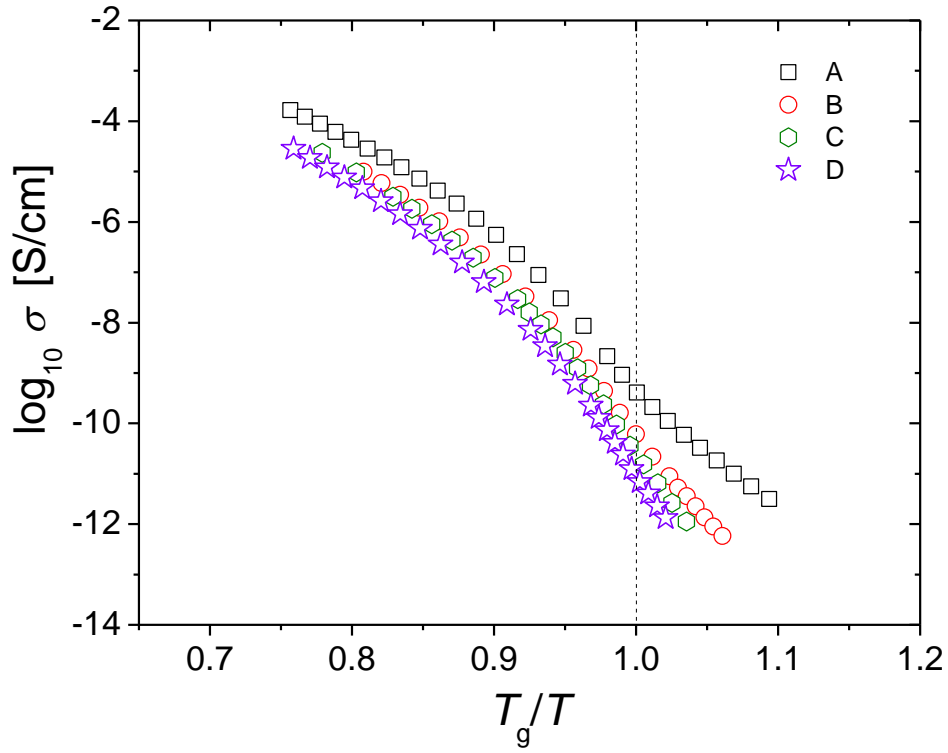
Figure 5.8. DC conductivity as a function of Tg/T. All our samples have conductivity significantly larger than 10^{-15} S/cm at their glass transition temperatures.

The decoupling ratio, R_τ, which is defined as the ratio of structural to conductivity relaxation times at Tg is summarized in Table 5.3. For polymer electrolytes in which the ionic transport is controlled by the structural dynamics of the polymer, R_τ is smaller than unity. For example, R_τ of poly(propylene oxide) (molecular weight= 4000g/mol) mixed with $NaCF_3SO_3$ salt, has very small values $\sim10^{-3}$.[213] Our PolyILs, on the other hand, show R_τ between 10^3 to $10^{4.9}$.

The Walden plot analysis serves as a very useful tool to study the relationship between ionic transport and segmental relaxation in polymer electrolytes.[228, 234, 235] In a Walden plot analysis modified for polymer electrolytes, the molar conductivity Λ of the sample is plotted against the inverse of segmental relaxation time on a double-logarithmic scale. Using the ion conductivity of a dilute aqueous solution as a reference (e.g., KCl, $LiClO_4$), an "ideal" Walden line with the slope of one can be drawn. This line presents the molar conductivity of a system where all ions contribute to the conductivity and their motion is completely coupled to the structural relaxation.

The modified Walden plot for all our samples is shown in Fig. 5.9. The dilute LiCl aqueous solution is used as the reference to draw the "ideal" Walden line. All of our samples' data fall above the "ideal" Walden line and exhibit a slope smaller than unity in the vicinity of Tg. This implies two things. First, the ionic conductivity has weaker temperature dependence than the segmental relaxation time. Second, the rate of ionic diffusion in our samples is much faster than the rate of structural relaxation in the entire studied temperature range. The Walden plot analysis (Fig. 5.9) clearly demonstrates that the ionic transport in all our samples
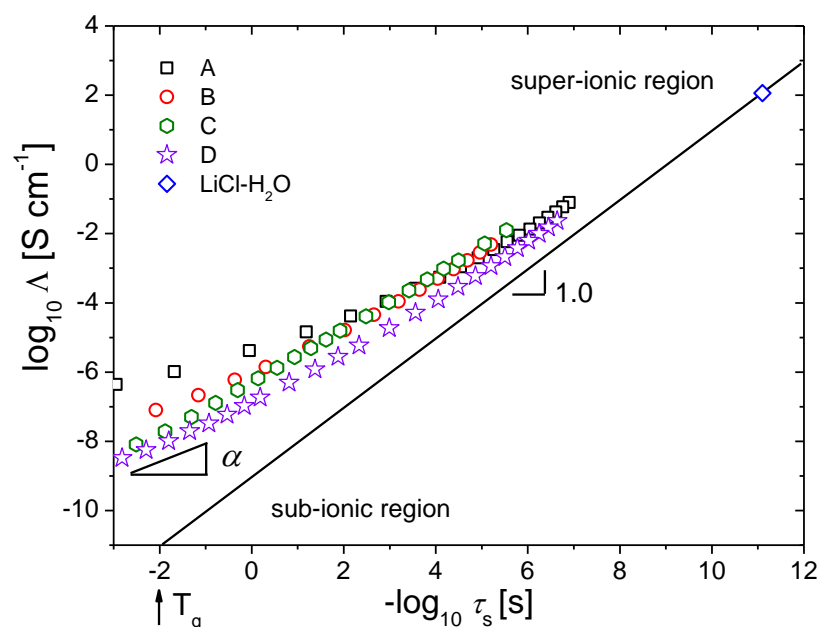
Figure 5.9. Walden Plot. Dilute LiCl aqueous solution is used as the reference to construct the "ideal" Walden line (black). All data points fall above the "ideal" Walden line. The relation between Λ and $1/\tau$ can be characterized by a power law: $\Lambda \tau_s^{\alpha}$ =Const. The decoupling exponent $\varepsilon = 1-\alpha$ reflects the degree of decoupling between the ion conductivity and segmental relaxation in the vicinity of the glass transition temperature.

is decoupled from the segmental relaxation, in strong contrast to their small molecule

analogue- aprotic ILs.[36, 198]

5.4.3 Correlation between Decoupling Exponent and Fragility

Analysis of the above data (Fig. 5.9) suggests that the degree of decoupling depends

on the structure of pedant groups, i.e. the variation of pendant group leads to different values

of the decoupling exponent ε. Based on our previous work[28] on polymer electrolytes and

analysis of other glass forming liquids with strong decoupling[223, 224], the fragility index (see

Chapter 1, eq.1.13) plays an important role in determining the degree of decoupling.[236, 237]

However, decoupling in aprotic ILs has been found to be very weak regardless of their

fragility.[36] It is far from clear what structural parameter controls the decoupling in PolyILs:

whether it will follow the change of fragility as it is in systems of polymers doped with salts,

or it will not depend on fragility as it is in regular aprotic ILs.

To estimate fragility of studied PolyILs we used τ_s from the mechanical

measurements. The decoupling exponent is plotted as a function of the fragility in Fig. 5.10.

More data points were obtained from Chapter 4 and the literature are put in Fig.5.10 together

to understand the correlation between the degree of decoupling and the fragility index in

polymeric samples

Indeed, the decoupling exponent increases with the increase of fragility in

polymerized ionic liquids, same as the trend found in polymers and polymer electrolytes

samples (Fig.5.10). It suggest that fragility might be the dominant factor that determines the

degree of decoupling in polymeric samples, in full analogy with earlier findings.[238, 239]

Unfortunately segmental dynamics and fragility of other polymeric systems reported by other

groups are not known, which precludes us from expanding the data in Fig.5.10.

To explain the correlation between fragility and the degree of decoupling, we turn to

the general entropy theory proposed by Dudowicz et al. and other recent theoretical and

experimental work.[17, 18, 81, 153, 176, 234, 235, 238-241] According to these studies, the "relative

rigidity" between the polymer backbone and side chain governs the chain packing efficiency
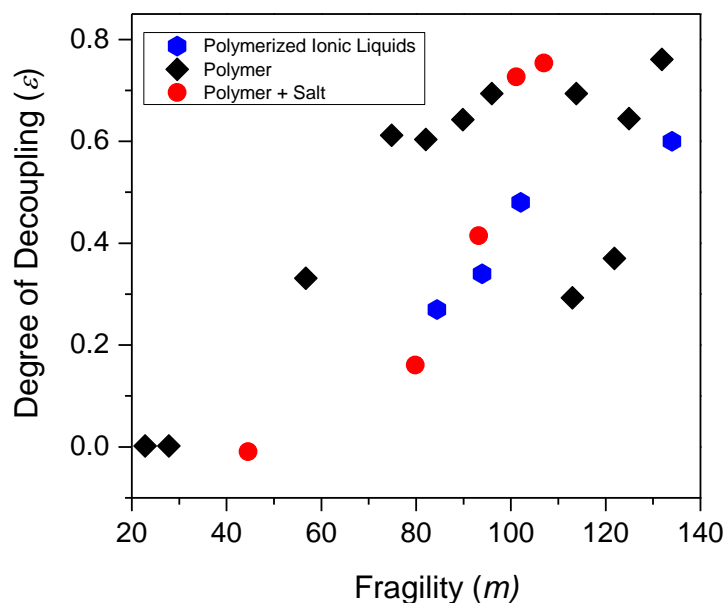
Figure 5.10 The decoupling exponent ε vs the polymer fragility m. Blue symbols represent the data from polymerized ionic liquids studied in this chapter; black symbols represent the data from ref.[27] and red symbols represent the data from Chapter 4 and ref. [28]

and thus affect the polymer fragility: the lower the chain packing efficiency, the higher the fragility. Flexible polymers can pack more efficiently, resulting in a tightly packed structure. For ion diffusion, a well packed polymer matrix presents more obstacles than that in a loosely packed polymer matrix. Thus the ionic transport requires larger rearrangement of polymer segments. On the contrary, ions may diffuse through the loosely packed polymer matrix even when the segmental dynamics is slow or "frozen". Analysis of our data shows that the decrease in the polymer fragility (through improved packing efficiency) leads to a decrease of the degree of decoupling between ion transport and segmental dynamics.

Table 5.3 Summary of Glass Transition Temperatures Obtained from Different Methods,

Fragility Index m, Decoupling Ratio R_τ and Decoupling Exponent ε

Sample Code	Tg-rheology	Tg-DSC	Tg-BDS	m	R_τ	ε
A	285.05	290.15	282.35	134	$10^{4.9}$	0.6
B	261.35	259.15	261.15	102.1	$10^{3.8}$	0.48
C	256.45	258.85	259.55	84.4	$10^{3.3}$	0.27
D	250.10	257.55	252.85	93.9	$10^{3.0}$	0.34

5.5 Conclusions

We have used broadband dielectric spectroscopy, together with rheology and differential scanning calorimetry to study the ionic transport in PolyILs with different pendant groups. We demonstrate that the main dielectric relaxation process in studied PolyILs is caused by conductivity relaxation and not by segmental dynamics. The variation of pendant groups alters the dielectric, mechanical and thermal properties of our samples. The Walden plot analysis demonstrates that the ionic transport is decoupled from the segmental relaxation in all our samples. The decoupling is also reflected in the conductivity values at the glass transition temperatures. All of our samples show conductivities at their Tgs much higher than the usually reported value $\sim 10^{-15}$ S/cm for polymer electrolytes, in which the ionic transport is closely coupled to the segmental dynamics (e.g. PEO). Our analysis shows that the degree of decoupling increases with the increase of the polymer fragility. We suggest that the higher

degree of decoupling in samples with larger fragility is caused by the packing frustration in those samples, i.e. ions can diffuse through the polymer matrix more easily when the polymer segments are loosely packed. For a further understanding of the correlation among glass transition temperature, fragility and degree of decoupling, and to better guide designs of PolyILs structures, an analysis of more PolyILs is necessary in the future.

CONCLUDING REMARKS AND FUTURE WORK

A great amount of effort has been put into the study of solid polymer electrolytes because of their advantages over the traditional liquid electrolytes and potential applications in energy storage and electrochemical devices.[47-50] However, none of the current dry polymer electrolytes exhibit conductivity greater than 10^{-3} S/cm at ambient temperature, which is mainly due to the fact that the mechanism of ion transport in the polymer electrolytes is not completely understood.

In this study, the ion transport mechanism in polymer electrolytes was studied. The main experimental techniques used were broadband dielectric spectroscopy, differential scanning calorimetry and rheology. By analyzing different polymer electrolyte systems, it was demonstrated that decoupling might be the key to achieve high ionic conductivity in polymer electrolytes at room temperature.

First, the ion transport mechanism was re-visited in a model system of PPG and LiClO$_4$ by systematically varying the experimental temperature, pressure, polymer molecular weight, and salt concentration. A micro-phase separation in "ion-rich" and "ion-depleted" domains was observed by both differential scanning calorimetry (PPG4000-LiClO$_4$, O:Li = 10, 15) and dielectric spectroscopy (PPG4000-LiClO$_4$, O:Li = 1000, 30, 15, 10; PPG1000-LiClO$_4$, O:Li = 30) in some of the samples. The analysis indicates that both the polymer molecular weight and the number of terminal hydroxyl groups contribute to the different thermal and dielectric behavior of PPG-LiClO$_4$. The classic Walden plot analysis was

modified to study the relationship between polymer dynamics and ion transport. In the modified Walden plot, the molar conductivity is plotted against the reciprocal segmental relaxation instead of fluidity on a double logarithmic scale. Data points corresponding to the segmental relaxation or the segmental relaxation of the "ion-rich" domain, if micro-phase separation is observed, fall close to the ideal Walden line, indicating that ion transport is strongly coupled with the segmental relaxation and the ionic conductivity is controlled by the "ion-rich" phase, not the "ion-depleted" phase in samples with micro-phase separation. In addition, dielectric spectroscopy measurements under high pressure were carried out. The degree of micro-phase separation was found to decrease with increased pressure. Most importantly, the close relationship between ionic transport and segmental relaxation breaks down at sufficiently high pressure, where the sample (PPG4000-LiClO$_4$, O:Li = 30) starts to resemble superionic conductors.

As demonstrated by the PPG-LiClO$_4$ system, because ion transport has to be facilitated by the segmental relaxation, the ion conductivity drops drastically with the slowing down of segmental relaxation as the system is cooled towards Tg. Inspired by the decoupling feature in several fast ion conductors and previous work done on rigid polymers, two types of polymer electrolytes based on polycarbonate and polystyrene were synthesized with a goal of decoupling ion migration from the polymer segmental dynamics. The results showed that decoupling was observed in those studied systems. The corresponding data points in the modified Walden plot displayed two types of decoupling features. First, a line with a slope less than one on the Walden plot indicates that ion conductivity and segmental relaxation have a different temperature dependence. Second, lines with a slope of one, yet above the idea

Walden line, indicates that ion transport is faster than the polymer segmental dynamics in the entire temperature range studied. The ion transport in those samples was compared with traditional polyether based polymer electrolytes and small molecules electrolytes. It is found that the ion transport mechanism is very different in polymeric materials and small molecules.

Lastly, the ion transport mechanism is studied in a new type of functional material, the so-called polymerized ionic liquids. A systematic study on several polymerized ionic liquids with different pendant groups is carried out. The variation of pendant groups greatly changes the thermal, dielectric, and mechanical properties of the samples. Comparison between dielectric and mechanical results, along with the modified Walden plot analysis reveals that the ion transport of PolyILs is very different from their small molecule analogue-aprotic IL. The former shows decoupling feature, while ion diffusion is strongly coupled to structural relaxation of the system in the later. Combining data from Chapter 4, literatures with data of the PolyILs studied, we found that the decoupling degree increases with the increase of fragility index of polymer. We suggest that this finding is related to the packing efficiency in polymeric samples. For polymers with high fragility, a loosely-packed structure should be expected due to rigidity of the polymer chains. Therefore, it is suggested that ions can diffuse through those systems without polymer segments rearrangements, resulting in a bigger degree of decoupling.

As it is demonstrated in Chapter 4, for traditional polymer electrolytes in which the ion conduction is coupled with segmental relaxation, the polymer segments have to reach a segmental relaxation rate as fast 10^{-8} s to be able to maintain an ionic conductivity of 10^{-3} S/cm at room temperature. The work presented here demonstrates that the concept of

"decoupling" is the most promising way if not the only way to obtain high ionic conductivity in polymer electrolytes at room temperature. Research presented in this dissertation could have a significant impact on the field of polymer electrolytes, providing an alternative approach to design polymer electrolytes with desired properties.

The highest ionic conductivity achieved in the polymer electrolytes studied here with the decoupling feature is of the order of 10^{-5} S/cm at room temperature. It out-performs one of the best conventional polymer electrolyte based on PEO-LiTFSI (wt45%). Future work would include development of advance polymer electrolytes as guided by the decoupling concept and exploring further the relationship between decoupling and polymer structural parameters.

Other methods of improving conductivity in polymer electrolytes have been briefly mentioned in Chapter 1. One way is to use polymer composites materials, in which "solid plasticizers", e.g. nano-scale Al_2O_3, SiO_2, TiO_2 are added to the polymer electrolytes. Due to the large surface area of nanoparticles, there are many interesting and unexpected properties of this new type of material. It has been reported that with the addition of nanoparticles the ionic conductivity of PEO based polymer electrolytes increased.[242] It was suggested that the increase of conductivity resulted from the reduced crystallinity with the introduction of nanocomposites. However, the enhancement of conductivity occurs in the entire temperature range, not just below T_m. It was proposed by Best et al.[243] that lithium cation experienced the same potential at TiO_2 filler surfaces and could move between these sites with a lowered activation energy barrier. A simulation study by Thomas et al.[244] showed that Li+ mobility was increased with the addition of particles. There is still a lot questions to be addressed in the nanocomposites polymer electrolytes field.

Another area that needs further investigation is the dynamics of polymerized ionic liquids. As mentioned in Chapter 5, by varying the structure of the polymer and pairing it with different ionic liquids, a large amount of PolyILs are potentially available. Thus, it is desirable to have an understanding of the structure-properties relationship in PolyILs. How do parameters like Tg, fragility, ionic conductivity change with the molecular weight? How does the side chain structure, cations, counter-ions affect properties of the system? How do ions diffuse in different PolyILs? There remains a lot of questions to be answered in this field.

LIST OF REFERENCES

1.   Corrie T. Imrie, M. D. I. *Electrochimica Acta* **2001,** 46, 1413–1417.

2.   Perzyna, K.; Borkowska, R.; Syzdek, J.; Zalewska, A.; Wieczorek, W. *Electrochimica Acta* **2011,** 57, 58-65.

3.   Meyer, W. H. *Adv Mater* **1998,** 10, (6), 439-+.

4.   Tarascon, J. M.; Armand, M. *Nature* **2001,** 414, (6861), 359-367.

5.   Malmberg, C. G.; Maryott, A. A. *J Res Nat Bur Stand* **1956,** 56, (1), 1-8.

6.   Chernyak, Y. *J Chem Eng Data* **2006,** 51, (2), 416-418.

7.   KRAUS, R. F. A. C. *J. Am. chem. Soc.* **1933,** 55, 2387.

8.   Marcus, Y.; Hefter, G. *Chem Rev* **2006,** 106, (11), 4585-4621.

9.   Ue, M.; Mori, S. *J Electrochem Soc* **1995,** 142, (8), 2577-2581.

10.   Ue, M. *J Electrochem Soc* **1994,** 141, (12), 3336-3342.

11.   Ue, M. *Denki Kagaku* **1994,** 62, (7), 620-623.

12.   Debye, P.; Hückel, E. *Physikalische Zeitschrift* **1923,** 24, 185–206.

13.   Angell, C. A. *Science* **1995,** 267, (5206), 1924-1935.

14.   Angell, C. A. *J Non-Cryst Solids* **1991,** 131, 13-31.

15.   Qin, Q.; McKenna, G. B. *J Non-Cryst Solids* **2006,** 352, (28-29), 2977-2985.

16.   Adam, G.; Gibbs, J. H. *J Chem Phys* **1965,** 43, (1), 139-&.

17.   Dudowicz, J.; Freed, K. F.; Douglas, J. F. *J Phys Chem B* **2005,** 109, (45), 21350-21356.

18.   Dudowicz, J.; Freed, K. F.; Douglas, J. F. *J Chem Phys* **2006,** 124, (6).

19.   Dudowicz, J.; Freed, K. F.; Douglas, J. F. *J Phys Chem B* **2005,** 109, (45), 21285-21292.

20.   Dimarzio, E. A.; Gibbs, J. H. *J Chem Phys* **1958,** 28, (5), 807-813.

21.   Dudowicz, J.; Douglas, J. F.; Freed, K. F. *J Chem Phys* **2014,** 141, (23).

22.   Walden, P. *Z. Physik. Chem.* **1906,** 55, 207-249.

23.   Lee, S.-Y.; Ueno, K.; Angell, C. A. *J. Phys. Chem. C* **2012,** 116, (45), 23915-23920.

24.   Angell, C. A.; Ansari, Y.; Zhao, Z. *Faraday Discuss.* **2012,** 154, 9-27.

25.   Belieres, J.-P.; Angell, C. A. *J. Phys. Chem. B* **2007,** 111, 4926-4937.

26.   Xu, W.; Angell, C. A. *Science* **2003,** 302, (5644), 422-425.

27.   Agapov, A. L.; Sokolov, A. P. *Macromolecules* **2011,** 44, 4410-4414.

28.   Wang, Y.; Agapov, A. L.; Fan, F.; Hong, K.; Yu, X.; Mays, J.; Sokolov, A. P. *Phys. Rev. Lett.* **2012,** 108, 088303.

29.   Imrie, C. T.; Ingram, M. D. *Electrochim. Acta* **2001,** 46, 1413-1417.

30.   Wei, X.; Shriver, D. F. *Chem. Mater.* **1998,** 10, 2307-2308.

31.   Ferry, A.; Edman, L.; Forsyth, M.; MacFarlane, D. R.; Sun, J. *J. Appl. Phys.* **1999,** 86, (4), 2346-2348.

32.   Ferry, A.; Edman, L.; Forsyth, M.; MacFarlane, D. R.; Sun, J. *Electrochim. Acta* **2000,** 45, (8–9), 1237-1242.

33.   Forsyth, M.; Jiazeng, S.; MacFarlane, D. R. *Electrochim. Acta* **2000,** 45, (8–9), 1249-1254.

34.   Angell, C. A. *Solid State Ionics* **1983**, 3-16.

35.   Angell. *Solid State Ionic* **1986**, 72-88.

36.   Griffin, P.; Agapov, A. L.; Kisliuk, A.; Sun, X. G.; Dai, S.; Novikov, V. N.; Sokolov, A. P. *J Chem Phys* **2011,** 135, (11).

37.   Xu, W.; Angell, C. A. *Science* **2003,** 302, (5644), 422-425.

38.   Fenton, D. E.; Parker, J. M.; Wright, P. V. *Polymer* **1973,** 14, (11), 589-589.

39.   Bruce, D. W.; O'Hare D.; I., W. R., *Energy materials*. 1 ed.; Wiley: 2011.

40.   Armand, M. *Solid State Ionics* **1994,** 69, (3-4), 309-319.

41.   Mullerplathe, F.; Vangunsteren, W. F. *J Chem Phys* **1995,** 103, (11), 4745-4756.

42.   Lightfoot, P.; Mehta, M. A.; Bruce, P. G. *Science* **1993,** 262, (5135), 883-885.

43.   Thomson, J. B.; Lightfoot, P.; Bruce, P. G. *Solid State Ionics* **1996,** 85, (1-4), 203-208.

44.   Bruce, P. G. *Philos T R Soc A* **1996,** 354, (1706), 415-436.

45.   Sylla, S.; Sanchez, J. Y.; Armand, M. *Electrochimica Acta* **1992,** 37, (9), 1699-1701.

46.   Agrawal, R. C.; Pandey, G. P. *J Phys D Appl Phys* **2008,** 41, (22).

47.   Scrosati, B.; Vincent, C. A. *MRS Bull.* **2000,** 25, 28-30.

48.   Wright, P. V. *MRS Bull.* **2002,** 27, (8), 597-602.

49.   Armand, M. *Solid State Ionics* **1983,** 9–10, Part 2, (0), 745-754.

50.   Tarascon, J.-M.; Armand, M. *Nature* **2001,** 414, 359-367.

51.   Watanabe, M.; Nagano, S.; Sanui, K.; Ogata, N. *J Power Sources* **1987,** 20, (3-4), 327-332.

52.   Huang, B. Y.; Wang, Z. X.; Li, G. B.; Huang, H.; Xue, R. J.; Chen, L. Q.; Wang, F. S. *Solid State Ionics* **1996,** 85, (1-4), 79-84.

53.   Croce, F.; Gerace, F.; Dautzemberg, G.; Passerini, S.; Appetecchi, G. B.; Scrosati, B. *Electrochimica Acta* **1994,** 39, (14), 2187-2194.

54.   Ferry, A.; Edman, L.; Forsyth, M.; MacFarlane, D. R.; Sun, J. Z. *J Appl Phys* **1999,** 86, (4), 2346-2348.

55.   Bohnke, O.; Frand, G.; Rezrazi, M.; Rousselot, C.; Truche, C. *Solid State Ionics* **1993,** 66, (1-2), 97-104.

56.   Bohnke, O.; Frand, G.; Rezrazi, M.; Rousselot, C.; Truche, C. *Solid State Ionics* **1993,** 66, (1-2), 105-112.

57.   Fan, L. Z.; Dang, Z. M.; Nan, C. W.; Li, M. *Electrochimica Acta* **2002,** 48, (2), 205-209.

58.   Michot, T.; Nishimoto, A.; Watanabe, M. *Electrochimica Acta* **2000,** 45, (8-9), 1347-1360.

59.   Jiang, Z.; Carroll, B.; Abraham, K. M. *Electrochimica Acta* **1997,** 42, (17), 2667-2677.

60.   Alamgir, M.; Abraham, K. M. *J Electrochem Soc* **1993,** 140, (6), L96-L97.

61.   Ramesh, S.; Arof, A. K. *Mat Sci Eng B-Solid* **2001,** 85, (1), 11-15.

62.   C. BERTHIER, W. G., M. MINIER. **1983,** 11, 91-95.

63.   Berthier, C.; Gorecki, W.; Minier, M.; Armand, M. B.; Chabagno, J. M.; Rigaud, P.
Solid State Ionics **1983,** 11, (1), 91-95.

64.   Druger, S. D.; Ratner, M. A.; Nitzan, A. *Solid State Ionics* **1983,** 9-10, (Dec), 1115-
1120.

65.   Druger, S. D.; Nitzan, A.; Ratner, M. A. *J Chem Phys* **1983,** 79, (6), 3133-3142.

66.   Ingram, M. D.; Imrie, C. T.; Stoeva, Z.; Pas, S. J.; Funke, K.; Chandler, H. W. *J Phys
Chem B* **2005,** 109, (35), 16567-16570.

67.   Wintersgill, M. C.; Fontanella, J. J.; Calame, J. P.; Figueroa, D. R.; Andeen, C. G.
Solid State Ionics **1983,** 11, (2), 151-155.

68.   Ngai, K. L.; Plazek, D. J. *Rubber Chem Technol* **1995,** 68, (3), 376-434.

69.   Stephan, A. M. *European Polymer Journal* **2006,** 42, 21–42.

70.   WRIGHT, P. V. *MRS BULLETIN* **2002**, 597-602.

71.   Vincent, B. S. a. C. A. *MRS BULLETIN* **2000**, 28-30.

72.   Vincent, P. G. B. a. C. A. *J. CHEM. SOC. FARADAY TRANS.* **1993**, 3187-3203.

73.   Pandey, R. C. A. a. G. P. *J. Phys. D: Appl. Phys.* **2008**, 18 pages.

74.   A. Manuel Stephan, K. S. N. *Polymer* **2006,** 47, 5952-5964.

75.   C. A. Angell, C. L. E. S. *Nature* **1993,** 362, 137-139.

76.   Wu Xu, L.-M. W., C. Austen Angell. *Electrochimica Acta* **2003,** 48, 2037-2045.

77.   Zlatka Gadjourova, Y. G. A., David P. Tunstall & Peter G. Bruce. *Nature* **2001**, 520-523.

78.   Sasabe, H.; Saito, S. *Polym J* **1972,** 3, (5), 624-&.

79.   Agapov, A. L.; Sokolov, A. P. *Macromolecules* **2011**, 4410-4414.

80.   Kumar Kunal, C. G. R., Sebastian Pawlus, Steven F. Hahn, and Alexei P. Sokolov. *Macromolecules* **2008,** 41, 7232-7238.

81.   Kumar, R.; Goswami, M.; Sumpter, B. G.; Novikov, V. N.; Sokolov, A. P. *Physical Chemistry Chemical Physics* **2013,** 15, (13), 4604-4609.

82.   Shengshui Zhang, Z. C., Kang Xu, C. Austen Angell. *Electrochimica Acta* **2000,** 45, 1229–1236.

83.   Takakazu Yamamoto, M. I., and Takaki Kanbara. *Chem. Mater.* **1994,** 6, 44-50.

84.   H. A. Every, F. Z., M. Forsyth and D. R. MacFarlane. *Electrochimica Acta* **1998,** 43, 1465-1469.

85.   Shriver, X. W. a. D. F. *Chem. Mater.* **1998,** 10, 2307-2308.

86.   C. T. Imrie, M. D. I., and G. S. McHattie. *J. Phys. Chem* **1999,** 103, (20), 4132-4138.

87.   Kremer, F.; Schohals, A., *Broadband Dielectric Spectroscopy*. Springer-Verlag: Berlin, 2002.

88.   Wübbenhorst, M.; van Turnhout, J. *J. Non-Cryst. Solids* **2002,** 305, 40-49.

89.   Zhang, S.; Runt, J. *J. Phys. Chem. B* **2004,** 108, (20), 6295-6302.

90.   MacDonald, J. R. *J. Phys. Rev.* **1953,** 92, 4.

91.   Coelho, R. *J. Non-Cryst. Solids* **1991,** 131-133, 1136-1139.

92.   Klein, R. J.; Zhang, S. H.; Dou, S.; Jones, B. H.; Colby, R. H.; Runt, J. *J. Chem. Phys.* **2006,** 124, 144903.

93.   Trukhan, E. M. *Sov. Phys. Solid State (Engl. Transl.)* **1963,** 4, 2560.

94.   Sørensen, T. S.; Compañ, V. *J. Chem. Soc. Faraday Trans.* **1995,** 91, (23), 4235-4250.

95.   Munar, A.; Andrio, A.; Iserte, R.; Compañ, V. *J. Non-Cryst. Solids* **2011,** 357, 3064-3069.

96.   Wang, Y. Y.; Sun, C. N.; Fan, F.; Sangoro, J. R.; Berman, M. B.; Greenbaum, S. G.; Zawodzinski, T. A.; Sokolov, A. P. *Phys Rev E* **2013,** 87, (4).

97.   Macdonald, J. R. *J Phys-Condens Mat* **2010,** 22, (49).

98.   Macdonald, J. R.; Evangelista, L. R.; Lenzi, E. K.; Barbero, G. *J Phys Chem C* **2011,** 115, (15), 7648-7655.

99.   Fragiadakis, D.; Dou, S.; Colby, R. H.; Runt, J. *Macromolecules* **2008,** 41, 5723-5728.

100.   Thomas, L. C., Modulated DSC® Paper #1 Why Modulated DSC®?; An Overview and Summary of Advantages and Disadvantages Relative to Traditional DSC. TA Instruments: New Castle, DE, 2005.

101.   Ferry, J. D., *Viscoelastic Properties of Polymers*. John Wiley & Sons, Inc: 1980.

102.   Williams, M. L.; Landel, R. F.; Ferry, J. D. *J Am Chem Soc* **1955,** 77, (14), 3701-3707.

103.   Plazek, D. J.; Orourke, V. M. *J Polym Sci A2* **1971,** 9, (2), 209-&.

104.   Plazek, D. J. *J Phys Chem-Us* **1965,** 69, (10), 3480-&.

105.   Armand, M.; Chabagno, J. M.; Duclot, M., Polyethers as Solid Electrolytes. In *Fast Ion Transport in Solids: Electrodes and Electrolytes*, Vashitshta, P.; Mundy, J. N.; Shenoy, G. K., Eds. North Holland Publishers: Amsterdam, 1979.

106.   Wright, P. V. *Br. Polymer J.* **1975,** 7, (5), 319-327.

107.   Fenton, D. E.; Parker, J. M.; Wright, P. V. *Polymer* **1973,** 14, (11), 589.

108.   Watanabe, M.; Ikeda, J.; Shinohara, I. *Polym. J.* **1983,** 15, 65-69.

109.   Watanabe, M.; Ikeda, J.; Shinohara, I. *Polym. J.* **1983,** 15, 175-177.

110.   Ferry, A.; Orädd, G.; Jacobsson, P. *Macromolecules* **1997,** 30, (23), 7329-7331.

111.   Schantz, S.; Torell, L. M.; Stevens, J. R. *J. Appl. Phys.* **1988,** 64, (4), 2038-2043.

112.   Schantz, S.; Torell, L. M.; Stevens, J. R. *J. Chem. Phys.* **1991,** 94, 6862-6867.

113.   Vallée, A.; Besner, S.; Prud'Homme, J. *Electrochimica Acta* **1992,** 37, (9), 1579-1583.

114.   Yoshida, K.; Manabe, H.; Takahashi, Y.; Furukawa, T. *Electrochim. Acta* **2011,** 57, 139-146.

115.   McLin, M. G.; Angell, C. A. *J. Phys. Chem.* **1996,** 100, (4), 1181-1188.

116.   Furukawa, T.; Mukasa, Y.; Suzuki, T.; Kano, K. *J. Polym. Sci. Part B: Polym. Phys.* **2002,** 40, (7), 613-622.

117.   Kano, K.; Takahashi, Y.; Furukawa, T. *Jpn. J. Appl. Phys.* **2001,** 40, 3246-3251.

118.   Berthier, C.; Gorecki, W.; Minier, M.; Armand, M. B.; Chabagno, J. M.; Rigaud, P. *Solid State Ionics* **1983,** 11, (1), 91-95.

119.   Gadjourova, Z.; Andreev, Y. G.; Tunstall, D. P.; Bruce, P. G. *Nature* **2001,** 412, (6846), 520-523.

120.   Scheirs, J.; Bigger, S. W.; Delatycki, O. *Eur. Polym. J.* **1991,** 27, (10), 1111-1120.

121.   Vachon, C.; Labreche, C.; Vallee, A.; Besner, S.; Dumont, M.; Prud'homme, J. *Macromolecules* **1995,** 28, (16), 5585-5594.

122.   Vachon, C.; Vasco, M.; Perrier, M.; Prud'homme', J. *Macromolecules* **1993,** 26, 4023-4031.

123.   Bergman, R.; Börjesson, L.; Fytas, G.; Torell, L. M. *J. Non-Cryst. Solids* **1994,** 172–174, Part 2, (0), 830-837.

124.   Gainaru, C.; Hiller, W.; Bohmer, R. *Macromolecules* **2010,** 43, (4), 1907-1914.

125.   Ferry, A. *J. Phys. Chem. B* **1997,** 101, (2), 150-157.

126.   Kaminski, K.; Kipnusu, W. K.; Adrjanowicz, K.; Mapesa, E. U.; Iacob, C.; Jasiurkowska, M.; Wlodarczyk, P.; Grzybowska, K.; Paluch, M.; Kremer, F. *Macromolecules* **2013,** 46, (5), 1973-1980.

127.   Gainaru, C.; Hiller, W.; Boehmer, R. *Macromolecules* **2010,** 43, (4), 1907-1914.

128.   Bernson, A.; Lindgren, J. *Polymer* **1994,** 35, (22), 4848-4851.

129.   Ferry, A. *J Phys Chem B* **1997,** 101, (2), 150-157.

130.   Roland, C. M.; Psurek, T.; Pawlus, S.; Paluch, M. *J. Polym. Sci. Part B: Polym. Phys.* **2003,** 41, (23), 3047-3052.

131.   Grzybowska, K.; Grzybowski, A.; Ziolo, J.; Rzoska, S. J.; Paluch, M. *J. Phys.: Condens. Matter* **2007,** 19, (37), 376105.

132.   Grzybowska, K.; Grzybowski, A.; Ziolo, J.; Paluch, M.; Capaccioli, S. *J. Chem. Phys.* **2006,** 125, (4), 044904.

133.   Andersson, S. P.; Andersson, O. *Macromolecules* **1998,** 31, (9), 2999-3006.

134.   Roland, C. M.; Hensel-Bielowka, S.; Paluch, M.; Casalini, R. *Rep. Prog. Phys.* **2005,** 68, (6), 1405.

135.   Fontanella, J. J. *J. Chem. Phys.* **1999,** 111, 7103-7109.

136.   Bendler, J. T.; Fontanella, J. J.; Shlesinger, M. F. *Phys. Rev. Lett.* **2001,** 87, (19), 195503.

137.   Bendler, J. T.; Fontanella, J. J.; Shlesinger, M. F.; Wintersgill, M. C. *Electrochim. Acta* **2003,** 48, (14–16), 2267-2272.

138.   Vachon, C.; Vasco, M.; Perrier, M.; Prudhomme, J. *Macromolecules* **1993,** 26, (15), 4023-4031.

139.   Mattsson, J.; Bergman, R.; Jacobsson, P.; Börjesson, L. *Phys. Rev. Lett.* **2003,** 90, (7), 075702.

140.   Schüller, J.; Mel'nichenko, Y. B.; Richert, R.; Fischer, E. W. *Phys. Rev. Lett.* **1994,** 73, (16), 2224-2227.

141.   Schonhals, A.; Stauga, R. *J. Chem. Phys.* **1998,** 108, (12), 5130-5136.

142.   Hayakawa, T.; Adachi, K. *Polymer* **2001,** 42, (4), 1725-1732.

143.   Schonhals, A.; Schlosser, E. *Prog. Colloid Polym. Sci* **1993,** 91, 158-161.

144.   Gainaru, C.; Bohmer, R. *Macromolecules* **2009,** 42, (20), 7616-7618.

145.   Paluch, M.; Pawlus, S.; Kaminski, K. *J. Chem. Phys.* **2011,** 134, 037101.

146.   Richert, R.; Agapov, A.; Sokolov, A. P. *J. Chem. Phys.* **2011,** 134, (10), 104508.

147.   Fragiadakis, D.; Dou, S.; Colby, R. H.; Runt, J. *J. Chem. Phys.* **2009,** 130, (6),
064907.

148.   Engberg, D.; Schuller, J.; Strube, B.; Sokolov, A. P.; Torell, L. M. *Polymer* **1999,** 40,
(17), 4755-4761.

149.   Bernson, A.; Lindgren, J. *Polymer* **1994,** 35, (22), 4848-4851.

150.   Rubinstein, M.; Colby, R. H., *Polymer Physics*. Oxford University Press: Oxford,
2003.

151.   Ratner, M. A.; Johansson, P.; Shriver, D. F. *MRS BULLETIN* **2000,** 25, (3), 31-37.

152.   Ratner, M. A.; Shriver, D. F. *Chem Rev* **1988,** 88, (1), 109-124.

153.   Agapov, A. L.; Sokolov, A. P. *Macromolecules* **2011,** 44, (11), 4410-4414.

154.   Imrie, C. T.; Ingram, M. D. *Electrochimica Acta* **2001,** 46, (10-11), 1413-1417.

155.   Wei, X. Y.; Shriver, D. F. *Chem Mater* **1998,** 10, (9), 2307-+.

156.	Hua, F. J.; Yuan, W. Z.; Britt, P. F.; Mays, J. W.; Hong, K. L. *Soft Matter* **2013,** 9, (37), 8897-8903.

157.	Walden, P. *Zeitschrift Fur Physikalische Chemie--Stochiometrie Und Verwandtschaftslehre* **1906,** 55, (2), 207-249.

158.	Haynes, W. M., *CRC handbook of chemistry and physics*. CRC Press: Boca Raton, 2012.

159.	Howell, F. S.; Bose, R. A.; Macedo, P. B.; Moynihan, C. T. *J. Phys. Chem.* **1974,** 78, 639-648.

160.	Malugani, J. P.; Wasniewski, A.; Doreau, M.; Robert, G. *Mat. Res. Bull.* **1978,** 13, 427-433.

161.	Takahashi, H.; Hiki, Y.; Kobayashi, H. *J. Appl. Phys.* **1998,** 84, 213-218.

162.	Robinson, R. A.; Stokes, R. H., *Electrolyte Solutions*. Second ed.; Butterworths Scientific Publications: London, 1959.

163.	Griffin, P. J.; Agapov, A. L.; Sokolov, A. P. *Phys Rev E* **2012,** 86, (2).

164.	Nakanishi, M.; Griffin, P.; Mamontov, E.; Sokolov, A. P. *J Chem Phys* **2012,** 136, (12).

165.	Howell, F. S.; Bose, R. A.; Macedo, P. B.; Moynihan, C. T. *J Phys Chem-Us* **1974,** 78, (6), 639-648.

166.	Sangoro, J. R.; Serghei, A.; Naumov, S.; Galvosas, P.; Karger, J.; Wespe, C.; Bordusa, F.; Kremer, F. *Phys Rev E* **2008,** 77, (5).

167.   Sangoro, J. R.; Iacob, C.; Serghei, A.; Friedrich, C.; Kremer, F. *Physical Chemistry Chemical Physics* **2009,** 11, (6), 913-916.

168.   Yoshida, K.; Manabe, H.; Takahashi, Y.; Furukawa, T. *Electrochimica Acta* **2011,** 57, 139-146.

169.   Furukawa, T.; Mukasa, Y.; Suzuki, T.; Kano, K. *J Polym Sci Pol Phys* **2002,** 40, (7), 613-622.

170.   Klein, R. J.; Zhang, S. H.; Dou, S.; Jones, B. H.; Colby, R. H.; Runt, J. *J Chem Phys* **2006,** 124, (14).

171.   Macdonald, J. R. *Phys Rev* **1953,** 92, (1), 4-17.

172.   Sorensen, T. S.; Compan, V. *J Chem Soc Faraday T* **1995,** 91, (23), 4235-4250.

173.   Trukhan, E. M. *Sov Phys-Sol State* **1963,** 4, (12), 2560-2570.

174.   Fragiadakis, D.; Dou, S. C.; Colby, R. H.; Runt, J. *Macromolecules* **2008,** 41, (15), 5723-5728.

175.   Angell, C. A.; Ansari, Y.; Zhao, Z. F. *Faraday Discuss* **2012,** 154, 9-27.

176.   Kunal, K.; Robertson, C. G.; Pawlus, S.; Hahn, S. F.; Sokolov, A. P. *Macromolecules* **2008,** 41, (19), 7232-7238.

177.   Kamaya, N.; Homma, K.; Yamakawa, Y.; Hirayama, M.; Kanno, R.; Yonemura, M.; Kamiyama, T.; Kato, Y.; Hama, S.; Kawamoto, K.; Mitsui, A. *Nat Mater* **2011,** 10, (9), 682-686.

178.   Bouchet, R.; Maria, S.; Meziane, R.; Aboulaich, A.; Lienafa, L.; Bonnet, J. P.; Phan, T. N. T.; Bertin, D.; Gigmes, D.; Devaux, D.; Denoyel, R.; Armand, M. *Nat Mater* **2013,** 12, (5), 452-457.

179.   Edman, L.; Ferry, A.; Doeff, M. M. *J Mater Res* **2000,** 15, (9), 1950-1954.

180.   Lee, S. Y.; Ueno, K.; Angell, C. A. *J Phys Chem C* **2012,** 116, (45), 23915-23920.

181.   Abouimrane, A.; Belharouak, I.; Amine, K. *Electrochem Commun* **2009,** 11, (5), 1073-1076.

182.   Xu, K. *Chem Rev* **2004,** 104, (10), 4303-4417.

183.   Kamaya, N.; Homma, K.; Yamakawa, Y.; Hirayama, M.; Kanno, R.; Yonemura, M.; Kamiyama, T.; Kato, Y.; Hama, S.; Kawamoto, K.; Mitsui, A. *Nature Mater.* **2011,** 10, 682-686.

184.   Song, J. Y.; Wang, Y. Y.; Wan, C. C. *J. Electrochem. Soc.* **2000,** 147, (9), 3219-3225.

185.   Stallworth, P. E.; Fontanella, J. J.; Wintersgill, M. C.; Scheidler, C. D.; Immel, J. J.; Greenbaum, S. G.; Gozdz, A. S. *J. Power Sources* **1999,** 81–82, (0), 739-747.

186.   Edman, L.; Ferry, A.; Doeff, M. M. *J. Mater. Res.* **2000,** 15, (09), 1950-1954.

187.   Galinski, M.; Lewandowski, A.; Stepniak, I. *Electrochimica Acta* **2006,** 51, (26), 5567-5580.

188.   Green, M. D.; Long, T. E. *Polym Rev* **2009,** 49, (4), 291-314.

189.   Armand, M.; Endres, F.; MacFarlane, D. R.; Ohno, H.; Scrosati, B. *Nat Mater* **2009,** 8, (8), 621-629.

190. Rogers, R. D.; Seddon, K. R. *Science* **2003,** 302, (5646), 792-793.

191. Greaves, T. L.; Drummond, C. J. *Chem Rev* **2008,** 108, (1), 206-237.

192. Mecerreyes, D. *Prog Polym Sci* **2011,** 36, (12), 1629-1648.

193. Yuan, J. Y.; Antonietti, M. *Polymer* **2011,** 52, (7), 1469-1482.

194. Yuan, J. Y.; Mecerreyes, D.; Antonietti, M. *Prog Polym Sci* **2013,** 38, (7), 1009-1036.

195. Nishimura, N.; Ohno, H. *Polymer* **2014,** 55, (16), 3289-3297.

196. Salamone, J. C.; Israel, S. C.; Taylor, P.; Snider, B. *Polymer* **1973,** 14, (12), 639-644.

197. Green, O.; Grubjesic, S.; Lee, S. W.; Firestone, M. A. *Polym Rev* **2009,** 49, (4), 339-360.

198. Sangoro, J. R.; Iacob, C.; Serghei, A.; Friedrich, C.; Kremer, F. *Physical Chemistry Chemical Physics* **2009,** 11, (6), 913-6.

199. Schreiner, C.; Zugmann, S.; Hartl, R.; Gores, H. J. *J Chem Eng Data* **2010,** 55, (10), 4372-4377.

200. Xu, W.; Cooper, E. I.; Angell, C. A. *J Phys Chem B* **2003,** 107, (25), 6170-6178.

201. Ohno, H.; Ito, K. *Chem Lett* **1998**, (8), 751-752.

202. Yoshizawa, M.; Hirao, M.; Ito-Akita, K.; Ohno, H. *J Mater Chem* **2001,** 11, (4), 1057-1062.

203. Ohno, H. *Electrochimica Acta* **2001,** 46, (10-11), 1407-1411.

204. Yoshizawa, M.; Ohno, H. *Electrochimica Acta* **2001,** 46, (10-11), 1723-1728.

205.   Yoshizawa, M.; Ogihara, W.; Ohno, H. *Polym Advan Technol* **2002,** 13, (8), 589-594.

206.   Yoshizawa, M.; Ohno, H. *Chem Lett* **1999**, (9), 889-890.

207.   Ohno, H.; Yoshizawa, M.; Ogihara, W. *Electrochimica Acta* **2004,** 50, (2-3), 255-261.

208.   Hirao, M.; Ito-Akita, K.; Ohno, H. *Polym Advan Technol* **2000,** 11, (8-12), 534-538.

209.   Lee, M.; Choi, U. H.; Colby, R. H.; Gibson, H. W. *Chem Mater* **2010,** 22, (21), 5814-5822.

210.   Choi, U. H.; Lee, M.; Wang, S. R.; Liu, W. J.; Winey, K. I.; Gibson, H. W.; Colby, R. H. *Macromolecules* **2012,** 45, (9), 3974-3985.

211.   Ogihara, W.; Washiro, S.; Nakajima, H.; Ohno, H. *Electrochimica Acta* **2006,** 51, (13), 2614-2619.

212.   U Hyeok Choi; Anuj Mittal; Jr., T. L. P.; Minjae Lee; Harry W. Gibson; James Runt; Colby, R. H. *Electrochimica Acta* **2014,** In Press.

213.   Mclin, M. G.; Angell, C. A. *Solid State Ionics* **1992,** 53, 1027-1036.

214.   Green, M. D.; Salas-de la Cruz, D.; Ye, Y. S.; Layman, J. M.; Elabd, Y. A.; Winey, K. I.; Long, T. E. *Macromol Chem Phys* **2011,** 212, (23), 2522-2528.

215.   Chen, H.; Choi, J. H.; Salas-de La Cruz, D.; Winey, K. I.; Elabd, Y. A. *Macromolecules* **2009,** 42, (13), 4809-4816.

216.   Nakamura, K.; Saiwaki, T.; Fukao, K. *Macromolecules* **2010,** 43, (14), 6092-6098.

217.   Nakamura, K.; Fukao, K. *Polymer* **2013,** 54, (13), 3306-3313.

218.   Agrawal, R. C.; Gupta, R. K. *J Mater Sci* **1999,** 34, (6), 1131-1162.

219.   Choi, U. H.; Ye, Y. S.; de la Cruz, D. S.; Liu, W. J.; Winey, K. I.; Elabd, Y. A.; Runt, J.; Colby, R. H. *Macromolecules* **2014,** 47, (2), 777-790.

220.   Sangoro, J. R.; Iacob, C.; Agapov, A. L.; Wang, Y.; Berdzinski, S.; Rexhausen, H.; Strehmel, V.; Friedrich, C.; Sokolov, A. P.; Kremer, F. *Soft Matter* **2014,** 10, (20), 3536-3540.

221.   Hutcheson, S. A.; McKenna, G. B. *J Chem Phys* **2008,** 129, (7), 074502.

222.   Nakamura, K.; Saiwaki, T.; Fukao, K.; Inoue, T. *Macromolecules* **2011,** 44, (19), 7719-7726.

223.   Nakamura, K.; Fukao, K.; Inoue, T. *Macromolecules* **2012,** 45, (9), 3850-3858.

224.   Ngai, K. L., *Relaxation and Diffusion in Complex Systems*. Springer: Berlin, 2011.

225.   Hodge, I. M.; Ngai, K. L.; Moynihan, C. T. *J Non-Cryst Solids* **2005,** 351, (2), 104-115.

226.   Wojnarowska, Z.; Knapik, J.; Diaz, M.; Ortiz, A.; Ortiz, I.; Paluch, M. *Macromolecules* **2014,** 47, (12), 4056-4065.

227.   Ngai, K. L.; Leon, C. *Phys Rev B* **1999,** 60, (13), 9396-9405.

228.   Fan, F.; Wang, Y. Y.; Sokolov, A. P. *Macromolecules* **2013,** 46, (23), 9380-9389.

229.   Karan, N. K.; Pradhan, D. K.; Thomas, R.; Natesan, B.; Katiyar, R. S. *Solid State Ionics* **2008,** 179, (19-20), 689-696.

230.   Wojnarowska, Z.; Wang, Y. Y.; Paluch, K. J.; Sokolov, A. P.; Paluch, M. *Physical Chemistry Chemical Physics* **2014,** 16, (19), 9123-9127.

231.   Wang, Y. Y.; Lane, N. A.; Sun, C. N.; Fan, F.; Zawodzinski, T. A.; Sokolov, A. P. *J Phys Chem B* **2013,** 117, (26), 8003-8009.

232.   Angell, C. A. *Solid State Ionics* **1983,** 9-10, (Dec), 3-16.

233.   Angell, C. A. *Solid State Ionics* **1986,** 18-9, 72-88.

234.   Wang, Y. Y.; Fan, F.; Agapov, A. L.; Yu, X.; Hong, K. L.; Mays, J.; Sokolov, A. P. *Solid State Ionics* **2014,** 262, 782-784.

235.   Wang, Y. Y.; Fan, F.; Agapov, A. L.; Saito, T.; Yang, J.; Yu, X.; Hong, K. L.; Mays, J.; Sokolov, A. P. *Polymer* **2014,** 55, (16), 4067-4076.

236.   Swallen, S. F.; Traynor, K.; McMahon, R. J.; Ediger, M. D.; Mates, T. E. *J Phys Chem B* **2009,** 113, (14), 4600-4608.

237.   Mapes, M. K.; Swallen, S. F.; Ediger, M. D. *J Phys Chem B* **2006,** 110, (1), 507-511.

238.   Wang, Y. Y.; Agapov, A. L.; Fan, F.; Hong, K. L.; Yu, X.; Mays, J.; Sokolov, A. P. *Phys Rev Lett* **2012,** 108, (8).

239.   Wang, Y. Y., Sokolov, A.P. *Current Opinion in Chemical Engineering* **2015,** 7, 113-119.

240.   Stukalin, E. B.; Douglas, J. F.; Freed, K. F. *J Chem Phys* **2009,** 131, (11).

241.   Noor, S. A. M.; Sun, J. Z.; MacFarlane, D. R.; Armand, M.; Gunzelmann, D.; Forsyth, M. *J Mater Chem A* **2014,** 2, (42), 17934-17943.

242.   Croce, F.; Appetecchi, G. B.; Persi, L.; Scrosati, B. *Nature* **1998,** 394, (6692), 456-458.

243.   Best, A. S.; Adebahr, J.; Jacobsson, P.; MacFarlane, D. R.; Forsyth, M. *Macromolecules* **2001,** 34, (13), 4549-4555.

244.   Kasemagi, H.; Klintenberg, M.; Aabloo, A.; Thomas, J. O. *Solid State Ionics* **2002,** 147, (3-4), 367-375.

VITA

Fei Fan was born in Suzhou, Jiangsu, China in the year of dragon (1988). Fei graduated from China Pharmaceutical University, Nanjing, Jiangsu in June, 2010 with a B.S. in pharmacy. After that, Fei came to the U.S. in August, 2010 to attend the University of Tennessee-Knoxville in pursuit of a PhD in chemistry. She joined Dr. Alexei P. Sokolov's group in Dec, 2010 with a focus on polymer electrolytes for energy storage applications. She won the POLY-IUPAC World Polymer Congress Travel Award 2012. She has presented posters and oral talks in POLY-IUPAC World Polymer Congress and two ACS national meetings. She was awarded the Burchfield Burridge Warner Fellowship in Polymer Chemistry from the chemistry department in 2014. She is the author or co-author of eight peer-reviewed publications.